

Institutionen för systemteknik

Department of Electrical Engineering

Examensarbete

Modeling and Control of Friction Stir Welding in 5 cm thick Copper Canisters

Examensarbete utfört i Reglerteknik
vid Tekniska högskolan vid Linköpings universitet
av

Isak Nielsen

LiTH-ISY-EX--12/4567--SE

Linköping 2012



Linköpings universitet
TEKNISKA HÖGSKOLAN

Department of Electrical Engineering
Linköpings universitet
SE-581 83 Linköping, Sweden

Linköpings tekniska högskola
Linköpings universitet
581 83 Linköping

Modeling and Control of Friction Stir Welding in 5 cm thick Copper Canisters

Master Thesis in Automatic Control
at the Institute of Technology at Linköping University
by


Isak Nielsen

LiTH-ISY-EX--12/4567--SE

Supervisors: **André Carvalho Bittencourt**
 ISY, Linköping University
 Lars Cederqvist
 SKB AB
 Olof Garpinger
 XDIN AB

Examiner: **Alf Isaksson**
 ISY, Linköping University

Linköping, 30 May, 2012

	Avdelning, Institution Division, Department Division of Automatic Control Department of Electrical Engineering Linköping University SE-581 83 Linköping, Sweden	Datum Date 2012-05-30
Språk Language <input type="checkbox"/> Svenska/Swedish <input checked="" type="checkbox"/> Engelska/English <input type="checkbox"/> _____	Rapporttyp Report category <input type="checkbox"/> Licentiatavhandling <input checked="" type="checkbox"/> Examensarbete <input type="checkbox"/> C-uppsats <input type="checkbox"/> D-uppsats <input type="checkbox"/> Övrig rapport <input type="checkbox"/> _____	ISBN _____ ISRN LiTH-ISY-EX--12/4567--SE Serietitel och serienummer ISSN Title of series, numbering _____
URL för elektronisk version http://www.control.isy.liu.se http://www.ep.liu.se		
Titel Title Modelling and Control of Friction Stir Welding in 5 cm thick Copper Canisters Författare Isak Nielsen Author		
Sammanfattning Abstract <p>Friction stir welding has become a popular forging technique used in many applications. The Swedish Nuclear Fuel and Waste Management Company (SKB) evaluates this method to seal the 5 cm thick copper canisters that will contain the spent nuclear fuel. To produce repetitive, high quality welds, the process must be controlled, and today a cascade controller is used to keep the desired stir zone temperature.</p> <p>In this thesis, the control system is extended to also include a plunge depth controller. Two different approaches are evaluated; the first attempt is a decentralized solution where the cascaded temperature controller is kept, and the second approach uses a non-linear model predictive controller for both depth and temperature. Suitable models have been derived and used to design the controllers; a simpler model for the decentralized control and a more extensive, full model used in the non-linear model predictive controller that relates all the important process variables.</p> <p>The two controller designs are compared according to important performance measures, and the achieved increase in performance with the more complex non-linear model predictive controller is evaluated. The non-linear model predictive controller has not been implemented on the real process. Hence, simulations of the closed loop systems using the full model have been used to compare and evaluate the control strategies.</p> <p>The decentralized controller has been implemented on the real system. Two welds have been made using plunge depth control with excellent experimental results, confirming that the decentralized controller design proposed in this thesis can be successfully used. Even though the controller manages to regulate the plunge depth with satisfying performance, simulations indicate that the non-linear model predictive controller achieves even better closed loop performance. This controller manages to compensate for the cross-connections between the process variables, and the resulting closed loop system is almost decoupled. Further research will reveal which control design that will finally be used.</p>		
Nyckelord Keywords Friction Stir Welding, Modeling, Control, Model predictive control, Depth control, Temperature control, Depth modeling		

Abstract

Friction stir welding has become a popular forging technique used in many applications. The Swedish Nuclear Fuel and Waste Management Company (SKB) evaluates this method to seal the 5 cm thick copper canisters that will contain the spent nuclear fuel. To produce repetitive, high quality welds, the process must be controlled, and today a cascade controller is used to keep the desired stir zone temperature.

In this thesis, the control system is extended to also include a plunge depth controller. Two different approaches are evaluated; the first attempt is a decentralized solution where the cascaded temperature controller is kept, and the second approach uses a non-linear model predictive controller for both depth and temperature. Suitable models have been derived and used to design the controllers; a simpler model for the decentralized control and a more extensive, full model used in the non-linear model predictive controller that relates all the important process variables.

The two controller designs are compared according to important performance measures, and the achieved increase in performance with the more complex non-linear model predictive controller is evaluated. The non-linear model predictive controller has not been implemented on the real process. Hence, simulations of the closed loop systems using the full model have been used to compare and evaluate the control strategies.

The decentralized controller has been implemented on the real system. Two welds have been made using plunge depth control with excellent experimental results, confirming that the decentralized controller design proposed in this thesis can be successfully used. Even though the controller manages to regulate the plunge depth with satisfying performance, simulations indicate that the non-linear model predictive controller achieves even better closed loop performance. This controller manages to compensate for the cross-connections between the process variables, and the resulting closed loop system is almost decoupled. Further research will reveal which control design that will finally be used.

Sammanfattning

”Friction stir welding” har blivit en populär svetsmetod inom många olika tillämpningar. På Svensk Kärnbränslehantering AB (SKB) undersöks möjligheten att använda metoden för att försegla de 5 cm tjocka kopparkapslarna som kommer innehålla det använda kärnbränslet. För att kunna producera repeterbara svetsar utav hög kvalitet krävs det att processen regleras. Idag löses detta med en temperaturregulator som reglerar svetszonens temperatur.

I detta examensarbete utökas styrsystemet med en regulator för svetsdjupet. Två olika lösningar har utvärderats; först en decentraliserad lösning där temperaturregulatorn behålls och sedan en lösning med en olinjär modellprediktiv reglering (MPC) som reglerar både djup och temperatur. Passande modeller har tagits fram och har använts för att designa regulatorerna; en enklare modell för den decentraliserade regulatorn och en utökad, komplett modell som används i den olinjära MPC:n och som beskriver alla viktiga variabler i processen.

Viktiga prestandamått har jämförts för de båda regulatorstrukturerna och även prestandaökningen med den olinjära MPC:n har utvärderats. Då denna regulator inte har implementerats på den verkliga processen har simuleringar av den kompletta modellen använts för att jämföra och utvärdera regulatorstrukturerna.

Den decentraliserade regulatorn har implementerats och testats på processen. Två svetsar har gjorts och de har givit utmärkta resultat, vilket visar att regulatorstrukturen som presenteras i rapporten fungerar bra för reglering av svetsdjupet. Trots att den implementerade regulatorn klarar av att reglera svetsdjupet med godkänt resultat, så visar simuleringar att den olinjära MPC:n ger ännu bättre reglerprestanda. Denna regulator kompenserar för korskopplingar i systemet och resulterar i ett slutet system som är nästan helt frikopplat. Ytterligare forskning kommer avgöra vilken av strategierna som kommer att användas i slutprodukten.

Acknowledgments

I would like to take the opportunity to express my gratitude to my examiner Prof. Alf Isaksson, my academic supervisor Lic. André Carvalho Bittencourt and my two industrial supervisors Dr. Lars Cederqvist and Lic. Olof Garpinger for their generous help, guidance and support. Their combined experience and competence regarding friction stir welding, modeling, system identification and design and implementation of control systems have made a major contribution to the completion of this thesis. I have always gotten professional, relevant and accurate feedback when discussing ideas and problems with them.

I also appreciate the help I received from Prof. John Hedengren at Brigham Young University, Provo, Utah, USA, regarding the modeling and optimization software APMONITOR. His extensive knowledge of this software and its algorithms has been very helpful. Without his generous help I would not have been using the user-friendly APMONITOR modeling language.

I would like to thank the Swedish Nuclear Fuel and Waste Management Company (SKB) for providing this interesting and challenging task for my Master Thesis. The task has been inspiring and demanded innovative solutions and the company has let me develop and test my own ideas, which I am most grateful for.

Also, Dr. Henrik Schmidt, HBS Engineering, Glostrup, Denmark, Lic. Peter Rosander, Division of Automatic Control, Linköping University and Dr. Larsgunnar Nilsson, Division of Solid Mechanics, Linköping University, have been helpful in their respective fields of interest.

Finally, I would thank my family for their support and for always believing in me.

Linköping, May Anno Domini 2012
Isak Nielsen

Contents

1	Introduction	3
1.1	Background	4
1.2	Related Work	4
1.3	Purpose	5
1.4	Scope	6
1.5	Methodology	6
1.6	Outline	6
2	Friction Stir Welding	9
2.1	Friction Stir Welding in General	9
2.2	Friction Stir Welding of Copper Canisters	10
2.2.1	Welding Equipment	11
2.2.2	Tool Geometry	12
2.2.3	Welding Sequences	12
2.2.4	Process Variables	14
2.2.5	Cascade Temperature Controller	15
2.2.6	Defects	16
3	Automatic Control	19
3.1	Open Loop Control	20

3.2	Closed Loop Control	21
3.3	Modeling	23
3.3.1	State Space Models	25
3.3.2	Transfer Functions	26
4	Modeling of Friction Stir Welding	29
4.1	Identification Experiments	30
4.2	Actuator	32
4.2.1	Oscillations	32
4.2.2	Dynamics	33
4.3	Sensors	34
4.3.1	Tool Position	35
4.3.2	Distance to Canister	36
4.4	Deflection	37
4.5	Thermal Expansion	39
4.6	Disturbances	41
4.7	Plunge Depth	41
4.7.1	Model I	41
4.7.2	Model II	44
4.8	Temperature	48
4.9	Torque	50
4.9.1	Friction	50
4.9.2	Spindle Torque	51
4.9.3	Complete Torque Model	53
4.10	Full Model	55
5	Controller Design & Comparison	61
5.1	Decentralized Controller I	61

Contents	xiii
5.1.1 Disturbance Suppression and Robustness	63
5.1.2 Reference Tracking	67
5.1.3 Comparison of PI and PID controllers	68
5.1.4 Discretization	70
5.1.5 Experimental Evaluation	71
5.2 Decentralized Controller II	74
5.2.1 Disturbance Suppression and Robustness	76
5.2.2 Reference Tracking	79
5.3 Non-linear Model Predictive Control	79
5.3.1 Optimization Problem	80
5.3.2 Controller Parameter Tuning	83
5.4 Comparison of Control Strategies	85
5.4.1 General Differences	87
5.4.2 Reference Tracking	87
5.4.3 Disturbance Suppression and Robustness	88
5.4.4 Violation of Bounds	91
5.4.5 Simplicity to Tune and Maintain	92
6 Results and Further Work	97
6.1 Results	97
6.2 Further Work	98
Bibliography	101

Acronyms

FEM	Finite element method
FFT	Fast fourier transform
FSW	Friction stir welding
IAE	Integrated absolute error
IMC	Internal model control
LP	Low-pass
LTI	Linear time-invariant
LVDT	Linear variable differential transformer
MIMO	Multiple-input-multiple-output
MPC	Model predictive control
NDT	Non-destructive testing
NLP	Non-linear programming
NMPC	Non-linear model predictive control
PI	Proportional-integral
PID	Proportional-integral-derivative
PRBS	Pseudo-random binary signal
SISO	Single-input-single-output
SKB	Svensk Kärnbränslehantering AB
TWI	The Welding Institute

Chapter 1

Introduction

The Swedish Nuclear Fuel and Waste Management Company (SKB) is responsible for the research and development of a long term storage solution for all radioactive waste from Swedish nuclear power plants. The final disposal consists of three barriers to ensure a high safety for humans and the environment, see Figure 1.1. The first barrier consists of a copper canister that encapsulates the nuclear fuel. The canisters are then placed in crystalline rock approximately 500 meters underground, SKB [27]. Bentonite clay is used to embed the canisters in the rock, and after disposal the tunnels and rock caverns are sealed. This long term storage must hold for about 100 000 years until the radioactivity has decayed to safe levels.

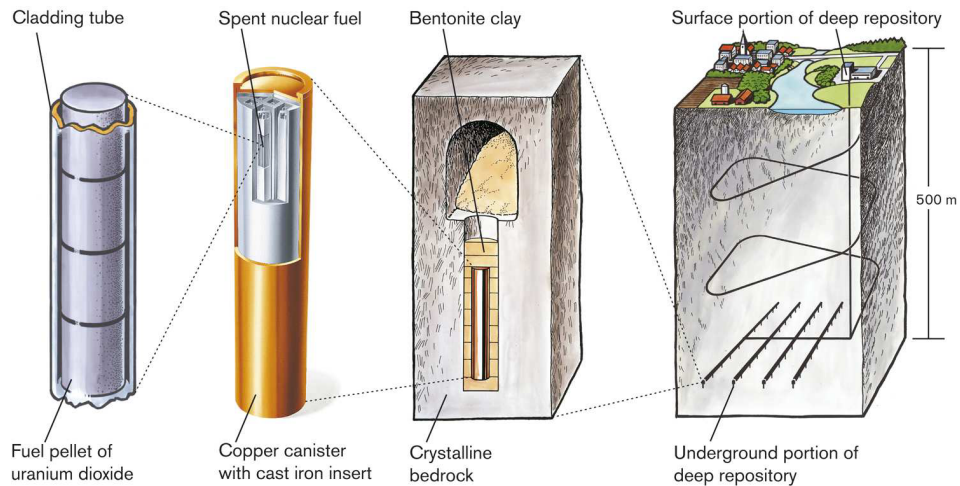


Figure 1.1. Schematic view of the planned storage of Sweden's spent nuclear waste. Three protective barriers ensure a high safety for human beings and the environment during 100 000 years.

The sealing of the nuclear waste containers has not yet started, but is in a research stage where suitable methods are investigated.

1.1 Background

A welding technique called friction stir welding (FSW) is currently under evaluation to be used to seal the copper canisters. This is a solid state joining method that was invented by The Welding Institute (TWI) in the early 90's, Thomas et al. [29]. Friction stir welding was chosen since it gives a more robust forging process than other methods, SKB [27], and Chapter 2 includes a detailed description of this method.

It is important that the sealing gives a solid corrosion barrier to fulfill the requirements from the authorities. It is crucial to keep the process in a window where there is a low risk of getting defects in the weld. Today, a feedback solution using a cascade controller keeps the stir zone temperature within the temperature range, but defects derived from the plunge depth of the welding tool have not yet been addressed. During welds, the tool is plunged into the copper with a constant axial force and due to variations in the process parameters, this will result in a non-constant plunge depth throughout the weld. This variation in depth may introduce hooking defects, see 2.2.6, which will reduce the corrosion barrier. To produce high quality repeatable defect free welds with the required corrosion barrier, a feedback solution where the plunge depth is controlled is thus needed.

1.2 Related Work

Much focus in the friction stir weld community regarding modeling and control have been related to the stir zone temperature, since this is an important process variable. There have been attempts of finding good models for simulating the heat generation and material flow using different software, e.g. Schmidt et al. [26], but these are computationally demanding and might not be useful in closed loop control.

Models that are used in closed loop control have been studied by several researchers e.g. Cederqvist et al. [2], Mayfield et al. [21] and Fehrenbacher et al. [8]. Common for these models are that they all consist of linear dynamic equations, and facilitating the control design based on those.

Research results regarding plunge depth modeling are more sparse. Mandal et al. [20] developed a numerical model using the constitutive temperature dependent Johnston-Cook law and simulations using Finite Element Method (FEM) with promising results. This type of models are however not useful in real-time control applications due to their computational complexity. In some FSW applications

with welding robots, position control of the tool is used, but this induces problems with compliance in the robots' linkages, Longhurst et al. [17]. An other research topic has been force control, since this is supposed to solve the problem with machine flexibility. The idea is that a constant force equals a constant depth, but this is not always true. Investigations on using torque as an indicator of plunge depth have been made by Longhurst et al. [18] and Lammlein et al. [15], and they state that torque is a better predictor of plunge depth than axial force.

1.3 Purpose

There are two main purposes with this thesis. The first one is to investigate the possibilities of using simple feedback control of the plunge depth, and second to verify the use of a more advanced controller structure called Non-linear Model Predictive Control (NMPC). The more advanced controller utilizes the cross-connections in the system to increase the performance.

Based on simulations, the performance gains achieved by using the advanced controller are evaluated. The criteria that are compared are

Reference tracking The performance for a change in reference is compared by looking at rise-time, settling-time and overshoot.

Robustness Robustness of the controller is important to get a control system that can handle modeling errors and disturbances. Simulations have been made for output disturbances and errors in the modeled gains.

Violation of bounds The bounds on states and control signals must not be violated during the weld. The NMPC can handle these bounds in the optimization, but the simple controller might sometimes calculate control signals that are out of these bounds.

Simplicity to maintain The controller will be used during several years while sealing approximately 12 000 lids, Cederqvist [5]. Hence, the controller will most probably be re-tuned some time in the future. It is thus desirable if the controller is intuitive and easy to tune for an operator with sparse knowledge in automatic control.

Besides the design and comparison of the two control structures, an evaluation of the sensors used to measure tool depth has been made. The investigation of the sensors was performed to realize which sensor is best to use in the feedback control loop.

1.4 Scope

The thesis is limited to the investigation of a simple plunge depth controller and a combined temperature and plunge depth controller. The controllers in this thesis are designed for the start and downward sequences, see 2.2.3. They are not tuned for use at the joint line, see 2.2.3.

All welds are made at SKB's Canister Laboratory in Oskarshamn and only the simple controller is implemented and tested on the real process. The more advanced NMPC is not possible to implement on the system with the current configuration. The comparison of the controllers are thus made through simulations. Further, the implementation of the simple controller is made by personnel from ESAB (the welding machine manufacturer).

The control signals available to use for the controllers in this thesis are merely reference signals to internal controllers in the machine. The tuning of these controllers should not be changed. The evaluation of the sensors are restricted to those which are currently available at SKB.

1.5 Methodology

The methodology used to solve the tasks of this thesis includes several steps. Data gathering has been made at SKB's location in Oskarshamn on their SuperStir welding machine. There are some inherent limitations in the welding machine that makes it hard to use advanced control signals and changes in references. The experiments have been designed given those limitations by the author together with the supervisors.

The next step has been to find a suitable model for the simple controller structure. This was done using linear models and the controller itself was designed using linear control theory.

Modeling for the advanced control structure uses a combination of empirical models and more fundamental modeling. This model has focused on capturing the most dominant cross-connections in the process. A software called APMONITOR, see [1], has been used to do parameter estimation of the non-linear models. APMONITOR has also been used to do the simulations of the two closed loop systems.

1.6 Outline

The report is divided into six chapters placed in logical order. There is a chapter dedicated to friction stir welding for readers with no or little knowledge of this

forging method. An introductory chapter on feedback control is also included to give the reader a brief overview of the concepts used in automatic control.

- 2. Friction Stir Welding** An overview of the friction stir welding process is given to introduce the basic concepts that are needed to understand the content of this thesis. In the beginning of the chapter, there is a section describing FSW in general, followed by a section that describes the use of FSW at the Swedish Nuclear Fuel and Waste Management Company. This section includes a description of the welding machine, the tool used, the process variables and some additional information of the process.
- 3. Automatic Control** The purpose of this chapter is to give the reader an overview of automatic control concepts and the ideas used by control engineers. The chapter introduces open and closed loop control, since it is important to understand the difference. Linear time-invariant systems will be described together with the use of transfer functions to represent them.
- 4. Modeling of Friction Stir Welding** Several models have been designed for different purposes and they are all presented in this chapter. There are two models derived for the plunge depth control, and one full model that is used in the non-linear model predictive controller.
- 5. Controller Design & Comparison** The two different controller structures are presented in this chapter. For the first approach, two different controller tunings are proposed. The chapter explains how the controllers have been designed and the last section is an evaluation and comparison of the two different controller structures. One of the controllers has been implemented and the experimental results are included in this chapter.
- 6. Results and Further Work** The results achieved in this thesis are summarized in this chapter. There is also a section with suggestions for further work that could be done to improve the plunge depth during the start and downward sequence. Additionally, some ideas regarding the control during the joint line is presented.

Chapter 2

Friction Stir Welding

The welding method was invented by The Welding Institute and patented in 1991, Thomas et al. [29]. It can be used to weld several different materials such as aluminum, copper and steel, Lohwasser et al. [16]. The technique is energy efficient and uses a non-consumable tool to combine pieces of material, Mishra et al. [22], and has become a popular technique for forging aluminum, Nandan et al. [23].

2.1 Friction Stir Welding in General

The main idea with FSW is to use a rotating tool that is plunged into the weld material and traversed along the joint line, see Figure 2.2. The rotating tool stirs the material and forges the work pieces without adding any additional material to the process. The weld material has to be hot enough to stir properly without getting defects, but the forging is done at temperatures below the melting temperature, making FSW a thermomechanical solid-state process. The heat needed to get the desired temperature of the stir zone is produced by frictional heat between the tool and the material together with heat generated by plastic deformation, Nandan et al. [23].

Since the actual forging of the materials are made with the tool, its geometry is one of the most important process parameters; it is critical to the behaviour of the material flow around the tool, Mishra et al. [22]. The basic geometry consists of a pin (sometimes called probe) and a shoulder, and the schematic configuration of the tool is visible in Figure 2.1. A common choice is to use a concave shoulder and a threaded pin, Mishra et al. [22] but other geometries are also used (see more in Section 2.2). The shoulder has two main purposes, first it generates heat input to the stir zone, Schmidt et al. [26], and second it applies pressure on the heated material. The applied pressure reduces the amount of material escaping the stir

zone. The shoulder also prevents formation of wormhole defects (see Section 2.2.6 for more information).

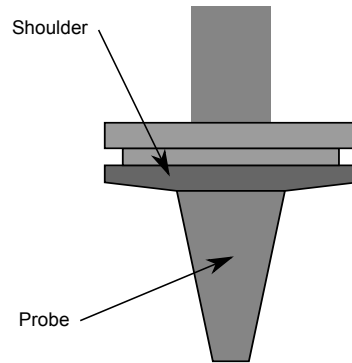


Figure 2.1. A schematic view of the tool used in friction stir welding. It consists of a shoulder and a probe that heats and stirs the material.

Since the tool rotates and is traversed, the material flow around the tool is not symmetric. The side where the rotation of the tool is in the same direction as the traverse speed is called the *advancing side*, whereas the side where the tool rotation is in the opposite direction is called the *retreating side*, see Figure 2.2.

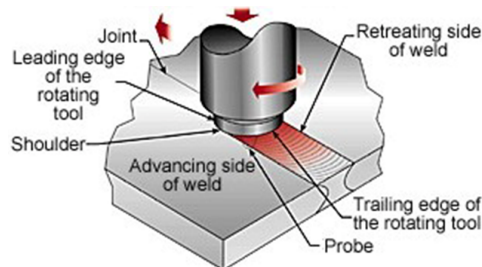


Figure 2.2. A figure from TWI depicting the tool and work piece configuration in a common FSW application. The tool is plunged into the material and traversed along the joint line. The material flow is not symmetric due to the traverse direction and the direction of the rotation of the tool.

2.2 Friction Stir Welding of Copper Canisters

SKB investigates the use of FSW to seal the copper canisters that will be used to encapsulate nuclear waste. The canisters consist of a tube made of 50 mm thick copper with an outer diameter of 1050 mm (1060 at the joint line) and a lid.

The canisters are 5 m high and weigh between 25 and 27 tonnes when filled with nuclear waste.

After every circumferential weld, the joint line will be examined using non-destructive testing (NDT). This test uses radiographic and ultrasonic testing to find deformations in the weld, see Figure 2.3 for a schematic view. The NDT performance increases when the sensors are closer to the actual weld, and hence some material will be machined off on the top of the lid and along the joint line (so the diameter is 1050 mm all over the tube).

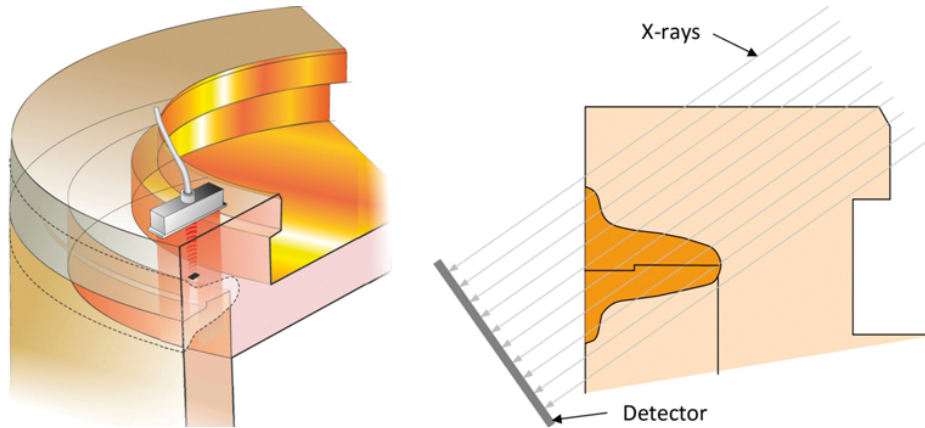


Figure 2.3. Schematic view of the non-destructive testing that will be performed after every full circumferential weld. The test is capable of detecting the defects that can occur during a weld.

2.2.1 Welding Equipment

The weld is performed by a SuperStir welding machine that was delivered by ESAB in Laxå in 2003. Figure 2.4 shows the machine with a canister mounted in weld position.

The canister is clamped into position by twelve clamps positioned around the tube with a combined force of 3200 kN, and the lid is clamped with a force of 390 kN distributed on the top of the canister. When the canister is properly clamped, a pilot hole is drilled and conically shaped to decrease the tool wear, Cederqvist [5], and the canister is ready for the welding sequences, described in Section 2.2.3.

During the circumferential weld, an argon gas chamber is used for shielding. It consists of several chambers, that embed the tool and welded sections, which are filled with argon. The argon gas reduces the shoulder wear and oxidation of the welded surfaces, Cederqvist et al. [3]. The use of argon shielding also decreases the variations in spindle torque, Cederqvist et al. [2].



Figure 2.4. The SuperStir friction weld machine is stationed at the Canister Laboratory in Oskarshamn. The machine was delivered by ESAB in 2003. In the centre of the machine, a copper canister is clamped into welding position.

2.2.2 Tool Geometry

The tool that is used to seal the copper canisters consists of a conical shaped probe and a convex scroll shoulder. The use of a convex shoulder instead of a concave was investigated by Cederqvist et al. [4]. The conclusion was that a convex scroll shoulder gave a more robust process with less variations in tool temperature and depth. The tool is shown in Figure 2.5.

The shoulder has an outer diameter of 70 mm while the conical probe has a base diameter of 30 mm and a tip diameter of approximately 7 mm. The length of the probe is around 50 mm, but the final length is still under investigation.

2.2.3 Welding Sequences

A full circumferential weld consists of five different stages, presented below. Figure 2.6 displays the different sequences and the numbers in the figure will be used to explain the weld stages.

1. **Dwell** During the initial plunging, the tool does not traverse. The tool has a constant rotation speed and axial force. The dwell sequence ends when



Figure 2.5. The tool that is used at SKB consists of a conically shaped probe and a convex scrolled shoulder. The diameter of the shoulder is 70 mm and the length of the probe is approximately 50 mm.

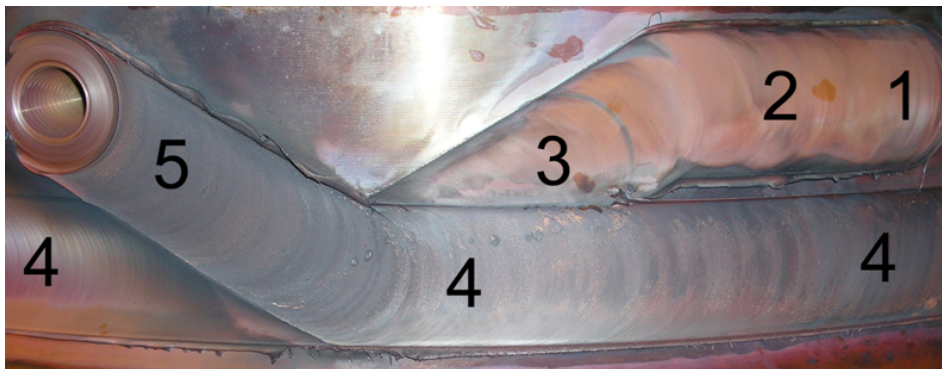


Figure 2.6. The five different weld stages: 1. Dwell, 2. Start, 3. Downward, 4. Joint line and 5. Parking.

a certain tool temperature where the tool can traverse without excessive stresses in the probe is reached.

2. **Start** The tool starts to traverse and accelerates to the welding speed. During the start sequence, the stir zone temperature is increased until a certain value is reached.
3. **Downward** The purpose of the downward sequence is to traverse the tool downwards to the joint line 75 mm below the start sequence.
4. **Joint line** When the tool reaches the joint line, the tool temperature is within the process window and the actual forging of the tube and lid starts. The

joint line sequence is a 360° weld and the figure only shows the start and end of the circumferential weld. When the whole joint line is forged, the parking sequence is initiated.

5. **Parking** The final sequence is the parking sequence. The tool starts to traverse upwards to move away from the joint line. When the tool is clear from the joint line, the weld is stopped and the tool is extracted from the material.

One reason for having different stages is because the process variables have to be within the process window during the weld at the joint line, hence it is not advisable to start the plunging there. Since the pilot hole is drilled in the lid (in the area which is machined off after the weld), it is possible to abort the weld if some error appears in the beginning of the weld before the joint line has been reached. Another weld can then be started in the same tube and lid without having to remove the nuclear waste and switch to a new canister.

2.2.4 Process Variables

Mayfield et al. [21] determines that there are three axes in friction stir welding, each with an effort and a flow. Either the effort or the flow can be chosen for every axis, and the other one is then given by the process. In SKB's application, the axial force acting on the tool (F_z), the spindle rotation rate (ω) and the tool traverse speed (v_w) are defined as manipulated variables. The dual variables tool depth (P_z), spindle torque ($M_{spindle}$) and the traverse force (F_t) are then given by the process. Besides those, the stir zone temperature (T) and power input (P) are very important process variables.

The manipulated variables are visualized in Figure 2.7, with tool rotation rate as number 1, tool traverse speed as number 2 and axial force as number 3.

It is preferred to keep the weld speed at a constant value, since relatively small changes in weld speed could decrease the process window significantly. Based on this, the weld speed is held constant at 86 mm/min during the full weld and the traverse force will fluctuate to keep this speed.

The two remaining manipulated variables, axial force (F_z) and spindle rotation rate (ω) are used to affect the process variables tool depth (P_z) and stir zone temperature (T). The torque will get the value that corresponds to a certain set of manipulated variables and controlled variables. Figure 2.8 shows a block diagram of the manipulated variables that can be used together with the most important process response output variables.

The process window for the stir zone temperature has a lower bound of $790^\circ C$ and an upper bound of $910^\circ C$. If the temperature is lower, there is an increased risk of wormhole formation (see Section 2.2.6) and at higher temperatures there is a great risk of tool breakage. The commanded axial force must be held within

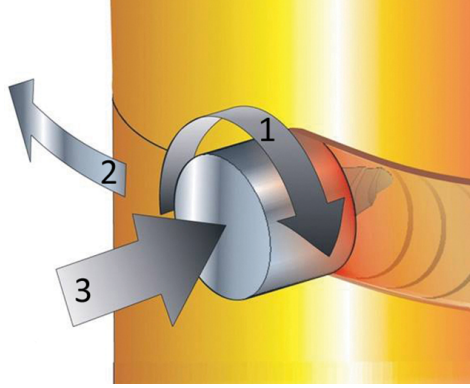


Figure 2.7. Manipulated variables in SKB's FSW application: 1. Tool rotation rate, 2. Traverse speed and 3. Axial force acting on the tool. The traverse speed is held constant throughout the whole weld.

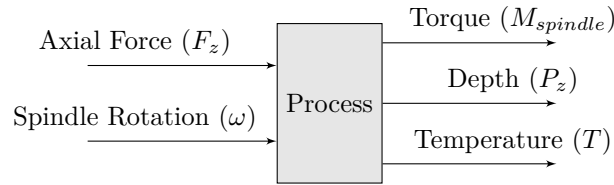


Figure 2.8. Block diagram of the process' manipulated variables axial force (F_z) and spindle rotation speed (ω) together with the important process response variables tool depth (P_z), spindle torque ($M_{spindle}$) and stir zone temperature (T).

the process window given by a lower bound on approximately 77 kN and an upper bound of approximately 91 kN. The lower bound is due to uncertainties in the relation between the temperature process window and axial force. The effects of too low force have not been evaluated, and thus this lower bound should not be violated. Excessively high axial forces will increase the risk of getting deep welds that are hard to recover from. Those limits are however not completely fixed, but further research will be made to find the best limits.

2.2.5 Cascade Temperature Controller

The stir zone temperature is controlled using a cascade controller (not designed by the thesis' author). The fast inner loop controls the power input to the process, whilst the outer, slower, loop controls the temperature. The outer loop thus calculates the required power, which is reference value to the inner loop. The stir zone temperature cannot be measured directly but is approximated with measurements from a thermo-couple placed inside the probe. This control structure is very useful when there are fast non-linear torque disturbances and slower disturbances

in temperature, Cederqvist et al. [2]. Figure 2.9 shows the schematic view of the cascaded temperature controller. Here G_P represents the process relating spindle rotation speed and power input, while G_T represents the relation between power input and temperature.

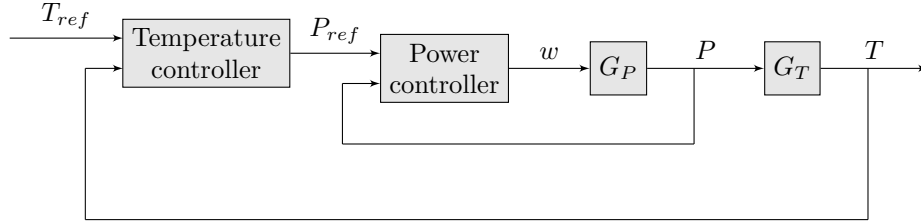


Figure 2.9. Schematic picture of the cascaded temperature controller. The inner loop controls the required power input to the process, while the outer loop controls the tool temperature. This controller was implemented before the work of this thesis started.

2.2.6 Defects

Defects in the weld will decrease the corrosion barrier, and if the defects are too severe the canister might have to be re-opened, which is very expensive. It is thus important to know what defects can appear and how to avoid them. There are two defects that have a major impact on the corrosion barrier; one is closely related to the stir zone temperature and the other one to the plunge depth.

A defect called *wormhole* can occur if the temperature of the stir zone is below the process window, and they are formed mainly on the advancing side of the tool, Cederqvist [5]. Figure 2.10 shows an example of a wormhole. This kind of defect can be avoided by keeping the weld in the process window for the temperature during the whole weld, and this is achieved with the cascade controller used today.

The other defect is called *hooking* and the main reason to the creation of this kind of defect is the plunge depth. Hooking is created at the interface between the tube and the lid (see Figure 2.11). If the tool is plunged too shallow into the material, then the joint line will not be forged all the way into the lid, leaving a gap in the corrosion barrier. If the plunge depth on the other hand is too deep, then there is a greater risk that the interface (on the back side of the tube) is bent outwards (due to material flow) and thus decreasing the corrosion barrier. This type of hooking is worse than the one where a piece of the joint line is not forged since it is difficult to determine where the hooking ends via NDT. Hence, it is important to be in control of how deep the tool is plunged into the material.

Besides those two defects, an unwanted blemish is the so-called flash. Flash is created when the shoulder plunges too deep into the copper and material from the stir zone is forced outwards. Hence, it is important to keep a shoulder depth



Figure 2.10. A massive wormhole formed due to a low stir zone temperature. This defect decreases the corrosion barrier that the canister should provide and may lead to re-opening of the canister.

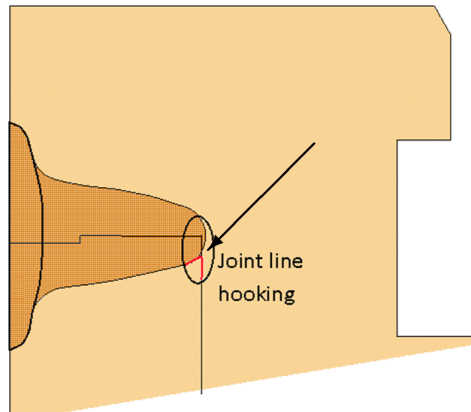


Figure 2.11. Joint line hooking is formed when the interface between the tube and the lid is moved outwards by the material flow induced by the tool. This defect can be formed when the tool is plunged too deep into the material.

that is large enough to produce welds without decreasing the temperature process window but at the same time small enough to avoid unnecessary flash formation. Figure 2.12 shows an example where excessive flash has been formed. Flash formation during the downward sequence will induce disturbances in depth and torque when the circumferential weld overlaps the flash in the end of the weld. This makes flash highly unwanted and should therefore be avoided if possible.

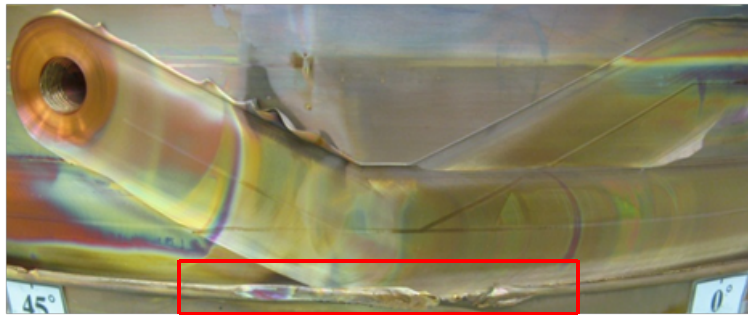


Figure 2.12. Extensive flash formation on the advancing side of the weld (the red box) due to excessive plunge depth.

Chapter 3

Automatic Control

The objective of automatic control is to manipulate the behaviour of a process according to a certain objective. A control law is a rule that determines how the system should be manipulated to achieve the objectives. This is an extensive field of research and there are a lot of different methods to design those rules in a suitable way.

The unit that calculates the control signals is often referred to as the *controller*, and the physical process that is controlled is called the *process* or the *system*. The process is manipulated via the *control signals* (u) and the process *outputs* (y) are measured. Very often there are *disturbances* (d) acting on the process. These can be seen as input signals that cannot be affected by the control system and can be measurable or non-measurable.

A *block diagram* of a process is shown in Figure 3.1. The use of block diagrams are common in automatic control and they give a visual picture of the components in the system. The arrows correspond to the flow of the signals, meaning that u and d affect the process, while y is produced by the process. The control system is often designed to suppress the influence of disturbances but at the same time keep the output variable y at a given reference r . The reference is the desired value of the output from the process, and is also called setpoint.

To describe the process, some kind of model is needed. A model describes the behaviour of the process, see Section 3.3. There are a lot of ways to model a process and the modeling technique may depend on the nature of the system and the performance requirements on the control system. The model is used to find a suitable controller with the desired properties (if possible).

Automatic control of the process given in Figure 3.1 can be made in two different ways; open loop control or closed loop control. It is of fundamental importance to understand the differences between the two methods when designing a control

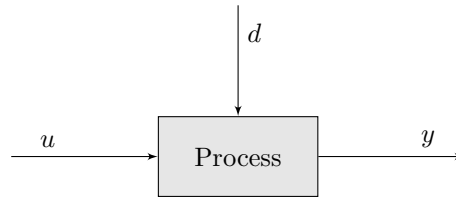


Figure 3.1. Block diagram of a process and its control signals (u), disturbances (d) and measured outputs (y). The arrows determine if the signal affects or is affected by the process. Here u and d affects the process while y is a process response.

system. Both approaches have drawbacks that must be taken into consideration to achieve satisfactory control performance.

Readers with no, or little, experience in automatic control are referred to basic control literature, e.g. Glad & Ljung [13] (in Swedish), Dorf & Bishop [7] and Ogata [24].

3.1 Open Loop Control

When a process is controlled with an open loop controller, the control signal is computed *without* any information of the real system's current state. In Figure 3.2 the block diagram for open loop control is shown. In this setting the controller calculates the control signal using only the reference signal (r) given by the operator.

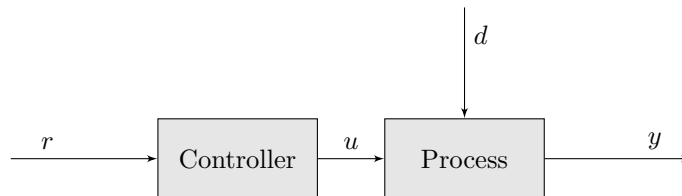


Figure 3.2. Block diagram of open loop control of a process. The controller calculates the control signal (u) using no real time information of the system. The process is also affected by disturbances (d) and the output is the variable that is controlled (y). The goal is to keep the output equal to the reference (r).

Open loop control demands an accurate model that describes the system's dynamic and static behaviour. The controller must know how to calculate the control signal given just the reference that the output should track. If the process is subjected to non-measurable disturbances, there are no chances to compensate for those. This makes open loop control quite tricky to use unless there are really good models of the process and the disturbances acting on it, or the specifications of control

performance are low. In Example 3.1, a tank is controlled in open loop, and the influence of a non-measurable disturbance is addressed.

Example 3.1

A water tank with an inflow $u(t)$ and an outflow $v(t)$ is depicted in Figure 3.3. The inflow is controlled by a controller and the level $y(t)$ should be kept at the reference level $r(t)$. In the bottom of the tank, there is an extra valve with flow $d(t)$, and the controller has no information of the state of this valve.

Figure 3.5 shows a simulation of a tank controlled with an open loop controller (the red line). If $d(t) = 0$, then the control signal $u(t) = 1$ gives $r(t) = y(t) = 1$ in steady state. When the valve is opened at 20 seconds, giving $d(t) = 0.2$, the controller still calculates the control signal $u(t) = 1$ and does not compensate for the extra outflow. The level $y(t)$ thus decreases to a value below $r(t)$, without the controller sensing this deviation from the reference.

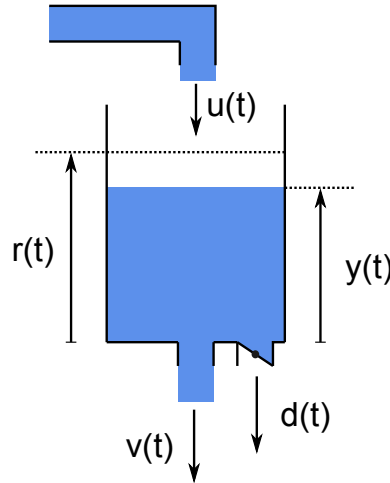


Figure 3.3. A tank system with inflow $u(t)$ and outflow $v(t)$. The level of the tank is $y(t)$ and the reference level is $r(t)$. A valve can be opened generating the extra outflow $d(t)$. The controller should keep the water level at the reference level, i.e. $y(t) = r(t)$.

3.2 Closed Loop Control

In contrast to open loop control, closed loop control (or feedback control) uses real time information about the process to calculate the control signal. The controller

uses measurements of the output from the process and hence it gets *feedback* of the output it is controlling. Figure 3.4 shows the principle configuration of a closed loop control system.

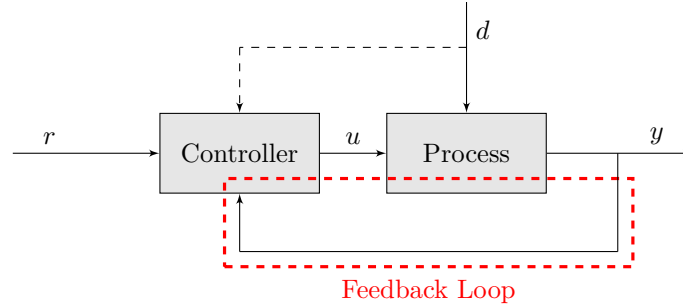


Figure 3.4. Block diagram of the closed loop control system. The controller gets feedback from the measured output (y) and uses this information to calculate a control signal (u) that makes the output track the reference signal (r). If the disturbances (d) are measurable, those could also be used by the controller.

Since the outputs are measured and fed back to the controller, the demands on the model accuracy are significantly decreased. The controller gets information of the output and it is thus possible to compensate for disturbances and modelling errors. Hence, a satisfactory performance can be achieved even if the model is not very accurate as in the case for open loop. In Example 3.2, the tank example is extended to closed loop control. The unknown outflow $d(t)$ is now compensated for.

Example 3.2

Consider again the tank system in Figure 3.3 and the simulation in Figure 3.5. Now suppose that a sensor is added to measure the water level $y(t)$ in the tank. This measurement is used in the feedback loop to the controller. When the extra valve is closed, i.e. $d(t) = 0$, then the closed loop controller calculates the same steady state control signal $u(t) = 1$ to keep the level at $y(t) = 1$.

When the valve is opened after 20 seconds, giving $d(t) = 0.2$, without the controller knowing it, the level of the tank starts to decrease. In opposite to the open loop controller, the closed loop controller however notices the decreasing water level via the measurements and compensates for the disturbance outflow by increasing the control signal to $u(t) = 1.2$ in steady state. In this example, the disturbance is fully compensated and the steady state inflow and outflows are the same.

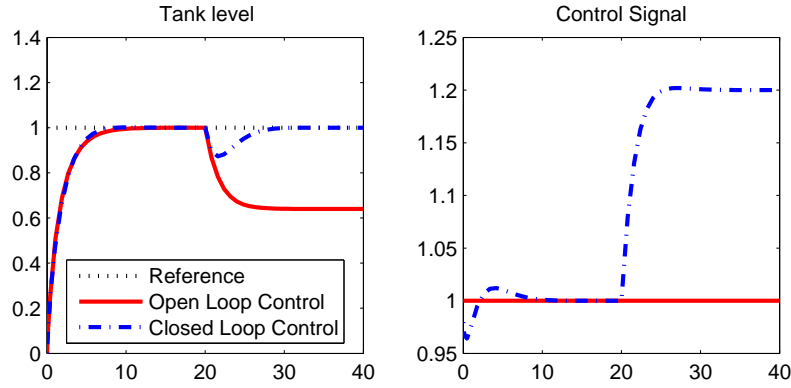


Figure 3.5. Simulation of the tank example using open and closed loop control. The reference level is $r(t) = 1$ and the corresponding control signal is $u(t) = 1$. At time 20 seconds, a disturbance $d(t) = 0.2$ is applied. The closed loop solution manages to compensate for this disturbance.

To get feedback from the system, sensors must be added, and this causes other problems that need to be addressed. It is important that the feedback sensor measures the output without too much measurement noise and bias. The result of a bad sensor might be that the controller drives the system to an undesired state.

3.3 Modeling

A model of a process is a set of rules that describes how the process will react to disturbances and control signals. Depending on the application, different levels of modeling are needed. If the model is used for simulation or open loop control of a process, then it must describe the process very well. On the other hand, if the model is used in feedback control, then the demands on the model are relaxed. It is important to choose a model that is suitable for the application; if it is too simple, then the performance of the simulation, control etcetera may be low. If it is unnecessarily complex, then it may be computationally demanding which can make real time control impossible.

The model could be focused on modeling the dynamics of the process, or it could be a static model or a combination of these. A static model describes the relationship of the process variables at some time point t (depending only on this time instance), while a dynamic model is also dependent on previous time points.

Process modeling is often based on physical relations that describe the system, and this approach will be used to find models for an example system. The examples illustrate and explain the basic concepts introduced in this section.

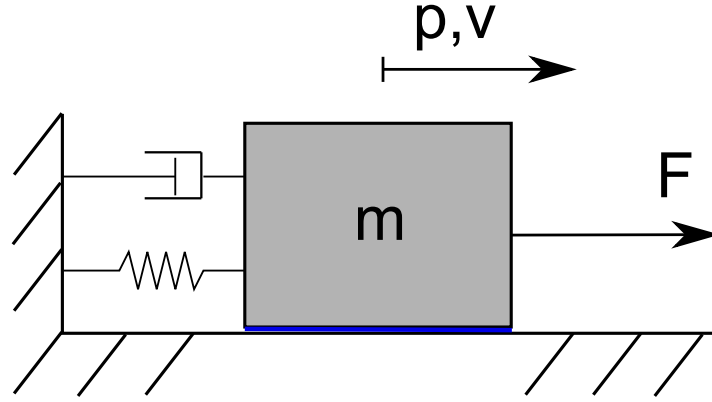


Figure 3.6. A box with mass m is sliding without friction. The box is connected to terra firma by a dashpot and spring element. An external force F is exerted on the box. The position measured from the equilibrium is p and the velocity is v .

Example 3.3

Figure 3.6 illustrates a rigid-body with mass m sliding without friction on a surface. The box is connected to terra firma by a spring and a damper, and a force F is exerted onto the box. The position deviation from the equilibrium (where the body is positioned when $F = 0$) is called p and the speed is v . The force exerted by the spring is a function of the position, $k(p)$, and the force from the damper is a function of velocity, $b(v)$. The motion of the sliding box is subjected to Newton's laws of motion, giving

$$\begin{aligned} m \cdot \ddot{p} &= F - k(p) - b(v) = \{\dot{p} = v\} = F - k(p) - b(\dot{p}) \iff \\ m \cdot \ddot{p} + b(\dot{p}) + k(p) &= F, \end{aligned} \quad (3.1)$$

which is a second order non-linear differential equation in p .

The differential equation obtained in Example 3.3 is a *non-linear model* of the position of the box, and given the initial position, initial velocity and the external force F , future positions can be calculated. If the functions k and b are linear, then the differential equation is linear, giving a *linear model* of the position. Further, if the model is not changing over time, then the model is time-invariant. For such systems (with given initial conditions), a control signal applied at time t_0 will give the same output as it would if applied at time t_1 (but time shifted). A system having both linear differential equation and time-invariance is called a Linear Time-Invariant (LTI) system. These have nice properties that make it easier to investigate certain issues of the controller (e.g. robustness and stability).

3.3.1 State Space Models

For a general system, a *state space model* is a set of connected first order differential equations and is often written

$$\begin{aligned}\dot{x} &= f(x, u) \\ y &= h(x, u),\end{aligned}$$

where x is an n -dimensional state vector, u is an m -dimensional input signal vector, y is a p -dimensional output signal vector, $f(x, u)$ is an $\mathbb{R}^{n \times m} \rightarrow \mathbb{R}^n$ function describing the dynamics and $h(x, u)$ is an $\mathbb{R}^{n \times m} \rightarrow \mathbb{R}^p$ function connecting the states to the output variables. n is referred to as the system's *order* (an n :th order differential equation requires at least n states). If $m = 1$ and $p = 1$, i.e. one input signal and one output signal, then the system is called a single-input-single-output system (SISO-system), whilst systems with $m > 1$ and $p > 1$ are called multiple-input-multiple-output-systems (MIMO-systems).

If the differential equations are linear, then a linear state space model could be derived, giving

$$\begin{aligned}\dot{x} &= Ax + Bu \\ y &= Cx + Du,\end{aligned}$$

where A , B , C and D are real matrices of appropriate dimensions. A non-linear system can often be *linearized* around some setpoint x_0 and is then described by a linear model close to this point. The linearization can be made using Taylor series expansions of $f(x, u)$ and $h(x, u)$. Around this setpoint, the validity of the model is good, but the model accuracy decreases further away. Depending on the system, the neighbourhood where the linear model is accurate can vary a lot.

Example 3.4

The second order differential equation (3.1) could be re-written as a system of first order differential equations. Introducing the *states* $x = (x_1 \ x_2)^T$, where

$$\begin{cases} x_1 = p \\ x_2 = v = \dot{p}, \end{cases}$$

gives the system of first order differential equations

$$\begin{aligned}\dot{x}_1 &= x_2 \\ \dot{x}_2 &= \frac{1}{m} (-k(x_1) - b(x_2) + F),\end{aligned}$$

where the position is given by $p = x_1$. This is one realisation of a state space model of the system in Example 3.3.

3.3.2 Transfer Functions

If the differential equation describing the system is linear (and time-invariant), then there is yet another way to describe the dynamics of the system. These models are widely used in control theory and are based on the Laplace operator (\mathcal{L}). This operator relates the differential equation in the time-domain with a complex rational function in the transformed domain.

A linear differential equation can be written (y and u are scalar)

$$y^{(n)} + a_1 y^{(n-1)} + \dots + a_n y = b_0 u^{(m)} + b_1 u^{(m-1)} + \dots + b_m u.$$

Assuming that all initial conditions are zero (the system is energy-free) and applying the Laplace operator on both sides of the equality sign gives

$$(s^n + a_1 s^{n-1} + \dots + a_n) Y(s) = (b_0 s^m + b_1 s^{m-1} + \dots + b_m) U(s),$$

where $Y(s)$ is the Laplace transform of the output signal and $U(s)$ is the Laplace transform of the input signal. The linearity of the Laplace operator and the fact that $\mathcal{L}(\dot{y}) = sY(s) - y(0) = sY(s)$ has been used here. The ratio of the output signal and the input signal in the Laplace domain (when the initial conditions are zero) is defined as the *transfer function* of the system (denoted $G(s)$). The relation is thus

$$G(s) = \frac{Y(s)}{U(s)} = \frac{b_0 s^m + b_1 s^{m-1} + \dots + b_m}{s^n + a_1 s^{n-1} + \dots + a_n},$$

and all realisable systems must have a *proper* transfer function, meaning that $m \leq n$.

Example 3.5

If the functions in Example 3.3 are linear ($k(p) = k \cdot p$ and $b(\dot{p}) = b \cdot \dot{p}$), then the linear differential equation is

$$m \cdot \ddot{p} + b \cdot \dot{p} + k \cdot p = F.$$

The transfer function relating the force F to the position p is

$$G(s) = \frac{\frac{1}{m}}{s^2 + \frac{b}{m}s + \frac{k}{m}}.$$

For a linear MIMO-system, there is a transfer matrix with a transfer function for every pair of input-output signal combination. For a system with two scalar inputs

(u_1 and u_2) and two scalar outputs (y_1 and y_2), the transfer function matrix has dimensions 2×2 and the structure is

$$\begin{bmatrix} Y_1(s) \\ Y_2(s) \end{bmatrix} = \underbrace{\begin{bmatrix} G_{11}(s) & G_{12}(s) \\ G_{21}(s) & G_{22}(s) \end{bmatrix}}_{G(s)} \begin{bmatrix} U_1(s) \\ U_2(s) \end{bmatrix},$$

where $G_{11}(s)$ is the transfer function from $U_1(s)$ to $Y_1(s)$, $G_{12}(s)$ from $U_2(s)$ to $Y_1(s)$ and so forth. If $G(s)$ is diagonal, then the system is decoupled and there are no cross-connections between the inputs and the outputs in the system (i.e. one input is affecting only one output). Further, the Laplace-transform of a time delayed signal $\bar{y}(t) = y(t - \tau)$ is given by

$$\bar{Y}(s) = Y(s) \cdot e^{-\tau \cdot s},$$

which allows models including dead time.

Chapter 4

Modeling of Friction Stir Welding

When designing a control system, some model of the process is often required. The model should describe the relations between the variables relevant to the controller, and the accuracy of the model is dependent on (among other) the desired control performance. This chapter presents three models; two linear SISO-models relating the axial force and the plunge depth, and one full model including also the important process variables stir zone temperature and torque. The linear SISO-models are used to design the decentralized controller, whilst the full model is used in the NMPC-structure. Since the controllers proposed in this thesis are designed to operate during the start and downward sequences, see 2.2.3, the modeling will focus on describing the process during this phase of the weld.

The full model has been divided into three sub-models that interact via cross-connections between the variables; a depth model, a temperature model and a torque model. In this approach, the depth is dependent on axial force and stir zone temperature, whilst the temperature in turn is dependent on torque and rotation speed. There are two slightly different torque models where one is dependent on plunge depth and axial force and the second includes a dependency on rotation speed as well. An evaluation of these two models is made but it is not determined which one is the best.

To display the physical relationships of the sensors, actuators and parts mentioned in this chapter, a schematic overview of the system set-up is given in Figure 4.1. The system consists of two different sensors for depth measurements, the spindle, the tool, the canister and the force actuator. The two different sensors are measuring different distances (depicted in the figure) and it is important to notice and understand the difference between these two measurements.

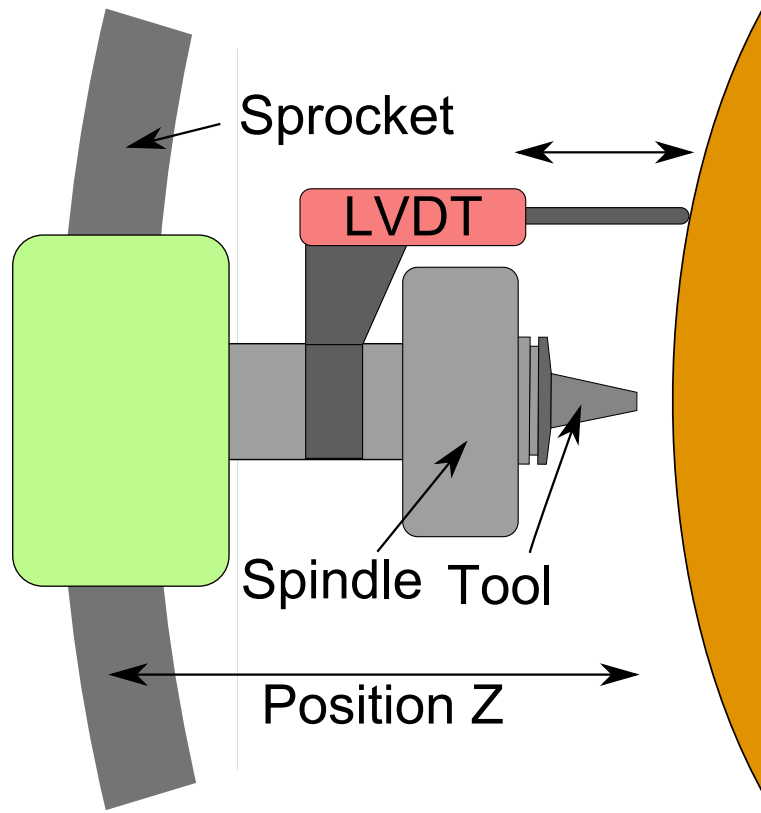


Figure 4.1. A schematic view of the physical connections in the system. The LVDT-sensor is measuring the distance from the tool to the canister surface, whilst the position sensor is measuring the tool position relative the sprocket. The force actuator (the green box) exerts a force that pushes the tool towards the canister.

The measurements from the tool position sensor is a composition of mainly three components; plunge depth (see Section 4.7), deflection (see Section 4.4) and thermal expansion (see Section 4.5). Figure 4.2 illustrates the logical connection between these three parts.

4.1 Identification Experiments

Experiments to gather data for the linear depth models have been performed in the lid with the cascade controller active. The identification experiments consist of steps and pseudo-random binary sequences (PRBS) which are input to the axial force command, and the process variables are measured. These are quite simple

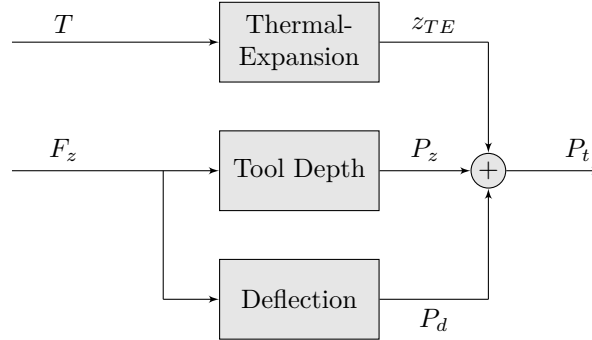


Figure 4.2. Block diagram of the three components in the position measurement. The thermal expansion is dependent on temperature whilst the other two are dependent on axial force.

experiments, but the current implementation of the control system prevents the use of more advanced control signals like e.g. sums of sinusoidal terms or chirp signals.

The step changes have been applied manually after the process has reached a steady-state behaviour. The amplitude of the steps and the values of the forces when the steps are applied have been changed to get data from different points in the process' state space. Gathering data from different parts of the process window makes it possible to evaluate if the process responses changes within this.

The settings of the PRBS have been chosen such that the frequency content in the signal is approximately the same as the bandwidth of the system. If it is much higher, then the process will attenuate the signal, and if it is much lower then the signal will not excite the system enough. Figure 4.3 shows one of the signals used in the experiments. Since the PRBS have been applied manually, the applied signals are approximations of PRBS-signals.

The data have been divided into estimation and validation data sets. The estimation sets have been used to identify the model parameters, whereas the validation data sets are used to validate the models. All linear models in this chapter have been estimated using Grey-box and process models in SYSTEM IDENTIFICATION TOOLBOX in MATLAB.

Data for the full model have been gathered without the cascaded controller, since this should not be used in the NMPC-approach. Step changes have been applied to the manipulated variables (spindle rotation speed and axial force command) and the responses were logged and saved. These data sets were divided into disjoint validation and estimation sets. The parameters in the full model have partly been estimated using SYSTEM IDENTIFICATION TOOLBOX, but parameters in the non-linear parts of the model have been estimated using the software APMONITOR.

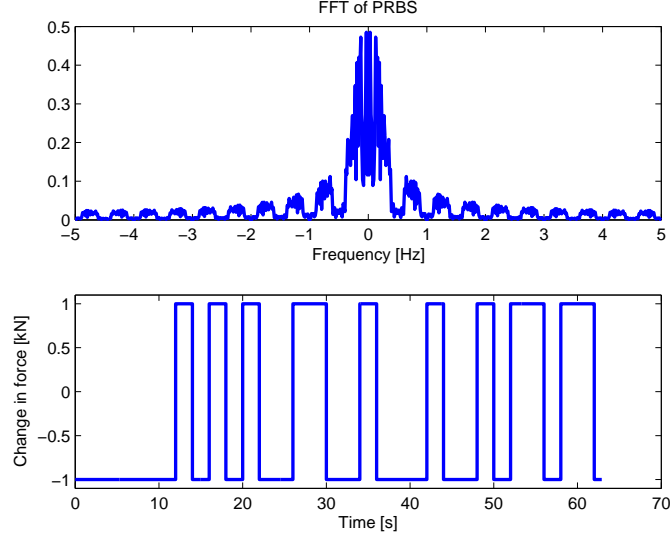


Figure 4.3. A PRBS used in an identification experiment. The upper subplot is the fast fourier transform (FFT) of the signal, showing the frequency content. The lower subplot is the signal in the time domain.

4.2 Actuator

The actuator that applies axial force on the tool consists of a hydraulic cylinder and a P-controller in a feedback loop. The use of a P-controller results in a force that is just below the commanded force. The force contains oscillations that most probably stem from backlash in the hydraulic cylinder. The oscillations have an amplitude of approximately 2.8 kN and these oscillations are propagated to other process variables such as torque and weld depth. This internal P-controller is not re-tuned in the thesis.

4.2.1 Oscillations

The oscillations have been investigated using FFT of the measured axial force, and the frequencies have been studied for different values of the commanded axial force within the process window. The result is seen in Figure 4.4 where the frequencies are in the set $\Omega_{osc} = [1.715 \text{ Hz}, 1.775 \text{ Hz}]$ with a mean of 1.74 Hz . There is no further investigation of the origin of the oscillations or means to prevent them. The measured axial forces can be recreated well by the equations for the dynamic response together with an additive sinusoidal with a frequency in the experimentally derived set Ω_{osc} . In this thesis, the frequency $f_{osc} = 1.74 \text{ Hz}$ is used throughout simulations. However, one should note that the oscillations are

not an additive disturbance in reality, but just modeled as one. This makes it possible to simulate the measured forces.

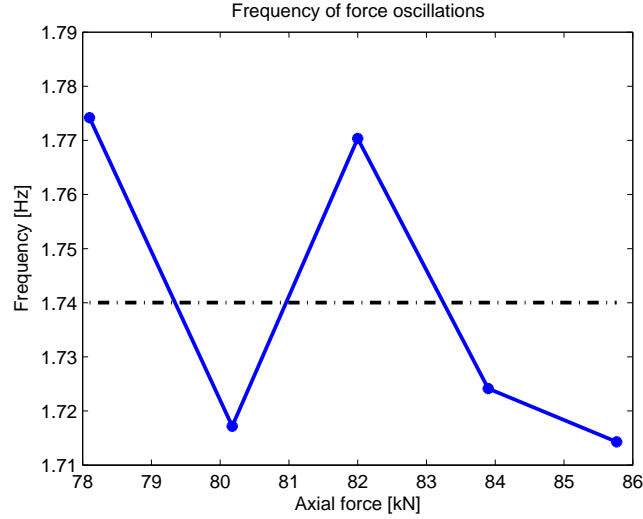


Figure 4.4. Measured frequencies for different commanded axial forces. The frequency has a small deviation from the measured mean of 1.74 Hz.

4.2.2 Dynamics

The linearized dynamic behaviour of the axial force can be described by a low order linear system with dead time. A simpler model is preferred over a high order model if the dynamics are modeled equally well. The validation of the first and second order model with damped poles and dead time are seen in Figure 4.5, where an added sinusoidal with amplitude 2.8 kN and frequency 1.74 Hz is used to model the oscillations. The simulated responses are almost the same and they both get just above 11% fit (without the sinusoidal), and the low order models capture the dynamics of the mean of the oscillations.

The simulations are very similar, hence the first order model is chosen and the final model has the form

$$G_{FA}(s) = \frac{0.967}{0.374 \cdot s + 1} e^{-0.4 \cdot s}.$$

This model was estimated using data for a step at a higher axial force than that used in the validation data. The system has also proved to have the same dynamics for steps downward in the axial force reference as well. This model is thus valid for the range of axial forces that are used in the process window, see Section 2.2.4.

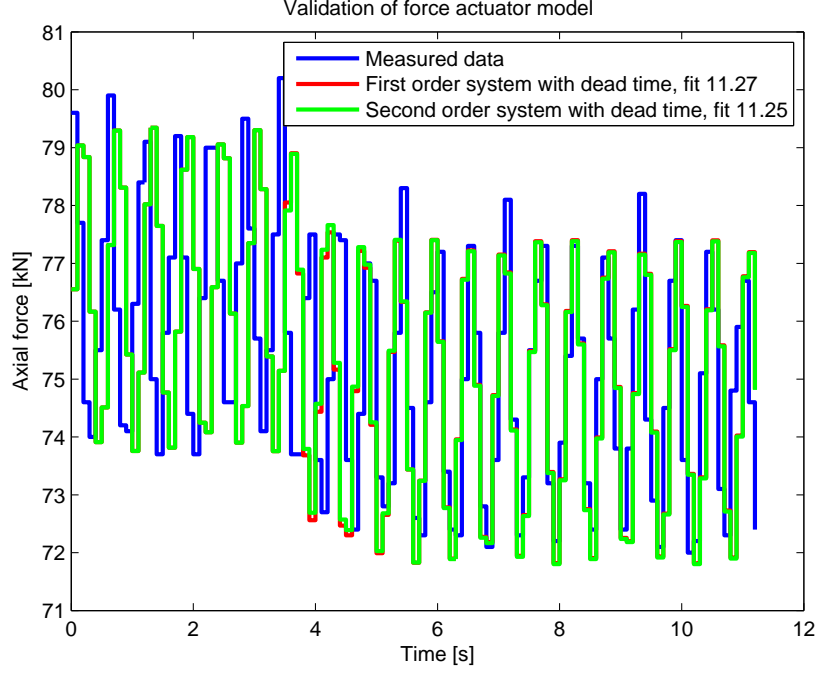


Figure 4.5. Validation of the models used to capture the dynamics of the force actuator. The force is modeled as a linear system with an additive sinusoidal with amplitude 2.8 kN and frequency 1.74 Hz.

If the system is linearized around the point $F_{z,r} = \bar{F}_{z,r}$ and $F_z = \bar{F}_z$, the dynamics can be written

$$\Delta F_z(s) = G_{FA}(s) \cdot \Delta F_{z,r}(s), \quad \begin{cases} \Delta F_{z,r}(s) = F_{z,r}(s) - \bar{F}_{z,r}(s) \\ \Delta F_z(s) = F_z(s) - \bar{F}_z(s) \end{cases}.$$

4.3 Sensors

There are two different sensors that are relevant for the plunge depth and they measure slightly different things. There is one position measurement that measures the tool position relative to the welding machine (called *Position Z* in Figure 4.1), and the other sensor measures the tool position relative to the canister surface (called *LVDT* in Figure 4.1).

An investigation of the two sensors and their usage as feedback sensors to plunge depth control has been made. The sensors are presented below.

4.3.1 Tool Position

The tool position sensor measures how far the tool has been moved from the welding machine (see Figure 4.1). This has some drawbacks since the distance to the surface (which can easily be translated to plunge depth) is not directly measured, and there are three problems related to this: flexibility and plastic deformation of the machine together with eccentricity. In this thesis, the canister is assumed perfectly circular. Hence, the eccentricity is only dependent on the displacement of the canister, and not the canister itself. The three uncertainties must all be compensated for if position measurements should be used as feedback to the controller. Besides, the thermal expansion of the canister will affect the position sensor measurements by decreasing its value with increasing expansion of the canister.

An obvious problem with this sensor is that the canister has to be perfectly centered for the tool position to be representative of the plunge depth. It has however shown to be very hard to clamp the canister perfectly centered, and this eccentricity needs to be compensated for. Lammlein et al. [15] have had similar problems when using FSW to weld hollow hemispheres and proposed a similar solution as is used here. A full circumferential measurement run is made pre-weld to determine the position of the canister, and this data can then be used to compensate for the non-centered clamping of the canisters. The result from such a run is seen in Figure 4.6. Measurements of the tool position contain peaks that stem from plastic deformation of the welding machine. As explained below, those peaks will be removed in the eccentricity compensator since otherwise they will be compensated for twice.

The large sprocket along which the tool moves seems to be plastically and elastically deformed. This is supposed to give rise to the peaks that are clearly visible in position weld data, see Figure 4.7. The plastic deformation can be seen in pre-weld measurements of the position, while the elastic deformation gives rise to larger peak amplitudes. In Figure 4.7, position data from three different full circumferential welds are presented. The peaks have a periodicity of 30° and they are very repetitive between welds, which makes it possible (in theory) to compensate for them. They are however not compensated for in the current implementation due to limitations in the control system. The conclusion that the peaks stem from deformation in the machine is confirmed by the fact that they are not seen in the LVDT-measurements, and the periodicity of 30° correlates well with the twelve clamps that fix the canister. It is a hypothesis of the author that those clamps deform the sprocket. The peaks always appear at the same *machine-fix* coordinates, so it is very likely that they stem from the machine and not the canister.

To get a good model of this sensor, the flexibility in the machine and the thermal expansion need to be considered. The deflection in the machine is addressed in Section 4.4 where a model of the flexibility is presented. Section 4.5 presents some observations of the thermal expansion.

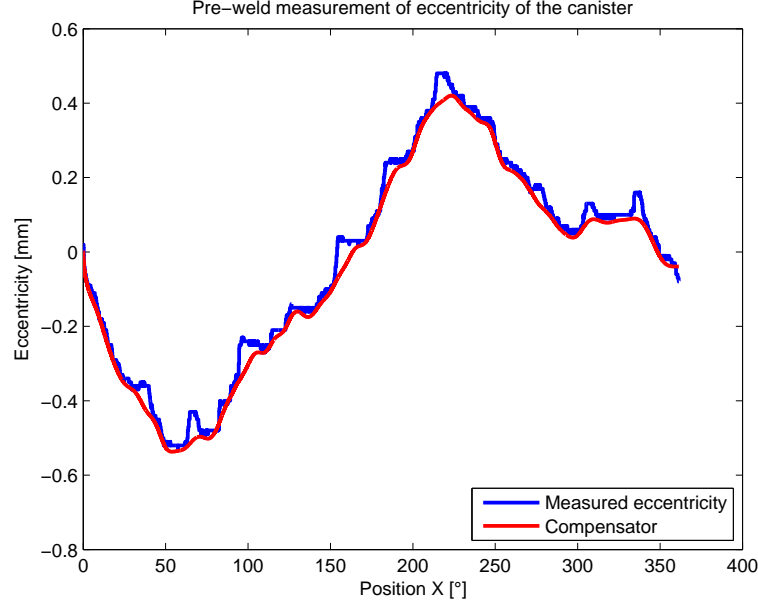


Figure 4.6. Measured eccentricity of a certain canister. The measurement contains peaks that are removed to not compensate for those twice.

4.3.2 Distance to Canister

The second sensor is the so called *LVDT*, which is an acronym for *Linear Variable Differential Transformer*, and this sensor is capable of measuring the actual distance between the tool and the canister surface. This distance is essentially the same as the plunge depth and is not affected by eccentricity due to the displacement of the canister.

When the full argon shield (that covers the whole circumferential weld) is used there is no space left for the LVDT-sensor. Hence, this sensor cannot be used when a full shield is needed. It is however not necessary to use full argon shielding during the research of the plunge depth control, which makes it possible to use this sensor for identification and validation of the controller.

The sensor is placed outside the main argon chamber (that is mounted around the tool) and measures the position at a point 13.5° ahead of the tool. A piston with a roll in the end is pushed towards the canister and the roll tracks the surface and the plunge depth is measured. The drawback with this sensor is that it is placed in front of the tool, so disturbances in the surface will be measured at the wrong position.

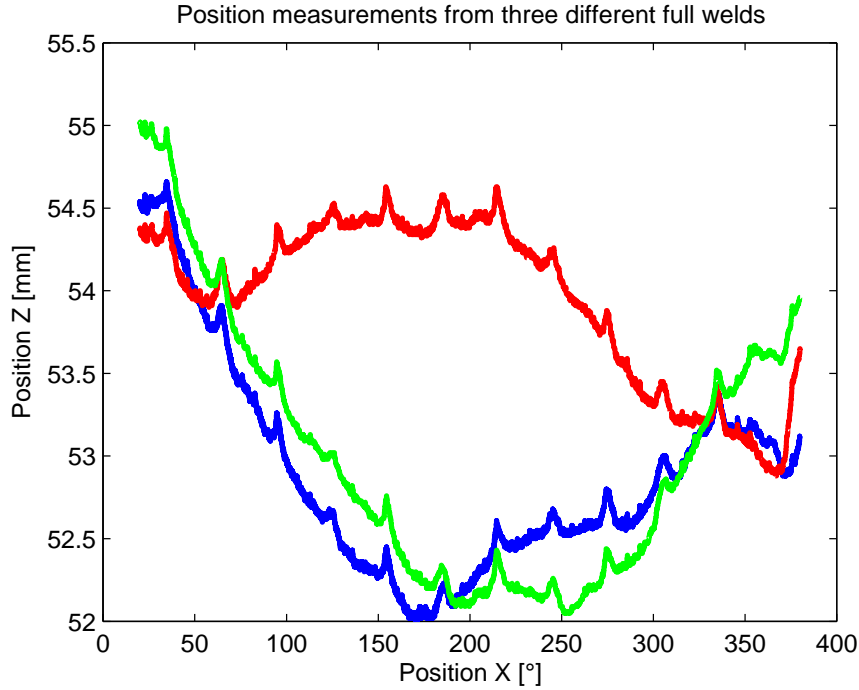


Figure 4.7. Position data from three full welds. The peaks are clearly visible and they are supposed to stem from plastic deformation and flexibility in the machine.

4.4 Deflection

Flexibility in the machine induces a deflection which affects the tool position measurements. The machine is bent and the distance between the machine and the canister surface is increased. This is a similar problem to the one encountered when using position control of FSW where robots are used, Longhurst et al. [18], but the SuperStir is purpose-built for FSW and copes with the high axial forces better. However, to get a good position measurement this deflection must be compensated for.

The deflection has been measured as the change of the difference between the position measurements and the LVDT-sensor. A change in plunge depth will be seen in both sensors and hence not contribute to the deflection. Even though the LVDT-sensor is placed ahead of the tool, a change in depth will be observed at the same time instance by both sensors. Hence, the fact that the LVDT-sensor is shifted in position has no effect on the measurement of the deflection. Using the measured data, a first order model was chosen to describe the dynamics of the deflection around an axial force close to the ones used during welding. Experiments

showed that the dynamics were very similar for the axial forces within the process window. Hence, the deflection seems to have linear characteristics with negligible non-linearities.

Figure 4.8 presents the measured deflection for a step change in the axial force together with the first and second order models. The model was estimated using a 4 kN step upwards in axial force from 80 kN, and the figure shows the validation of the model for a 2 kN step downwards from 82 kN. The fit for the process models are around 50% and the first order model gets slightly better fit. Since a less complex model is preferred if they have comparable fits, the first order model is chosen to describe the dynamics of the deflection.

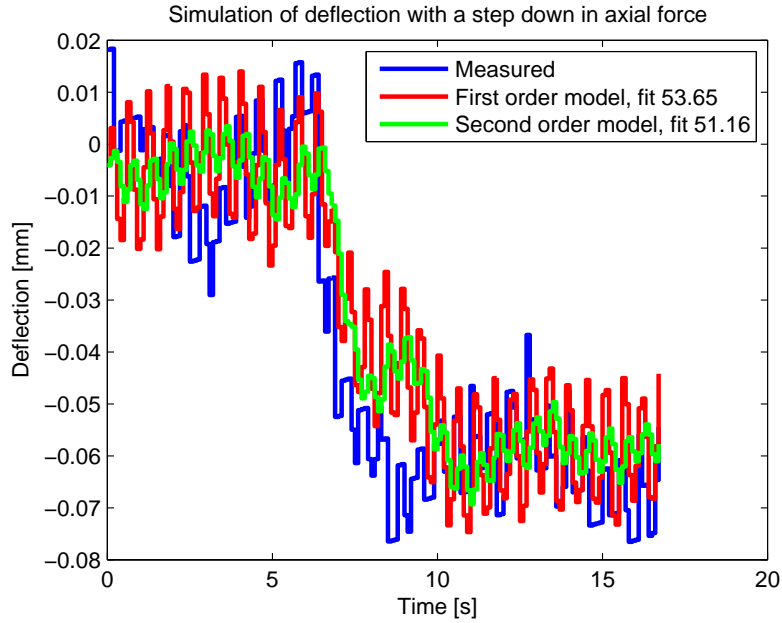


Figure 4.8. Validation of the models for the deflection. The first order model has a slightly better fit than the second order system.

The first order process model that fits the measurements best is

$$G_{defl}(s) = \frac{0.0304}{0.56 \cdot s + 1}, \quad (4.1)$$

and it has proven to describe the dynamics well for different welds, which indicates that the deflection is not dependent on the welding parameters. Figure 4.9 shows measurements of the deflection for a wide range of axial forces, and the linear polynomial has a very good fit to measured data. The gain is approximately the same as in the dynamic model.

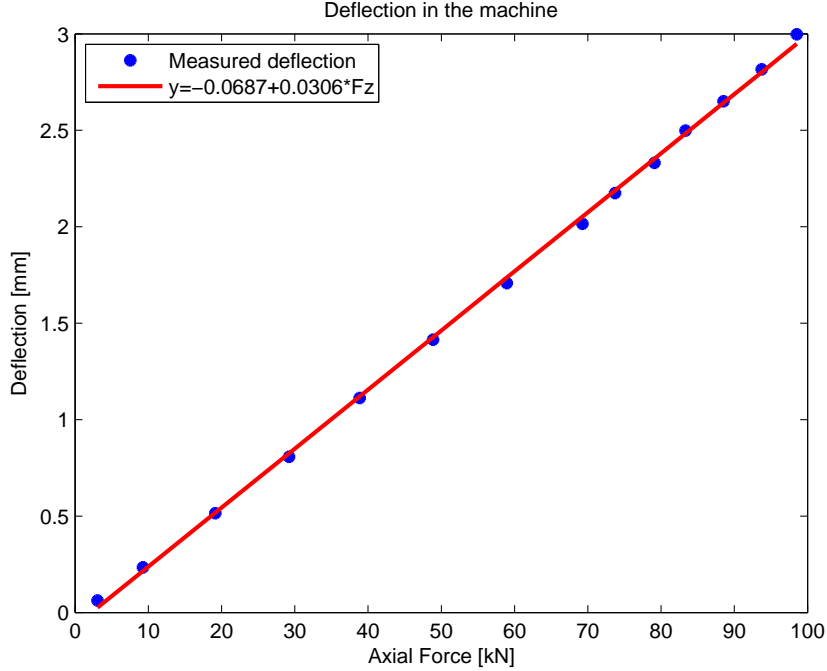


Figure 4.9. Measured deflection for a range of axial forces. The fit of a first order polynomial is good, giving the same gain as the dynamic model, but with a small bias.

4.5 Thermal Expansion

Thermal expansion of the canister has not been thoroughly investigated, but some observations have been made. The thermal expansion has been measured using the difference between the position measurements and the LVDT-measurements. By compensating the position measurement with the deflection, the thermal expansion can be calculated as

$$z_{TE} = P_{LVDT} - P_t + P_d,$$

where z_{TE} is the thermal expansion, P_{LVDT} is the LVDT-measurements, P_t is the position measurements and P_d is the deflection. Calculating the thermal expansion in this way assumes that the expansion at the LVDT is the same as at the tool, and this is the best way to do it today. This assumption might however not be true since the expansion at the LVDT is unknown in reality and has not been measured. Hence, the results in this section are merely hints of the thermal expansion and must be further investigated to get good measurements from the position sensor.

The thermal expansion was calculated for three different welds, and the result is seen in Figure 4.10. The dwell sequence ends at time zero and the initial thermal expansion is almost the same for the three welds. During the start and downward

sequences (for positive time values) the expansion is slight different; the blue and green curves seem to represent thermal expansions that decrease less than for the red curve. This could be explained by the fact that the weld corresponding to the red curve was performed in the lid (i.e. the downward sequence was aborted) and the two other had complete downward sequences. This observation is somewhat strange since intuitively the thermal expansion should increase in the lid. It is however possible that the thermal expansion at the LVDT is different depending on whether the weld is performed in the lid or if a full downward sequence is performed. Neither the validity of this assumption nor an accurate model of the thermal expansion are further investigated in this thesis. Since the thermal expansion seems to be quite constant (varying approximately 0.1 mm) for a weld with a full downward sequence, the thermal expansion will be compensated for by a constant in the plunge depth reference.

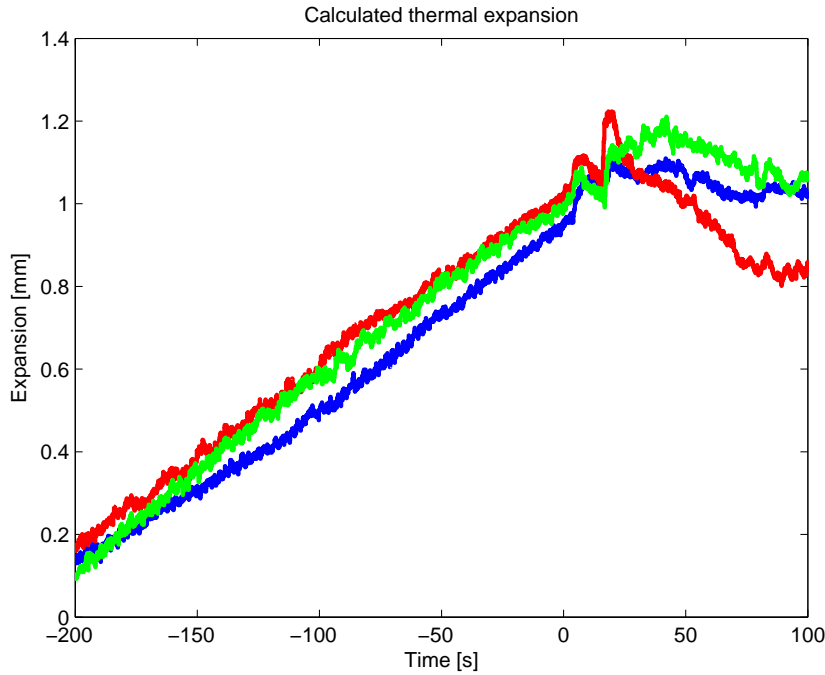


Figure 4.10. Calculated thermal expansion from three different welds. The blue and green are welds with a full downwards sequence, while the red weld is only in the lid. The start sequence begins at time zero.

4.6 Disturbances

The disturbances acting on the process have not been fully investigated, but some observations have been made. In Cederqvist [5], the disturbances are mostly related to the temperature via changes in the thermal boundary conditions and heat conduction. Those disturbances will affect the plunge depth since the material softens with increasing temperatures. This type of disturbance will change the parameters of the model, and can thus be seen as modelling errors. Also other material parameters e.g. hardness can change during the welds and induce errors in the models used to design the controller.

4.7 Plunge Depth

One of the controlled variables is the plunge depth, and this is assumed to be the same as the LVDT-measurements. Observing measured data reveals that the response in plunge depth due to changes in axial force may vary. Some of the steps act as if the depth settles at a constant depth, whilst others have a behaviour that indicates that the material creeps under constant force. Hence, two different models have been evaluated for the plunge depth dynamics. Both are derived in a neighbourhood around the linearization point $z_{SD} = \bar{z}_{SD}$. Here z_{SD} is the shoulder depth, which is connected to the tool depth by the relation

$$P_z = z_{SD} + PL,$$

where PL is the probe length.

The two models are both derived using rheology approximations of the heated copper material, and they are referred to as "Model I" (without creep) and "Model II" (with creep) and are presented in this chapter. "Model II" also includes the depth dependence on stir zone temperature.

4.7.1 Model I

To find a simple linear model for the plunge depth without the creep, a rheology model has been used. The rheology model is an approximative visco-elastic model that can be used to describe the behaviour of metals at high temperatures, Flügge [9]. The idea is to describe the heated copper as an elastic material that can be modelled as a Kelvin material, built by a spring (Hooke-element) and a dashpot (Newton-element) in parallel.

In order to use the rheology model, several approximations have to be made. Figure 4.11 visually describes the approximation. In this model it is assumed that the copper closest to the tool is heated to a temperature where it can be described

as a visco-elastic material. This property is valid up to a distance of l_0 from the tool, and further away the material is assumed to be completely stiff. The value of l_0 is assumed constant during the weld. Further, it is assumed that the heated copper behaves as if it was subjected to a 1-D deformation. The parameters of the Hooke- and Newton-elements are supposed to be constant.

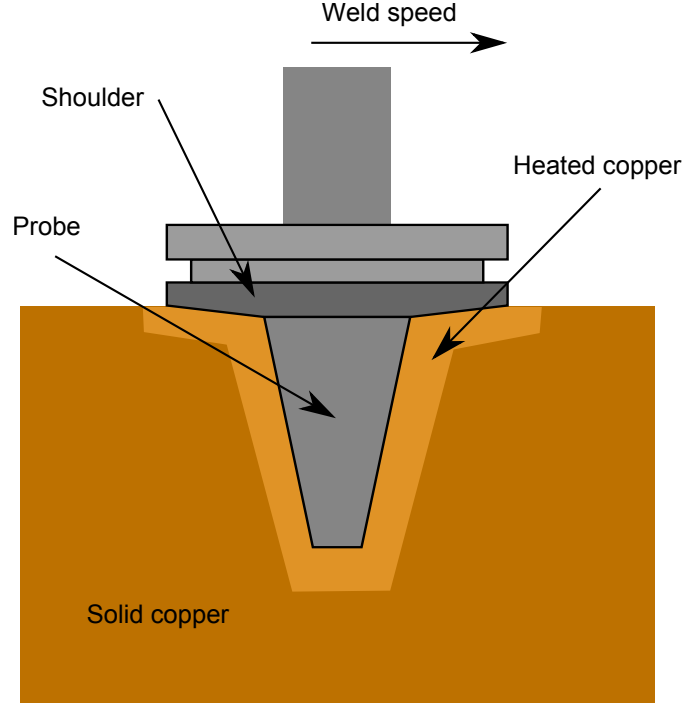


Figure 4.11. Schematic view of the approximations made in the depth model. The copper closest to the tool is assumed isothermally heated and acting as visco-elastic material, while the copper further away is assumed completely stiff.

Using the simplest Kelvin material and the approximations stated above, the expression of stress becomes

$$\sigma(t) = \bar{K} \cdot \epsilon(t) + \bar{B} \cdot \dot{\epsilon}(t),$$

where \bar{K} and \bar{B} are constants and $\epsilon(t)$ is the strain given by (Δl is the deformation)

$$\epsilon(t) = \frac{\Delta l(t)}{l_0}.$$

Assuming that the contact area is constant at all times and using the formula

$$\sigma(t) = \frac{F(t)}{A}$$

together with the expression for the deformation

$$\Delta l(t) = z_{SD}(t) - \bar{z}_{SD}$$

gives

$$F(t) = K \cdot \Delta l(t) + B \cdot \dot{\Delta l}(t)$$

as the expression of the force exerted on the tool by the copper.

The deformation $\Delta l(t)$ is the deviation from a given shoulder depth \bar{z}_{SD} , and this deviation is created by the motion of the spindle and tool along the z-axis. This motion is subjected to Newton's second law and can be expressed

$$m \cdot \ddot{\Delta l}(t) = \Delta F_z(t) - F(t) = \Delta F_z(t) - K \cdot \Delta l(t) - B \cdot \dot{\Delta l}(t),$$

where m is the mass of the moving parts. This is a linear differential equation in $\Delta l(t)$ and re-writing this, using the Laplace-operator, gives the transfer function

$$G_{depth}(s) = \frac{1}{m \cdot s^2 + B \cdot s + K} \quad (4.2)$$

from the change in axial force ΔF_z , to the deviation from the shoulder depth \bar{z}_{SD} . Since the change in plunge depth is the same as the deviation, this transfer function models the plunge depth dynamics.

Using LVDT-measurements from a step change in axial force, the parameters in (4.2) and a first order process model were estimated. The rheology model was implemented as a Grey-box model in SYSTEM IDENTIFICATION TOOLBOX. Validation of the models were made using new data from another step response and the results are presented in Figure 4.12.

The rheology model describes the measured change in plunge depth better and the estimated model is given by the transfer function

$$G_{depth}(s) = \frac{1}{14.8 \cdot s^2 + 58.6 \cdot s + 36.2},$$

which has the static gain

$$G_{depth}(0) = \frac{1}{36.2} \approx 0.0277$$

Validation

The model of the actuator, the deflection and model I for the plunge depth were combined into a complete model and simulated for a step change in the commanded axial force. The simulated change in position is compared to the measured change, and the result is seen in Figure 4.13.

The figure shows that the dynamics of the measured position, for the case without creep, can be modeled using these three models. The data used for this validation have not been used to estimate any of the subsystems' models.

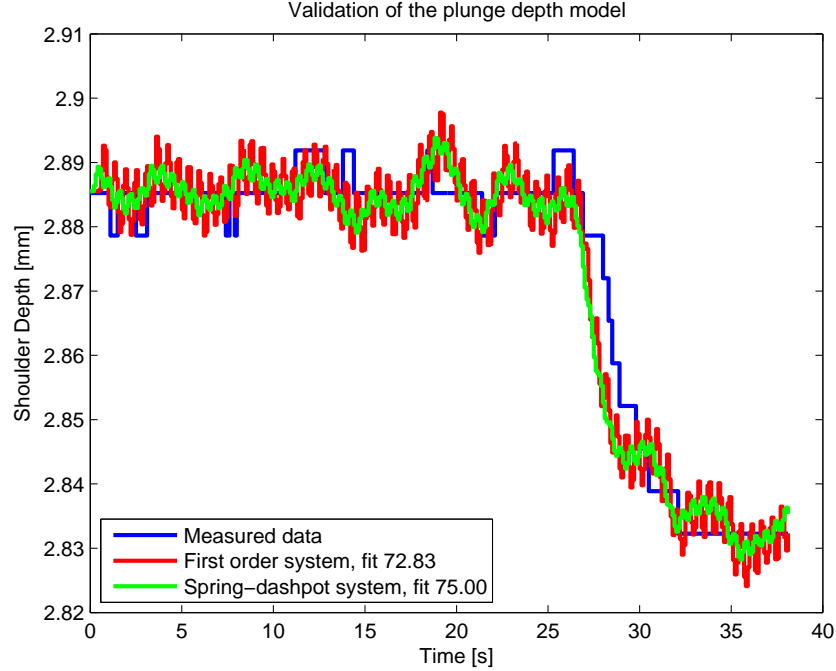


Figure 4.12. Validation of the experimental first order LTI-system and the rheology model using data from a step downwards in axial force. The fit for the rheology model is better and is therefore used to describe the plunge depth dynamics.

4.7.2 Model II

Measurement data from several different welds have been used to draw the conclusion that axial force and stir zone temperature are the major process variables that determine the tool depth. The model proposed in this sub-section is derived from rheology approximations of visco-elastic materials, just like the model derived in Section 4.7.1, combined with an ad hoc correction factor for temperature. The same assumption of a homogeneous width (called l_0) of the heated copper is assumed here. However, a slightly different rheology model is used in this approach to model the creep tendencies of the material. Creep is an increase in strain under constant stress and it is common in metals at high temperatures, Flügge [9]. The rheology model used here is called a 3-parameter fluid model and consists of two dashpot elements and one spring, connected according to Figure 4.14.

The leftmost part of the figure has the same structure as in the previous depth model and the rightmost dashpot is added to describe the creep. The equation

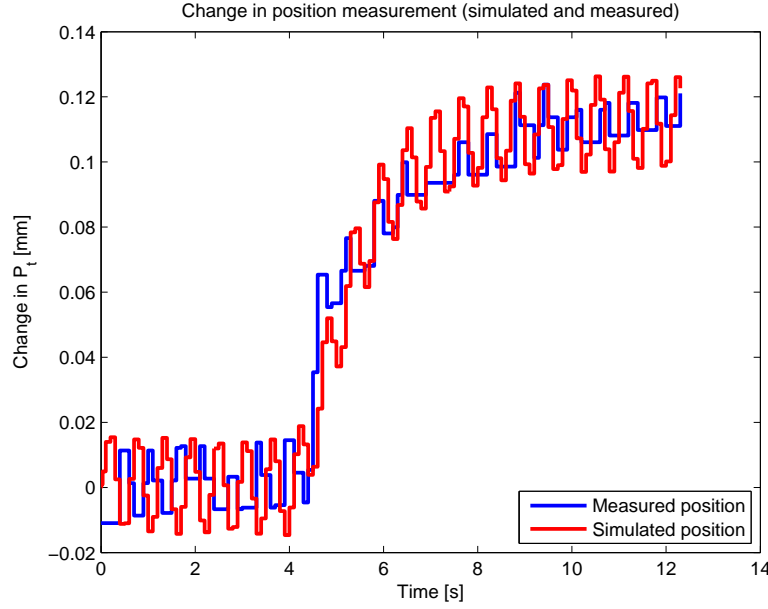


Figure 4.13. Simulation of the dynamics in the position measurement plotted together with the measured change in position. The full model is a decomposition of the sub-systems.

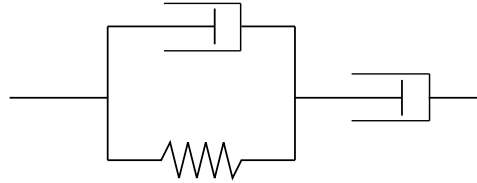


Figure 4.14. Schematic view of the rheological 3-parameter fluid model used to describe the plunge depth. The rightmost dashpot element is added to model creep tendencies in the material.

describing the relation between stress ($\sigma(t)$) and strain ($\epsilon(t)$) is given by

$$\sigma(t) + p_1 \dot{\sigma}(t) = \bar{q}_1 \dot{\epsilon}(t) + \bar{q}_2 \ddot{\epsilon}(t), \quad (4.3)$$

where p_1 , \bar{q}_1 and \bar{q}_2 are constants. By introducing the deformation $\Delta l(t)$ one could express the strain as

$$\epsilon(t) = \frac{\Delta l(t)}{l_0},$$

which inserted in (4.3) gives

$$\sigma(t) + p_1 \dot{\sigma}(t) = \bar{q}_1 \frac{\Delta \dot{l}(t)}{l_0} + \bar{q}_2 \frac{\Delta \ddot{l}(t)}{l_0} = q_1 \Delta \dot{l}(t) + q_2 \Delta \ddot{l}(t), \quad (4.4)$$

as the relation between stress and deformation (q_1 and q_2 are constants). Continuing by using Newton's laws of motion and noting that the deformation is the change in plunge depth gives a relation from the axial force to the change in tool depth. The assumption states that $\Delta l(t) = z_{SD}(t) - \bar{z}_{SD}$, giving

$$m \cdot \Delta \ddot{l}(t) = \Delta F_z(t) - F_c(t) = \Delta F_z(t) - A \cdot \sigma(t), \quad (4.5)$$

where $F_c(t)$ is the force exerted by the material on the tool, A the area of the tool in contact with the copper (assumed constant here), m the mass of the moving spindle and $\Delta F_z(t) = F_z(t) - \bar{F}_z$ is the deviation of the axial force from the point \bar{F}_z .

By using the Laplace transform, (4.4) and (4.5) can be written

$$\begin{aligned} (1 + p_1 \cdot s) \sigma(s) &= (q_1 \cdot s + q_2 \cdot s^2) \Delta l(s) \\ A \cdot \sigma(s) &= \Delta F_z(s) - m \cdot s^2 \cdot \Delta l(s). \end{aligned}$$

Combining these give

$$\Delta l(s) = \frac{1}{mp_1} \cdot \frac{1 + p_1 s}{s \cdot \left(s^2 + \frac{Aq_2 + m}{mp_1} s + \frac{Aq_1}{mp_1} \right)} \Delta F_z(s),$$

which is a second order system with a zero and an integrator. Using MATLAB and SYSTEM IDENTIFICATION TOOLBOX, a process model with the same structure was estimated from LVDT-measurements. The transfer function of the linear model is

$$G_D(s) = 0.001592 \cdot \frac{1 + 29.56 \cdot s}{s \cdot (1 + 14.67 \cdot s) \cdot (1 + 0.00095 \cdot s)}.$$

The plunge depth is given by

$$P_z(t) = z_{SD}(t) + PL = \Delta l(t) + \bar{z}_{SD} + PL.$$

The dependence on temperature is introduced as a multiplicative correction factor of the plunge depth. This is an ad hoc solution that is sometimes used to model the static behaviour around a setpoint. The correction factor is estimated using data from a weld with constant axial force and oscillating temperature, see Figure 4.15. Although the change in depth is delayed approximately 6 seconds in this data set, other observations indicates that the delay can be less. In some data sets, the change in depth seems to not be delayed at all. This data set was however chosen to estimate the correction factor since there is an oscillating temperature during a long time period. The correction factor is introduced to describe the static dependence on temperature, and an approximation with no time delay should not

affect the steady state model. Further, the correction factor is assumed linear in temperature deviation and the polynomial

$$CF_T(\Delta T) = 1 + 0.0021 \cdot \Delta T$$

has been estimated using the least-squares method. Here $\Delta T(t) = T(t) - T_0$ is the deviation in temperature around the temperature $T_0 = 816.4^\circ C$. This ad hoc solution might only be valid in a region near T_0 , and more experiments need to be done to evaluate the validity of this approximation.

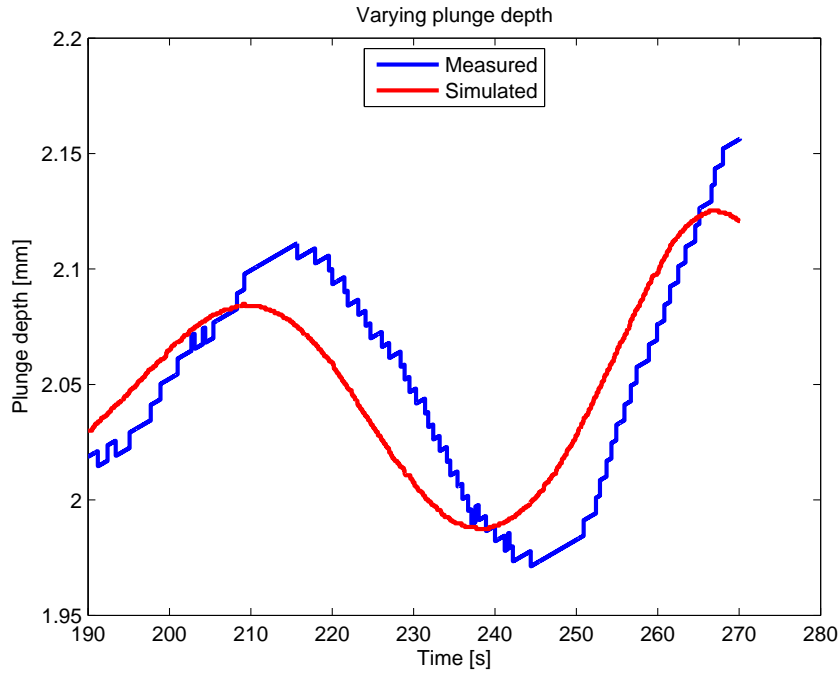


Figure 4.15. Variations in plunge depth due to oscillations in temperature. This data have been used to estimate a correction factor for the plunge depth.

The linear rheology model combined with the correction factor gives the complete model

$$\Delta l(s) = 0.001592 \cdot \frac{1 + 29.56 \cdot s}{s \cdot (1 + 14.67 \cdot s) \cdot (1 + 0.00095 \cdot s)} \Delta F_z(s)$$

$$z_{SD}(t) = (\Delta l(t) + \bar{z}_{SD}) \cdot (1 + 0.0021 \cdot \Delta T(t)).$$

The validation of the model has been made using measured data from a weld in the lid. Figure 4.16 shows the simulated and the measured shoulder depth. The accuracy is not perfect, but it captures the main cross-correlation between axial force, temperature and plunge depth.

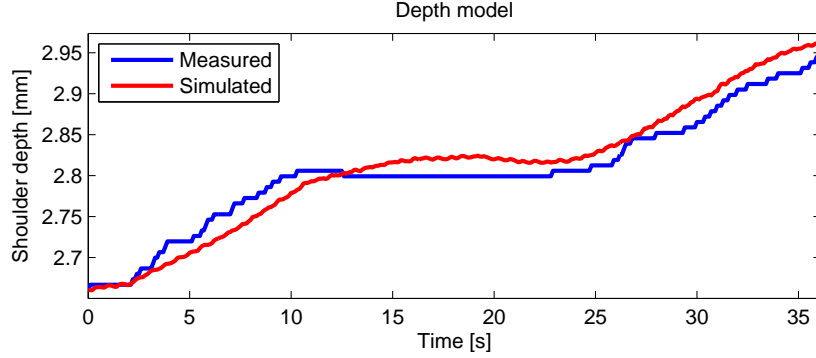


Figure 4.16. Validation of the second depth model. It consists of a rheology model and a correction factor for the temperature dependence. The first increase in depth is due to a step change up and down in the axial force. The second part is due to an increase in temperature.

4.8 Temperature

The heating of the stir zone is complex but can be approximated with a linear differential equation relating temperature and power input. Cederqvist et al. [2] used a linear second order process model with a time delay and Mayfield et al. [21] derived a first order linear differential equation based on a set of approximations and assumptions. The power input to the process is given by

$$P = \bar{\omega} \cdot M + F_v \cdot v$$

where M is the torque exerted by the tool in Newton meter ([Nm]), $\bar{\omega}$ is the spindle rotation speed in radians per second ([rad/s]), F_v is the traverse force in Newton ([N]) and v is the traverse speed in meters per second ([m/s]). The major part of the power is due to the rotation of the tool, and hence the contribution from the traverse is negligible, Cederqvist [5], which gives the approximative relation

$$P = \frac{\pi}{30000} \cdot \omega \cdot M$$

for the power input. Here the rotation speed (ω) has been transformed into revolutions per minute ([RPM]) instead of radians per second.

Experimental data from a weld in the lid were used to fit linear process models of varying orders. A first order model was not sufficient to explain the measured data, but a second order linear model with dead time worked well. Introducing higher orders of the models seemed to be unnecessary since the fit was not improved. The final model was estimated using a process model in SYSTEM IDENTIFICATION TOOLBOX in MATLAB and is described by the transfer function

$$G_T(s) = \frac{18.118}{(1 + 30.487 \cdot s) \cdot (1 + 1.15459 \cdot s)} e^{-2.8151 \cdot s}.$$

The validation of the model using measured data is shown in Figure 4.17, where the first step increase in power is generated by a step change in the axial force, and the second step is generated by a change in spindle rotation speed. The model was estimated from measured temperature data generated by changes in axial force. As can be seen, the measured increase in temperature for the second step is not properly modeled. This phenomenon will be further discussed in Sections 4.9 and 4.10 where there are two hypotheses presented to explain this behaviour.

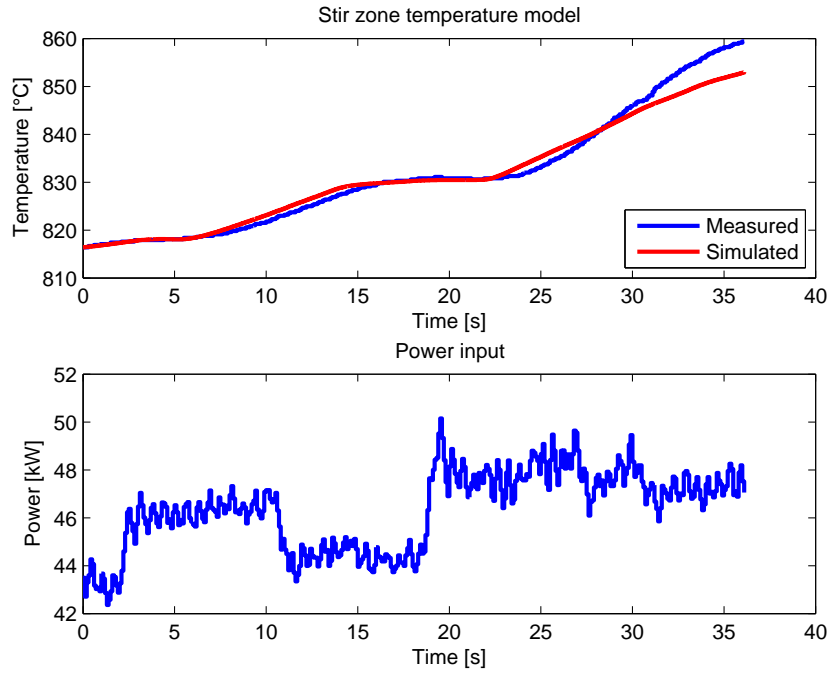


Figure 4.17. Validation of the second order dead time model for the temperature. The increase in power has been generated in two different ways; first there is an increase in axial force and second an increase in rotational speed.

It is a hypothesis of the author that the temperature model is actually two models in series; one describing the heating of the copper (which could be described by a first order linear differential equation according to Mayfield et al. [21]), and one describing the heating of the tool. The thermo-couple that measures the temperature is placed inside the probe, and therefore the tool temperature is measured, not the stir zone temperature. This sensor has however performed well with the cascaded temperature controller and is used in this approach as a controlled variable. The model derived in this section assumes an isothermal condition at the tool-matrix interface, which has proven to work well in the existing cascade controller used today.

4.9 Torque

The torque sensor used today measures the torque exerted by the motor and not the torque input to the process. The motor torque is thus a composition of spindle torque (torque exerted by the tool), friction torque and torque used to accelerate the spindle.

4.9.1 Friction

The friction torque data have been gathered by measuring steady state motor torque when the tool rotates in air (which gives negligible spindle torque). Measurements were made before and after welding, but no differences in friction torque could be seen. Figure 4.18 shows the measured torque when steps downwards are made (starting at 600 RPM ranging down to 50 RPM).

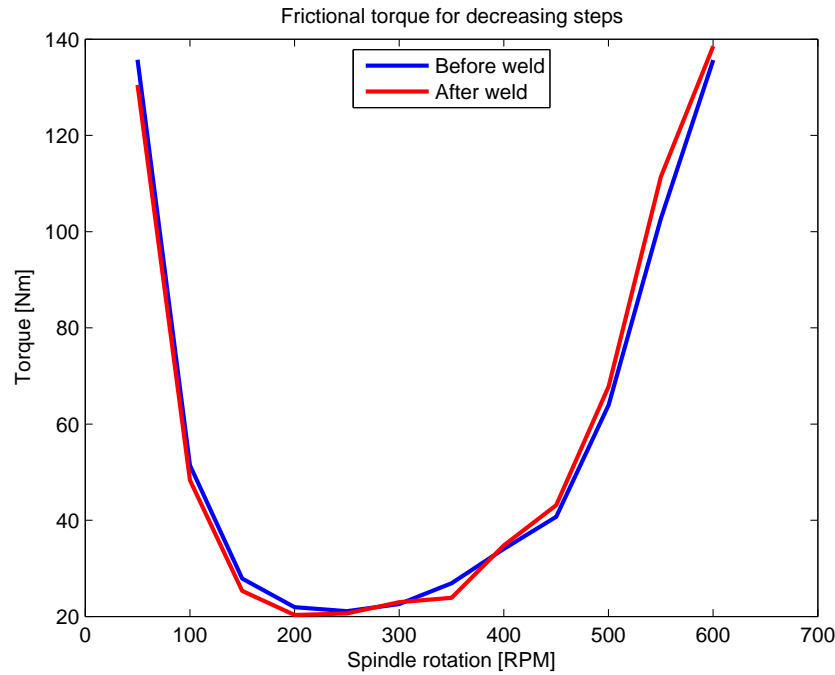


Figure 4.18. Measured friction torque for different spindle rotation speeds. The friction has been measured before and after a weld, and the results are very similar.

During a weld, the rotational speed is varying in a band ranging from approximately 300 to 550 RPM, and a second order polynomial is fitted to the measured

data in this interval. The model of the friction torque is

$$M_{fric}(\omega) = 243.11 - 1.305 \cdot \omega + 0.001927 \cdot \omega^2.$$

Figure 4.19 shows the measured data together with the fitted polynomial in the interesting band.

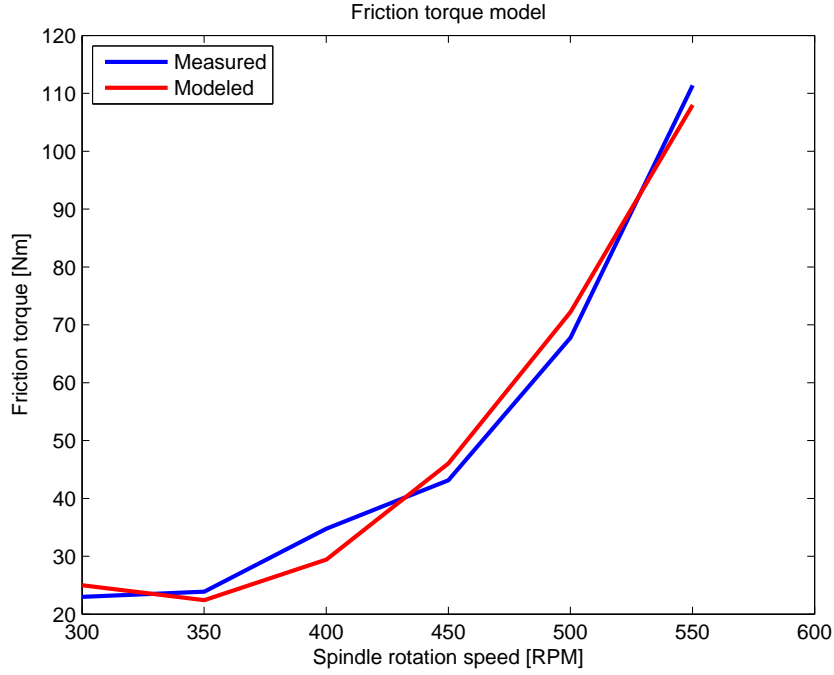


Figure 4.19. Validation of the friction torque model consisting of a second order polynomial. The polynomial was fitted to measured data in the interval 300 to 550 RPM.

4.9.2 Spindle Torque

The torque exerted by the tool is described using a model proposed by Schmidt [26] with some changes to fit this process. The idea is that torque is produced in two different ways; slipping and sticking. The slipping condition means that the tool velocity is higher than the material's at the interface, resulting in a Coulomb friction between the tool and the copper. When sticking condition is present, the material is assumed to rotate with the tool and the torque is produced by shear stresses due to plastic deformation of the material. Which of these conditions that are most valid in FSW has not yet been determined. Schmidt et al. [26] argue that it could be a combination of these two conditions that together produces the

torque. Qian et al. [25] have observed that the ratio of torque produced by the sticking and sliding conditions varies during one rotation of the tool, and the ratio might also change during the weld. However, in this thesis a constant ratio is used.

Introducing the constant state parameter $\delta \in [0, 1]$ gives

$$M_{spindle} = \delta M_{sticking} + (1 - \delta) M_{sliding},$$

where $M_{sticking}$ is the contribution from the sticking condition and $M_{sliding}$ is the contribution from the sliding condition. Looking at an infinitesimal part of the tool, the torque is described by

$$dM_{contact} = r \cdot dF = r \cdot \tau_{contact} \cdot dA,$$

where $\tau_{contact}$ is the contact shear stress (either $\tau_{sticking}$ or $\tau_{sliding}$), r is the radius and dA is an infinitesimal area section. Integrating this over the tool surface yields

$$M_{contact} = G(z_{SD}) \cdot \tau_{contact}.$$

The geometric quantity $G(z_{SD})$ is dependent on the tool geometry and the plunge depth. Assuming that the probe is always penetrated into the copper, the shoulder is not fully penetrated and that the shoulder geometry is a cut cone (see Figure 2.1), the relation is

$$G(z_{SD}) = G_{probe} + \frac{2\pi}{3} \frac{z_{max}}{R_o - R_i} \left(1 + \frac{1}{\tan \alpha} \right) \cdot \left(\left(R_i + \frac{R_o - R_i}{z_{max}} \cdot z_{SD} \right)^3 - R_i^3 \right),$$

where all constants are given by the tool geometry, see Table 4.1. The two contributions of torque are then

$$\begin{aligned} M_{sliding} &= G(z_{SD}) \cdot \tau_{sliding} \\ M_{sticking} &= G(z_{SD}) \cdot \tau_{sticking}, \end{aligned}$$

where the expression for the sliding shear stress is given by the Coulomb friction

$$\tau_{sliding} = \mu \sigma.$$

Here, μ is the coefficient of friction and σ is the contact pressure. The sticking shear stress is assumed to be the same as the copper yield stress, giving

$$\tau_{sticking} = \tau_{yield},$$

where τ_{yield} is assumed constant in the relatively narrow band of temperatures used in FSW of copper canisters. The contact pressure σ is calculated as force divided by area;

$$\sigma(t) = \frac{F_z(t)}{A(z_{SD}(t))},$$

Name	Value	Description
G_{probe}	$2.3 \cdot 10^{-5} [m^3]$	Geometric quantity for the probe
z_{max}	$0.003 [m]$	The height of the convex part of the shoulder
R_o	$0.035 [m]$	Shoulder outer radius
R_i	$0.015 [m]$	Shoulder inner radius
α	$0.1489 [rad]$	Angle of the convex shoulder

Table 4.1. Table with the geometric constants of the tool used to derive the torque.

where $A(z_{SD})$ is the depth dependent area given by the tool's projection on the canister surface. The tool geometry gives

$$A(z_{SD}) = \pi \left(R_i + \frac{R_o - R_i}{z_{max}} z_{SD} \right)^2.$$

Observations show that the measured torque is dependent on the spindle rotation speed as well but the origin of this dependence is not yet fully investigated. There are two hypotheses that could explain the observed measurements; either the torque exerted by the tool/material contact is dependent on the tool rotation speed or some part of the power transmission is dependent on the rotation speed (besides the friction). Observations that indicate that the first hypothesis is correct are made by e.g. Cui et al. [6] where a spindle rotation rate dependent torque model is derived. However, in this thesis the first hypothesis is investigated using an ad hoc approach with a multiplicative correction factor on the form

$$CF_M = 1 - \tau_\omega \Delta\omega |\Delta\omega|,$$

where $\tau_\omega = 1.42 \cdot 10^{-5}$ was estimated using measured data. The correction factor is based on the deviation in spindle rotation speed from a given speed, giving $\Delta\omega = \omega - \omega_0$. The spindle torque is thus given by

$$M_{spindle} = (\delta\tau_{yield} + (1 - \delta)\mu p) \cdot G(z_{SD}) \cdot (1 - \tau_\omega \Delta\omega |\Delta\omega|).$$

The hypotheses will be compared in Section 4.10 and a discussion of their validity is presented.

4.9.3 Complete Torque Model

The torque used to accelerate the spindle and the dynamics in the gear box have not been fully considered in the model. The moment of inertia of the spindle and gear box have a filtering effect on the spindle torque. A fast oscillation in spindle torque will not be measured by the torque sensor. This phenomenon has been modeled using a first order low-pass filter (LP-filter) on the motor torque. The resulting model is

$$\tau_M \dot{M}_{motor} = -M_{motor} + M_{spindle} + M_{fric},$$

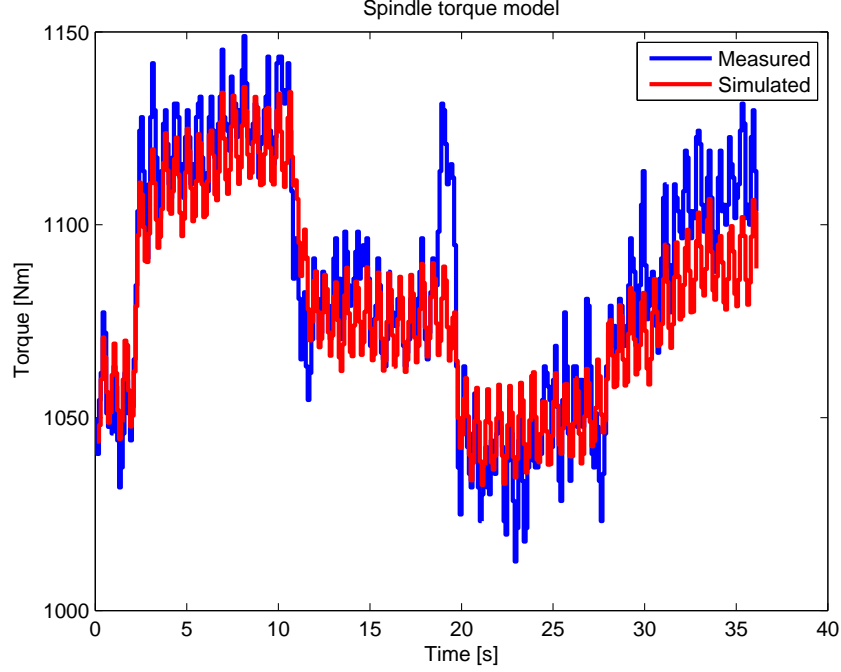


Figure 4.20. Validation of the torque model. In the first part of the data set, the axial force is changed whilst the spindle rotation is instead changed in the second half. An increase in spindle rotation speed results in a decrease in torque.

where τ_M is the filter time constant.

The constants related to the tool have been calculated analytically, except for the parameter G_{probe} . This has been estimated together with the parameters δ , μ , τ_{yield} and τ_M using measured data from a weld in the lid. The estimated values are

$$\begin{aligned} G_{probe} &= 0.00002308 [m^3] \\ \delta &= 0.1528 [-] \\ \tau_{yield} &= 1 [MPa] \\ \tau_M &= 0.27 [s] \end{aligned}$$

and the validation of the model is seen in Figure 4.20. Estimation and validation data is extracted from the same weld, but from non-overlapping sequences. The peak in motor torque measurements at approximately 19 seconds is due to the acceleration of the spindle, but since this is not modeled, the simulated torque does not include this peak. Also, the torque response to changes in the rotational speed is not modeled as good as for the changes in axial force. This is most likely because the ad hoc solution is not derived from fundamental physical relations. If

the LP-filter had not been used, then the simulated torque would have oscillated much more due to the fluctuations in the axial force.

4.10 Full Model

The models of the sub-systems (plunge depth model II, torque model and temperature model) are combined into one full model for friction stir welding. All parameters that were estimated in each model are used in the full model without any changes. An evaluation of the torque dependence on spindle rotation speed is also added to this section. The linear parts of the model are derived at the linearization point where

$$\begin{aligned} F_z &= 78.4 \text{ kN} \\ T &= 816.4 \text{ }^\circ\text{C} \\ z_{SD} &= 2.66 \text{ mm} \\ \omega &= 404 \text{ RPM.} \\ P &= 43.6 \text{ kW} \end{aligned}$$

The final model with the correction factor on the torque is

$$\begin{aligned} \Delta T &= \frac{18.118}{(1 + 30.487 \cdot s) \cdot (1 + 1.1546 \cdot s)} e^{-2.8151 \cdot s} \Delta P \\ \Delta l &= 0.0016 \cdot \frac{1 + 29.56 \cdot s}{s \cdot (1 + 14.67 \cdot s) \cdot (1 + 0.00095 \cdot s)} \Delta F_z \\ 0.27 \cdot \dot{M} &= -M + (152800 + 0.435 \cdot \sigma) \cdot G(z_{SD}) \cdot (1 - 1.42 \cdot 10^{-5} \Delta \omega \cdot |\Delta \omega|) + M_{fric} \\ \sigma &= \frac{F_z}{A(z_{SD})} \\ A(z_{SD}) &= \pi \left(0.015 + \frac{20}{3} z_{SD} \right)^2 \\ G(z_{SD}) &= 2.3 \cdot 10^{-5} + 2.408 \cdot \left(\left(0.015 + \frac{20}{3} z_{SD} \right)^3 - 0.015^3 \right) \\ M_{fric} &= 243.11 - 1.305 \cdot \omega + 0.001927 \cdot \omega^2 \\ \Delta P &= \frac{(M - M_{fric}) \cdot \omega \cdot \pi}{30000} - 43.6 \\ \Delta F_z &= \frac{0.967}{0.374 \cdot s + 1} e^{-0.4 \cdot s} \Delta F_{z,r} \\ F_z &= \Delta F_z + 78.4 \\ T &= \Delta T + 816.4 \\ z_{SD} &= (\Delta l + 2.66) \cdot (1 + 0.0021 \cdot \Delta T) \\ \omega &= \Delta \omega + 404, \end{aligned}$$

and the model without the correction factor is the same except for the torque. The relation for torque in this approach is

$$0.27 \cdot \dot{M} = -M + (152800 + 0.435 \cdot \sigma) \cdot G(z_{SD}) + M_{fric}.$$

The model includes linearized parts, and hence it will be valid in a neighbourhood close to the corresponding point. This linearization point will be used in all simulations of the model to get a good accuracy of those.

Simulations of both models give different results in the second half of the data set. Figure 4.21 displays the results for the model with the correction factor, and Figure 4.22 shows the same validation of the model without the dependence on rotation speed. The two models are exactly the same in the first half of the validation data set. The depth model has a slight bias in the beginning, resulting in a simulated torque lower than the measured one. Since the cross-connections are modeled, this error in the torque results in a simulated temperature that is just below the measured temperature.

When steps are applied to the spindle rotation speed, the first approach manages to model the measured torque in a better way than the second approach. However, the second approach simulates the temperature more accurately. This could be explained by the fact that the change in torque is due to the machine, and not the tool/matrix interface. To verify this, further investigations must be made, and it could be possible that a part of the change is due to the material response (like the one observed by Cui et al. [6]). The controllers will be simulated for the model using the second approach, where the torque is not dependent on spindle rotation rate.

The model proposed in this section relates the two manipulated variables commanded axial force and spindle rotation speed to the three important process variables plunge depth, stir zone temperature and torque. The most important cross-connections are modeled and Figure 4.23 reveals that they are quite severe. The response in depth and temperature to a 1 kN step change applied in the axial force command is seen in the first column, and the second column contains the response for a step change of magnitude 10 RPM applied in spindle rotation speed. The cross-connections are not negligible and the ability of the controllers to cope with them will be quite important.

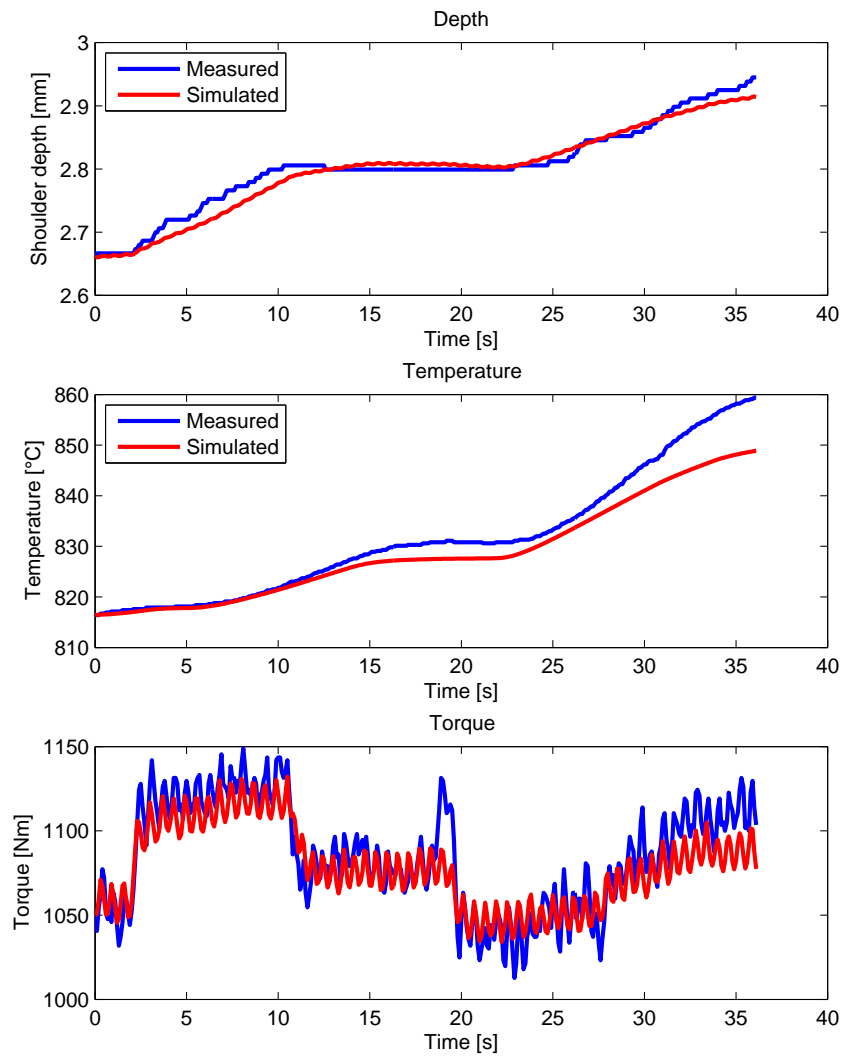


Figure 4.21. Validation of the full model with the cross-connection between spindle rotation speed and spindle torque.

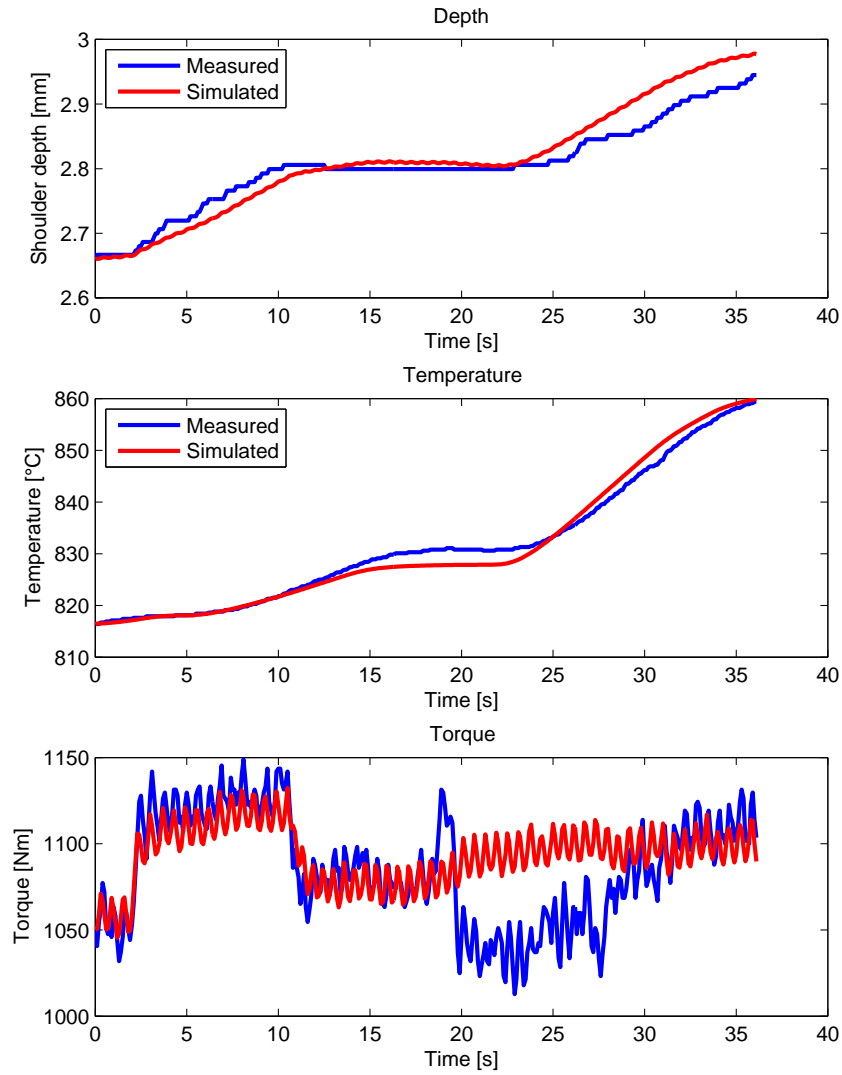


Figure 4.22. Validation of the full model that does not consider the relation between spindle rotation speed and spindle torque.

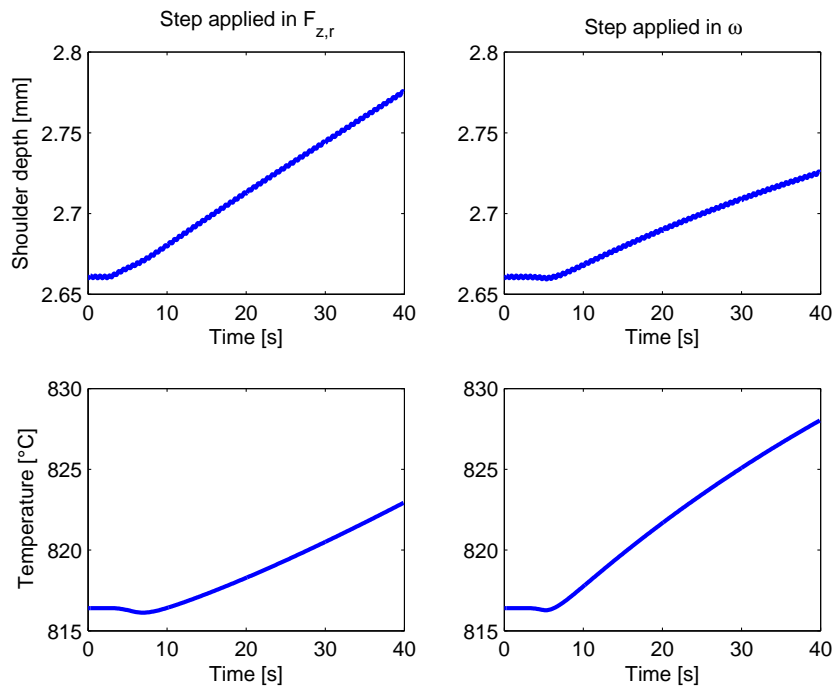


Figure 4.23. The first column contains the results from a step change of 1 kN in the axial force command, and the second column illustrates the response to a step change of magnitude 10 RPM in the spindle rotation speed. There are quite severe cross-connections in the system.

Chapter 5

Controller Design & Comparison

Two different controller strategies are proposed in this chapter. First, the decentralized control is addressed and two different controller tunings are presented. Second, the NMPC-design is investigated and in the end the two controller structures are compared.

5.1 Decentralized Controller I

This first controller is based on Model I presented in Section 4.7.1. This is a decomposition of the depth model and the force actuator model, resulting in a SISO LTI-model. The model is described by the transfer function

$$G_I(s) = \frac{0.967}{0.374 \cdot s + 1} \cdot \frac{1}{14.8 \cdot s^2 + 58.6 \cdot s + 36.2} e^{-0.4 \cdot s}, \quad (5.1)$$

that relates the commanded axial force to the change in plunge depth.

Since a simple controller structure is desired in the decentralized control solution, PID and PI controllers are investigated. A model based control design approach is considered which is based on the model given by (5.1). The control structure is depicted in Figure 5.1, where the PI/PID controller is combined with two low order linear filters.

The PID controller uses a proportional part (P), an integral part (I) and a derivative part (D) to calculate the control signal given the filtered control error, which is the difference between the filtered reference and output. In this control structure, the filtered reference and measurements are used instead of the original signals.

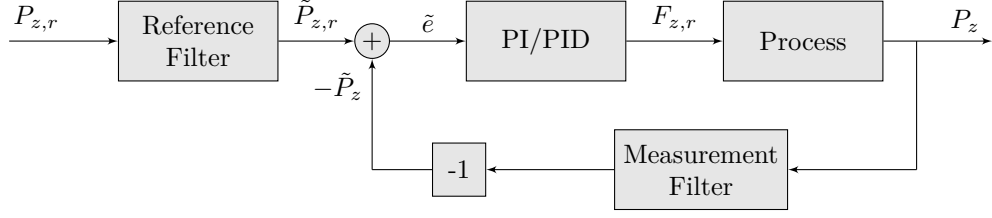


Figure 5.1. Block diagram of the control structure with a PI or PID controller together with filters for the reference and measurements. The filters on reference and measurements are necessary to give an implementable controller when PID is used.

The control law for the PID controller is then

$$F_{z,r}(t) = K_P \tilde{e}(t) + K_I \int_0^t \tilde{e}(\tau) d\tau + K_D \frac{d}{dt} \tilde{e}(t)$$

$$\tilde{e}(t) = H_r(p) \cdot r(t) - H_y(p) \cdot y(t),$$

where K_P is the proportional gain, K_I the integral gain, K_D is the derivative gain, \tilde{e} is the filtered control error, $H_r(p)$ is the reference filter, $r(t)$ is the reference, $H_y(p)$ is the measurement filter and $y(t)$ is the measurement. The derivative term cannot be directly implemented, but the low order filters make the implementations possible.

The PI controller does not have the derivative part, and the control law is thus

$$F_{z,r}(t) = K_P \tilde{e}(t) + K_I \int_0^t \tilde{e}(\tau) d\tau.$$

The transfer functions for the PID and PI are

$$F_{PID}(s) = K_P + \frac{K_I}{s} + K_D s$$

$$F_{PI}(s) = K_P + \frac{K_I}{s}.$$

The block diagram from Figure 5.1 can be re-written to get a two degrees of freedom controller, see Figure 5.2. Since transfer functions are linear, the two controllers F_r and F_y can be defined as

$$\begin{aligned} F_r(s) &= F(s) \cdot H_r(s) \\ F_y(s) &= F(s) \cdot H_y(s), \end{aligned} \tag{5.2}$$

which are both possible to implement if the filters are chosen such that the complete system is proper (here $F(s)$ could be replaced with $F_{PID}(s)$ or $F_{PI}(s)$ depending on which controller is used).

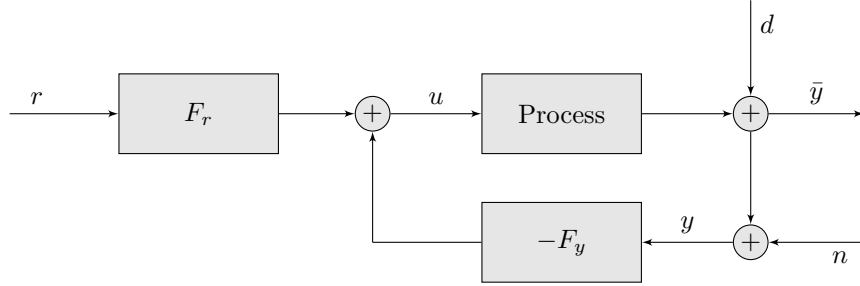


Figure 5.2. Control structure of a two degrees of freedom controller. The measured output is y and the calculated control signal is u . An output disturbance d is acting on the system and the real output \bar{y} is measured with an additive noise n . The closed loop robustness and disturbance compensation is determined by the controller F_y , while the closed loop response is also affected by F_r .

Although there is a time delay in the system, this is not compensated for in the proposed controller structure. A step response for the dynamics from a change in axial force to the corresponding change in tool depth is seen in Figure 5.3. By calculating

$$\tau = \frac{L}{L + T},$$

it is possible to conclude if the process is lag dominated (with τ close to zero) or delay dominated (τ close to one), see e.g. Garpinger et al. [12]. Using the values for this system ($L = 0.82$ and $T = 1.65$) gives $\tau = 0.33$ which is a balanced system and hence the time delay is not dominant in the process. A robust controller that does not consider the time delay should therefore work well.

Changing the controller parameters to get a desired behaviour of the closed loop system is referred to as controller tuning. There exist several tuning methods, such as λ -tuning and Ziegler-Nichols-tuning, with rules of thumb on how to choose the controller gains. Two tuning methods are used to find suitable gains for this controller; an algorithm proposed by Garpinger [11], that optimizes the controller for a given cost function and constraints, and the frequently used λ -tuning. The reference and measurement filters are manually tuned.

The task can be divided into determining $H_y(s)$ and $F(s)$ to get the robustness and disturbance compensation needed, and then tune the filter $H_r(s)$ such that the reference tracking is as desired.

5.1.1 Disturbance Suppression and Robustness

Disturbance suppression is often an important task for a control system. The effect of a process disturbance $D(s)$ entering the system at the output of the

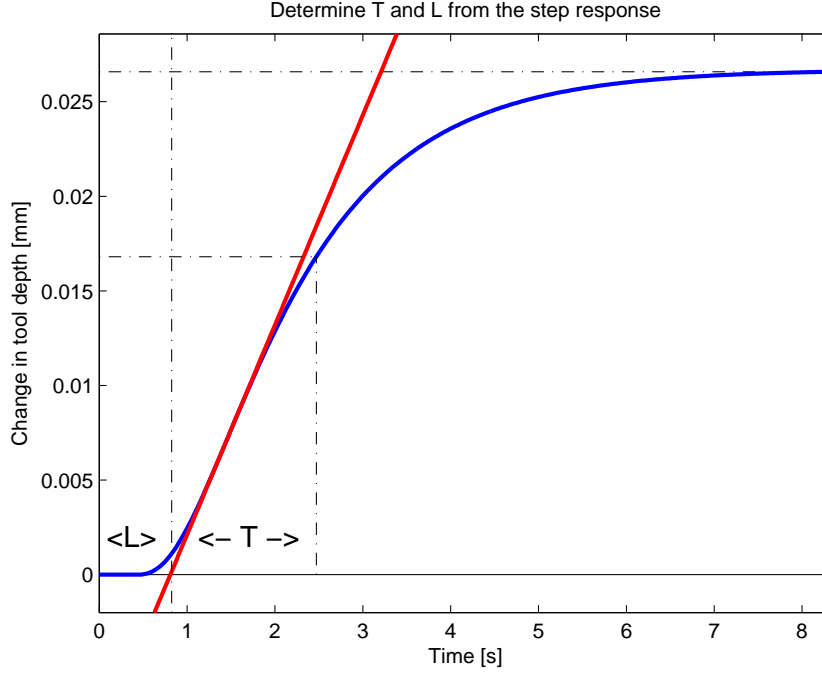


Figure 5.3. A unit step response for the dynamic model from the change in axial force command to the change in tool depth. The parameters L and T are determined from the response, giving $\tau = 0.33$ which denotes a balanced process that is neither lag dominant nor delay dominant.

process (see Figure 5.2) is given by the sensitivity function

$$S(s) = \frac{1}{1 + G(s) \cdot F_y(s)},$$

where $G(s)$ is the model of the system and $F_y(s)$ is one of the transfer functions in the two degrees of freedom controller, see Figure 5.2. A disturbance with frequency ω_0 is attenuated by the factor $|S(i\omega_0)|$. Hence, small values of this factor are desired at all frequencies, but there are fundamental limitations of how small $|S(i\omega)|$ can be (e.g. Bode's integral theorem, Glad & Ljung [13]). A common choice is to make the static gain of the sensitivity function very small and constrain the maximum value of $|S(i\omega)|$ to avoid excessive amplification of disturbances.

Another very important property of a control system is robustness towards modeling errors and measurement noise. Both are closely related to the complementary sensitivity function

$$T(s) = \frac{G(s) \cdot F_y(s)}{1 + G(s) \cdot F_y(s)}.$$

The complementary sensitivity function is the transfer function from measurement

noise $N(s)$ (see Figure 5.2) to the output signal. Hence, a small value of $|T(i\omega)|$ is desired for all frequencies, but the relation $S(s) + T(s) = 1$ must always hold. A common choice is thus to make the factor $|T(i\omega)|$ small at high frequencies. Most measurement noises are high frequent, and they are then attenuated by the control system. Modeling errors may lead to instability of the closed loop system, but the robustness criteria presented in basic control literature states under what conditions stability is preserved. If all conditions are fulfilled, and

$$|\Delta G(i\omega)| < \frac{1}{|T(i\omega)|}, \quad \forall \omega \in \mathbb{R}^+,$$

then the closed loop system is guaranteed to be stable. $\Delta G(s)$ is the relative modeling error describing the relative deviation from the nominal plant model, i.e.

$$\Delta G(s) = \frac{G^0(s) - G(s)}{G(s)},$$

where $G^0(s)$ is the real plant and $G(s)$ is the plant model. A small value of $|T(i\omega)|$ is thus preferred (giving a higher bound on the relative modeling error).

Garpinger's algorithm

This algorithm designs a controller on the form given by (5.2) where

$$H_y(s) = \frac{1}{1 + T_f s}, \quad (PI)$$

$$H_y(s) = \frac{1}{1 + T_f s + \frac{(T_f s)^2}{2}}, \quad (PID)$$

and the cost function is

$$IAE = \int_0^\infty |e(t)| dt.$$

The optimization is constrained by

$$\begin{aligned} |S(i\omega)| &\leq M_S, \quad \forall \omega \in \mathbb{R}^+ \\ |T(i\omega)| &\leq M_T, \quad \forall \omega \in \mathbb{R}^+, \end{aligned}$$

with equality for at least one of the two inequalities at some angular frequency ω^S or ω^T . In Garpinger [11], the IAE is calculated for a disturbance entering the system at the input of the process, but this has been changed for the tuning of the controller in this thesis. The disturbance is now entering at the output of the process, which is assumed to reflect the real system more accurately. The values of M_S and M_T are set to small values to get good disturbance suppression and robustness.

The time constants of the filters are tuned manually. If T_f is chosen low, then measurement noise will have large effect on the control signal, whilst a large value of T_f gives poorer disturbance suppression. The time constants have been chosen differently for the PI and the PID controllers, resulting in

$$\begin{aligned} T_f &= 0.001 \text{ [s]}, & (PI) \\ T_f &= 0.1 \text{ [s]}, & (PID) \end{aligned}$$

The PID needs a filter with lower bandwidth to reduce the oscillations in the control signal. The derivative term amplifies high frequency oscillations in the measurement signal, which thus have to be attenuated by the LP-filter.

Using $M_S = 1.2$, $M_T = 1.2$ and the filter constants above, the optimization gives the following two sets of controller gains:

$$\begin{aligned} PID : & \begin{cases} K_P = 22.23 \\ K_I = 16.6 \\ K_D = 12.9 \end{cases} \\ PI : & \begin{cases} K_P = 11.32 \\ K_I = 7.86 \\ (K_D = 0) \end{cases} . \end{aligned}$$

λ -tuning

The optimal values for the PI-controller are compared with the controller gains calculated using the λ -tuning method. The idea with the λ -tuning method is to define

$$\lambda = \frac{T_c}{T}$$

where T_c is the desired closed loop time constant and T is the time constant of the open loop system. Choosing $\lambda = 3.3$ gives approximately the same closed loop time constant as when the optimal values are used. This gives the PI-controller gains

$$PI : \begin{cases} K_P = 10.52 \\ K_I = 7.2176 \\ (K_D = 0) \end{cases} .$$

Creating a trade-off plot visualizes the relation between IAE, M_S and M_T , Garpinger et al. [12], and in Figure 5.4 the IAE and $\|S\|_\infty$ are plotted in the $K_P - K_I$ -plane for the PI controllers. The red curves are the values of $\|S\|_\infty$ and the blue curves are the IAE (which decreases to the top right part of the figure). The black star is the controller tuning that the optimization algorithm calculated and the green star is the controller parameters calculated using the λ -tuning rules. A similar plot of $\|T\|_\infty$ is given in Figure 5.5.

The figures reveal that increasing the proportional gain (from the one calculated in the optimization) will not decrease IAE significantly, but merely increase the maximum amplitude of the sensitivity function. Increasing the integral gain (especially in combination with a slightly higher proportional gain) could however decrease IAE quite significantly, but at the cost of a higher peak in the sensitivity function. This change of gains is however not increasing the peak in the complementary sensitivity function significantly. The result using λ -tuning is very similar to the optimal values when the closed loop system time constants are the same.

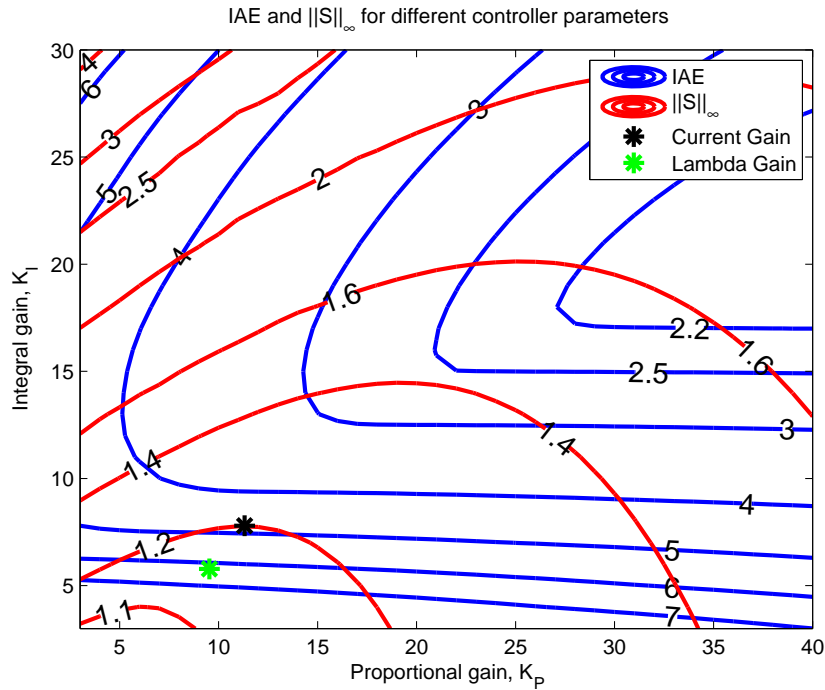


Figure 5.4. Contour plot of IAE and maximum value of the sensitivity function plotted for different values of proportional and integrator gains. IAE is calculated for a step disturbance in tool depth and decreases towards the upper right part of the figure.

5.1.2 Reference Tracking

The reference filter $H_r(s)$ can be chosen to get a desired behaviour of the reference tracking of the closed loop. The reference will not be changed very often, so the tuning has been made to get a static gain of one in the closed loop and a quite slow response in the tracking to avoid excessive control signal amplitudes.

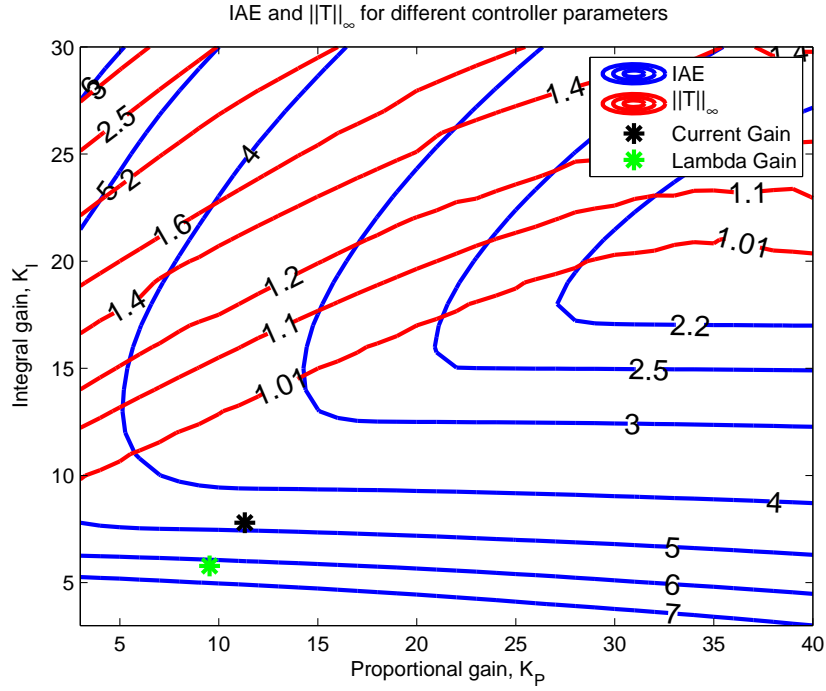


Figure 5.5. Contour plot of IAE and maximum value of the complementary sensitivity function plotted for different values of proportional and integrator gains. IAE is calculated for a step disturbance in tool depth. IAE decreases for gains in the upper right corner of the figure.

Choosing

$$H_r(s) = \frac{1}{1 + T_r s}, \quad (PI)$$

$$H_r(s) = \frac{1}{1 + T_r s + \frac{(T_r s)^2}{2}}, \quad (PID)$$

gives a smooth response for the change in reference. By changing the parameter T_r , the response can be tuned as desired. In the simulations to compare PI and PID, $T_r = 5$ [s] is used. This choice makes it possible to do step changes in the reference without a large transient behaviour, but it is still fast enough for acceptable reference tracking.

5.1.3 Comparison of PI and PID controllers

To decide which controller to use, a comparison of the control performance has been made using simulations. The simulations are made in SIMULINK with Model I

and the control performance for a step change in the reference tool depth has been made together with simulated errors in the model.

During the design of Model I, it was noted that the gain seemed to differ quite a lot, possibly due to fluctuations in temperature and other process variables. It is therefore thought that the most severe modeling errors are connected to the stiffness of the heated material (and hence also the static gain). The simulations have thus also included different disturbances in the stiffness to evaluate how well the two controllers cope with them.

The change in stiffness is tested for two different cases; step changes and ramps. The idea is that the step change could model abrupt changes in stiffness when entering regions with other material properties, whilst the ramping could simulate increasing temperature of the material. This heating of the material will make it softer and hence it should have less stiffness.

The result of the simulation with a step change in stiffness is shown in Figure 5.6. The stiffness is changed to half its value after 110 seconds. The PID controller has a quicker response to both reference changes and stiffness changes, but it seems to have a slightly higher tendency to oscillate. The two PI-controllers performs equally well for both the reference tracking and the modeling error.

When the ramp change in stiffness is applied, the results look quite different. Figure 5.7 shows that neither of the controllers manage to compensate for the disturbance in stiffness completely. It is however clear that the PID controller gives a smaller static control error. The use of the derivative part makes it possible to achieve a higher gain in the controller, but still having the same robustness, which gives a lower static error. The slope of the ramp is such that after 50 seconds (i.e. at 160 seconds of simulation) the stiffness has decreased to half its original value, which is a quite severe disturbance.

Based on those simulations, a PI controller was chosen for the decentralized control. The added complexity from the derivative part does not give much increase in performance. The higher orders of the transfer functions and the extra parameter to tune does not add enough performance to motivate the use of a PID controller. The faster response in the reference tracking is not so important, since the reference will not be changed very often. Besides this, the commanded axial force is smoother with the PI controller, which is seen in Figure 5.8 and a noisy control signal is seldom desired.

Although λ -tuning is a simple tuning method that gives almost the same results as the optimized controller tuning, Garpinger's algorithm will be used to tune the PI-controller. The software is easy to use, and an operator with sparse experience in automatic control should be able to use this software without problem. Besides, it gives guarantees on robustness and disturbance suppression which can easily be changed.

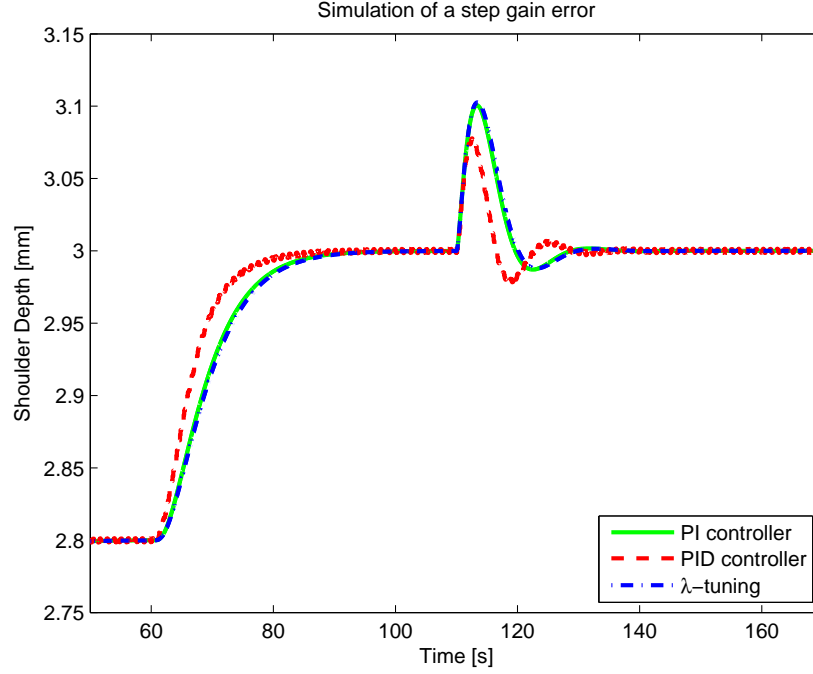


Figure 5.6. Simulated closed loop system with a step in reference at 60 seconds and a step change in stiffness at 110 seconds. The two PI controllers perform equally well while the PID controller has a faster response.

5.1.4 Discretization

The proposed PI controller is described in continuous time (and frequency domain) but since the controller should be implemented on the real time computerized system, it has to be discretized. There are different ways of discretizing a continuous controller, but the controller proposed in this thesis uses Euler forward to get an approximate discrete PI controller. The approximation of the derivative is

$$s \approx \frac{z - 1}{T_s} \quad (5.3)$$

where z is the z-transform variable and $T_s = 0.1$ [s] is the sample time in the system. There are however better methods to discretize, like Tustin's formula, where the derivatives are approximated with

$$s \approx \frac{2}{T_s} \frac{z - 1}{z + 1}$$

giving a more accurate approximation with more complex controller implementation.

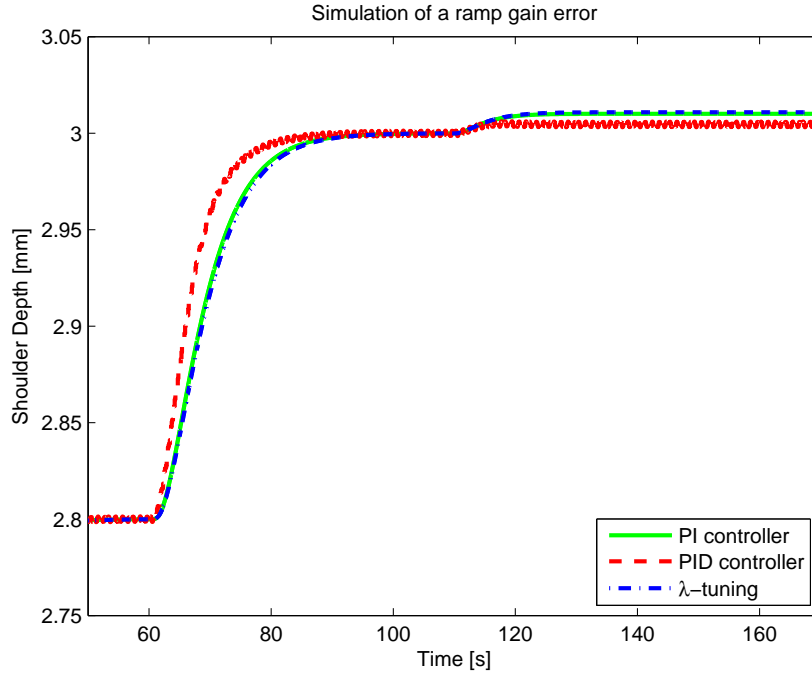


Figure 5.7. Simulation of the closed loop system when a ramp disturbance on the stiffness is applied. At 60 seconds there is a step change in the reference and at 110 seconds the ramp disturbance is applied. The PID controller performs slightly better than the two PI controllers.

The sample time is however more than ten times faster than the time constant of the process (from commanded axial force to shoulder depth), so Euler forward should give a good approximation in this case. Figure 5.9 shows the Bode diagram for the continuous and discrete PI controllers. The discrete approximation is very similar to the continuous controller. Simulation results using the continuous and discrete controllers give almost exactly the same results. The conclusion is thus that the approximation given by (5.3) can be used in this application.

5.1.5 Experimental Evaluation

The decentralized controller has been implemented and added to the existing control system by ESAB. The current implementation uses the position measurements and not the LVDT, and hence the deflection and thermal expansion have to be compensated for. The deflection is calculated according to the model described by (4.1), while the thermal expansion is just included as a constant in the reference. The limits for the force are 77 kN and 91 kN in the first weld and 71 kN to 93 kN

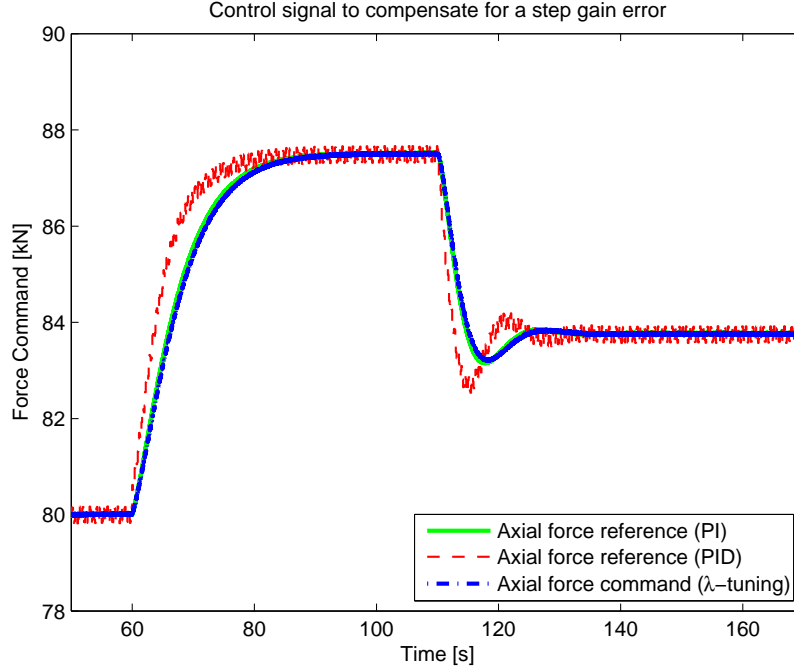


Figure 5.8. The simulated commanded axial forces for the controllers. The PID gives oscillating control signals and slightly higher amplitudes.

in the second, and they are implemented as saturations of the control signal.

The results from two welds are seen in Figure 5.10, where the shoulder depth reference is 1.5 mm. This value will give a real shoulder depth of approximately 2.7 mm with the thermal expansion added. In the first weld, an initialization bug in the code gives a drop from 87 kN to 77 kN (instead of starting at 87 kN) and this drop propagates to the plunge depth which is slightly lower than the reference in the beginning. This bug was fixed and the second weld had a better reference tracking during the start. The downward sequence starts at approximately 14 seconds and ends at 134 seconds for both welds, and after 134 seconds, the welds are performed in the joint line. In the second weld, the upper limit was raised to 93 kN instead of 91 kN in an attempt to find a suitable value.

In the controller used on the real process, the reference filter has a time constant of 20 seconds ($T_r = 20\text{ s}$) and the depth is kept close to the filtered reference during the start and downward sequences. The peaks at approximately 200 and 340 seconds respectively are due to the deformation in the machine. Limitations in the software currently prevents compensating for those. The decrease in depth after 200 seconds in the first weld is due to saturations of the control signal. It is a hypothesis of the author that during the joint line the feedback signal is invalid

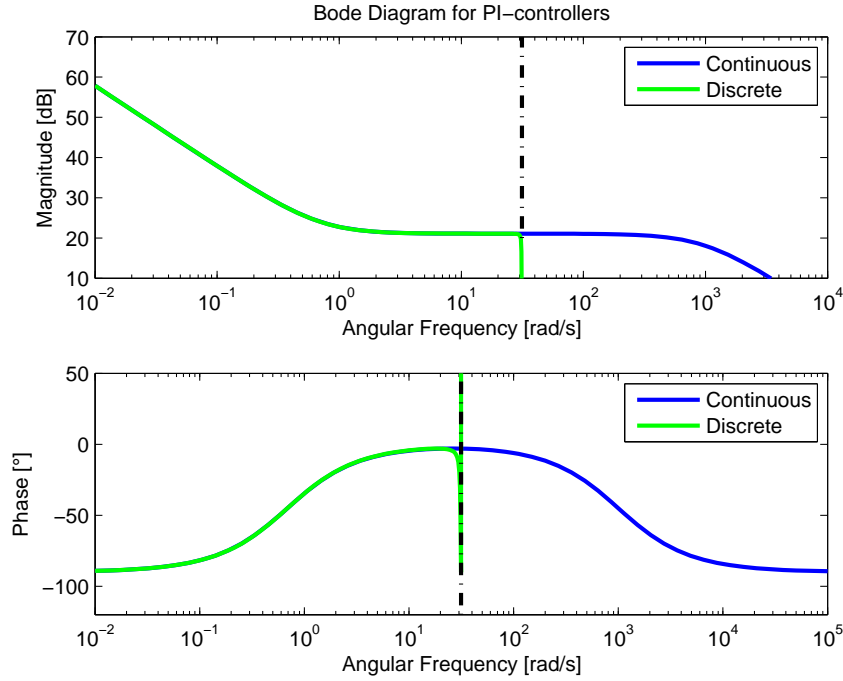


Figure 5.9. Bode diagram for the PI controller. The blue curve is the continuous controller and the green curve is the discrete.

due to uncertainties in thermal expansion and eccentricity. The controller gets a faulty feedback and it is no longer the real depth that is measured because the model of a constant thermal expansion is not valid during the joint line. A similar observation is made for weld number two, but the increased upper limit in the force makes it possible to keep the reference longer. However, more welds need to be done to validate this hypothesis.

The control signals for the two different welds are quite different; in the first weld, the force is high at all time while it is noticeably lower for the second weld. It could be due to a too aggressive tuning of the depth controller which gives a rapid decrease in force when the control error is negative. Such drop in the force will induce a quite severe drop in the torque, which will affect the cascaded temperature controller. Such fast and large changes are thus unwanted, and the controller might need to be re-tuned to get a slower response.

The results from those two welds are promising and a feedback solution using the decentralized controller seems to work well. The influence of the depth controller on the temperature must be evaluated with more welds, and the need for re-tuning the controller could be investigated by observing how well the cascaded controller copes with the torque changes.

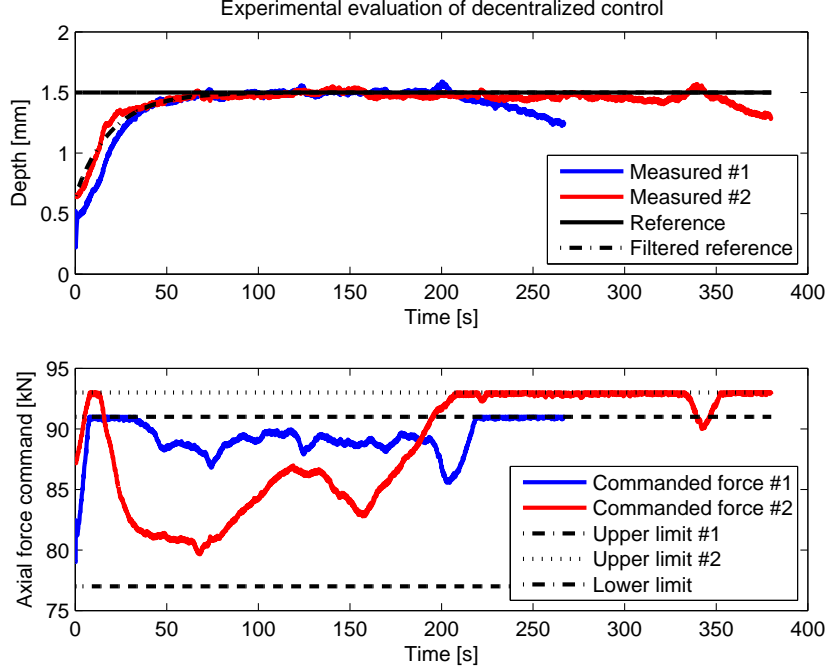


Figure 5.10. Measured data from two welds with the depth controller active. In the first weld, an initialization bug triggers a force drop from 87 kN to 77 kN which affects the depth. After 134 seconds, the welds are performed in the joint line.

5.2 Decentralized Controller II

The second decentralized controller is based on the depth model proposed in Section 4.7.2, called Model II. The linear SISO-system obtained is a decomposition of the depth model and the force actuator, and is described by

$$G_{II}(s) = 0.001592 \cdot \frac{0.967}{0.374 \cdot s + 1} \cdot \frac{1 + 29.56 \cdot s}{s \cdot (1 + 14.67 \cdot s)(1 + 0.00095 \cdot s)} e^{-0.4 \cdot s}, \quad (5.4)$$

which is the transfer function relating the commanded axial force and the change in plunge depth.

This controller has the same structure as the one proposed in Section 5.1, with the same filters on the measurements and reference. However, it is tuned differently since (5.4) has an integrator to describe the creep tendencies. Garpinger's algorithm and the standard λ -tuning rules can not be applied to this system, and the tuning rules used in this section are proposed by Skogestad [28]. Those rules

are designed for the model structure

$$G(s) = \frac{b}{s} e^{-L \cdot s},$$

which is a single integrator with a time delay. The process model II can be approximated with the two parameters b and L according to Figure 5.11. The red curve approximates the slope of the response, giving $b = 0.00268$ and $L = 0.55$. The rule used in this thesis is the one called Skogestad's IMC tuning, Foley et

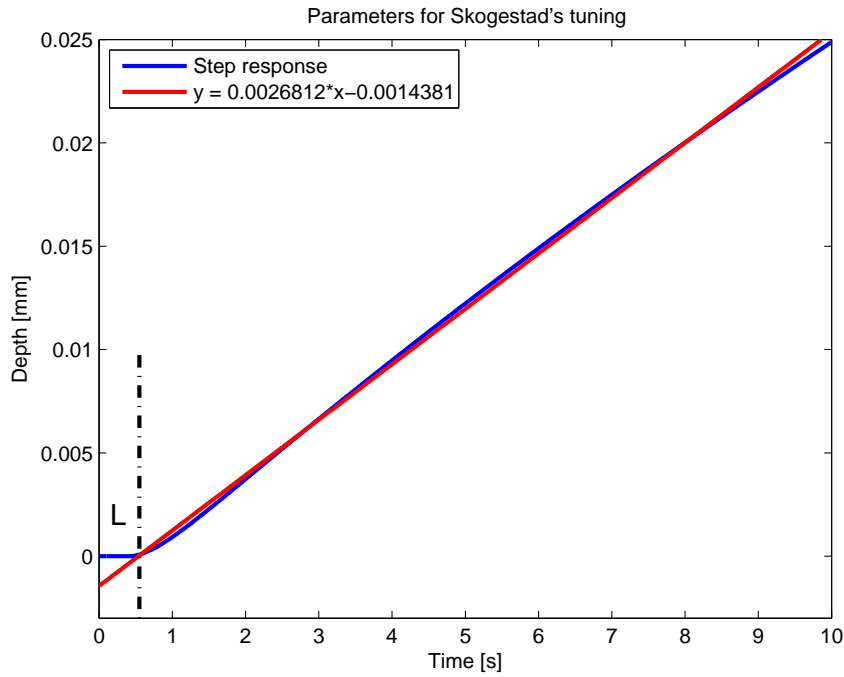


Figure 5.11. The parameters b and L can be derived from the step response by looking at the slope of the response.

al. [10], and this method states that $K_D = 0$. Hence, a PI-controller is tuned for this process using the rules

$$K_P = \frac{1}{b \cdot (\gamma + L)}$$

$$K_I = \frac{K_P}{4 \cdot (\gamma + L)},$$

where γ is a tuning parameter that is used to get the desired time constant for the closed loop system. Here $\gamma = 9 \cdot L$ which gives a closed loop time constant of

approximately 5 seconds. The corresponding controller parameter values are

$$\begin{cases} K_P = 67.8 \\ K_I = 3.08 \\ (K_D = 0) \end{cases}.$$

The proportional gain is about six times larger than in Controller I, but the integral gain is approximately half of the one used in Controller II. This might impose an excessive control signal, which could be solved by increasing the closed loop time constant. No experimental welds using this tuning have been made, and further research is needed to validate the performance of this tuning. Since this controller has the same structure as Controller I (which is implemented on the real system), those controller parameters could easily be tested and evaluated on the real process.

5.2.1 Disturbance Suppression and Robustness

The sensitivity function in Figure 5.12 and the complementary sensitivity function in Figure 5.13 are seen as the blue lines. The magnitude for the sensitivity function decreases for low angular frequencies. Hence, the controller will compensate well for static or low frequent disturbances. With those controller parameters, the peak in the sensitivity function is $M_S = 1.145$, giving

$$|S(i\omega)| \leq M_S = 1.145, \quad \forall \omega \in \mathbb{R}^+,$$

and no sinusoidal disturbance will be amplified more than 14.5%. This value is in the same magnitude as the one chosen in Section 5.1 where Controller I was tuned. The absence of large peaks in the sensitivity function should give good disturbance suppression without any oscillating responses.

The magnitude of the complementary sensitivity function is decreasing for higher angular frequencies, meaning that measurement noise and influences from high frequency modeling errors are attenuated. The large phase lag is due to the time delay in the system. A time delay of L seconds will give a negative contribution to the phase of ωL which is large for high angular frequencies. The magnitude is subjected to

$$|T(i\omega)| \leq M_T = 1.09, \quad \forall \omega \in \mathbb{R}^+,$$

giving good robustness towards modeling errors.

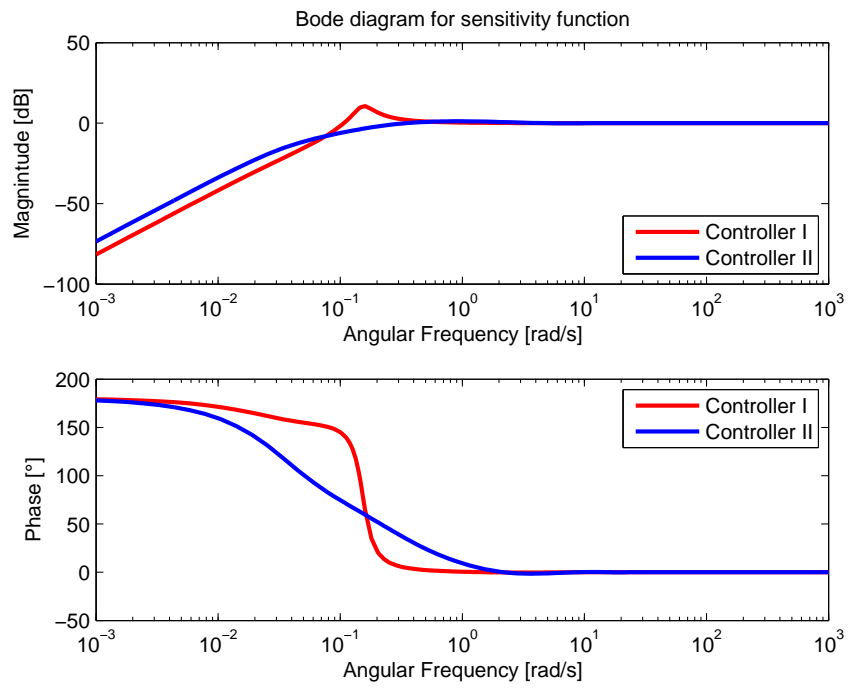


Figure 5.12. Sensitivity function for the closed loop system using Model II and Controller I (red) and Controller II (blue). Controller I has a clear peak in the amplitude.

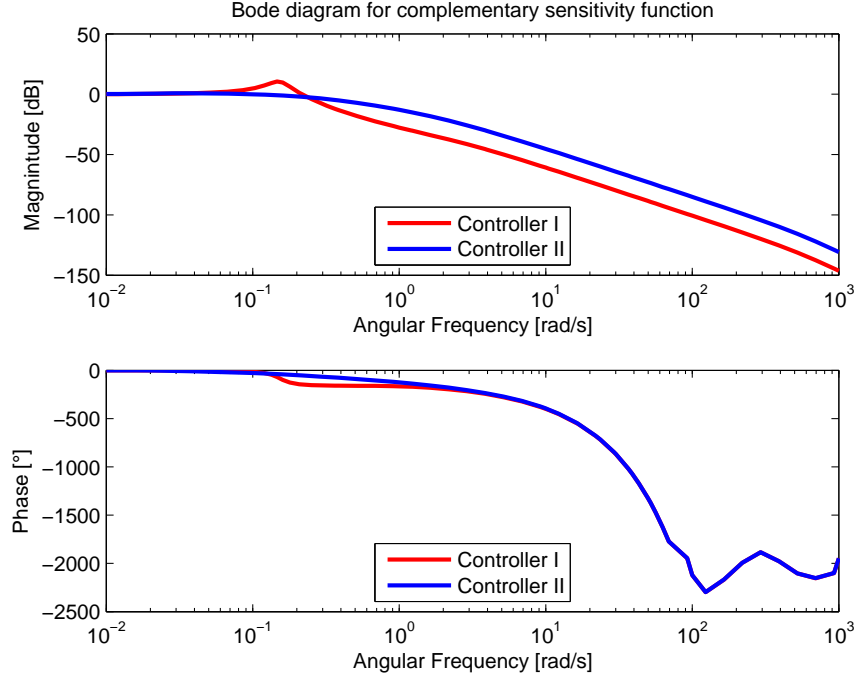


Figure 5.13. Complementary sensitivity function for the closed loop system using Model II and Controller I (red) and Controller II (blue). Controller I gives a closed loop system with a complementary sensitivity function with a clear peak in amplitude.

When Controller I is used to control the depth model II (5.4), the sensitivity function and complementary sensitivity function are given by the red lines in Figures 5.12 and 5.13. There are clear amplitude peaks for both functions, and the corresponding M_S and M_T values are summarized in Table 5.1. If Model II is used, then Controller I has higher M_S and M_T , resulting in a less robust closed loop system. The conclusion is that if Model II is the most valid plunge depth model, then Controller II should perform better than Controller I. Figure 5.14 reveals that a step response in the closed loop system using Controller I oscillates more than when Controller II is used, which is confirmed by the result in Table 5.1.

	M_S	M_T
Controller I	3.37	3.34
Controller II	1.15	1.09

Table 5.1. M_S and M_T for the two controllers when the second depth model is used. Controller I is less robust than Controller II when Model II is used.

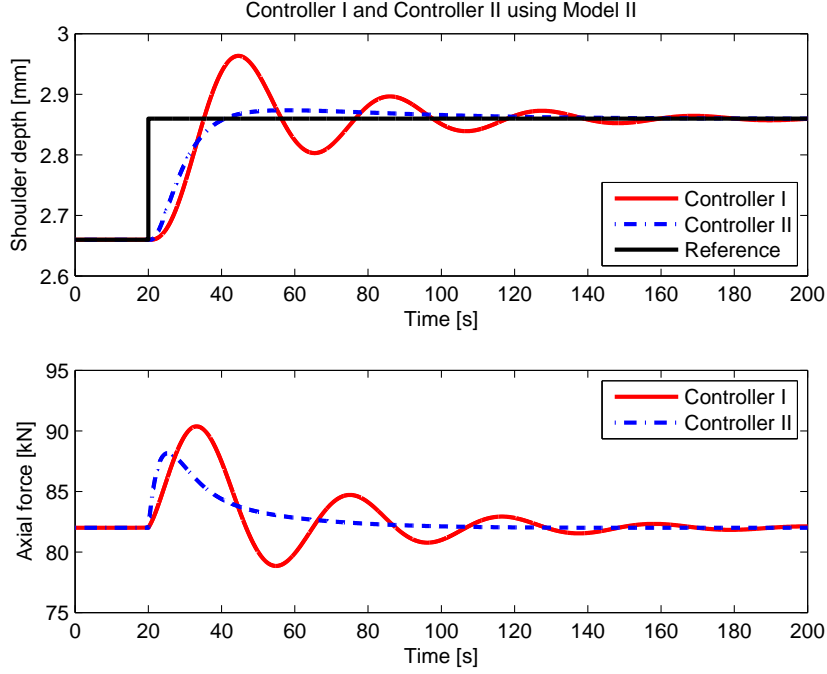


Figure 5.14. Closed loop simulation using Model II. Controller II has a higher performance without the oscillations that appear when using Controller I.

5.2.2 Reference Tracking

The reference filter is a first order linear filter with time constant T_r , just as the case for Controller I. The time constant is tuned to get an acceptable reference tracking without excessive control signals. The final tuning will be done when evaluating the controller on the real process. In the simulation in Figure 5.15, $T_r = 5$ is used. At time 20 seconds, a step in reference from 2.8 mm to 3 mm is made, and at time 200 seconds, a step change by a factor 1.5 in the gain is made. The step response has an overshoot but seems to be without oscillations and the modeling error appearing at 200 seconds is handled well.

5.3 Non-linear Model Predictive Control

In non-linear model predictive control, a model of the process is used to optimize the control signal. The optimization is given as a Non-linear Programming (NLP) problem that is solved by a suitable solver over a finite time interval. The problem consists of an objective function and a set of constraints that must be satisfied.

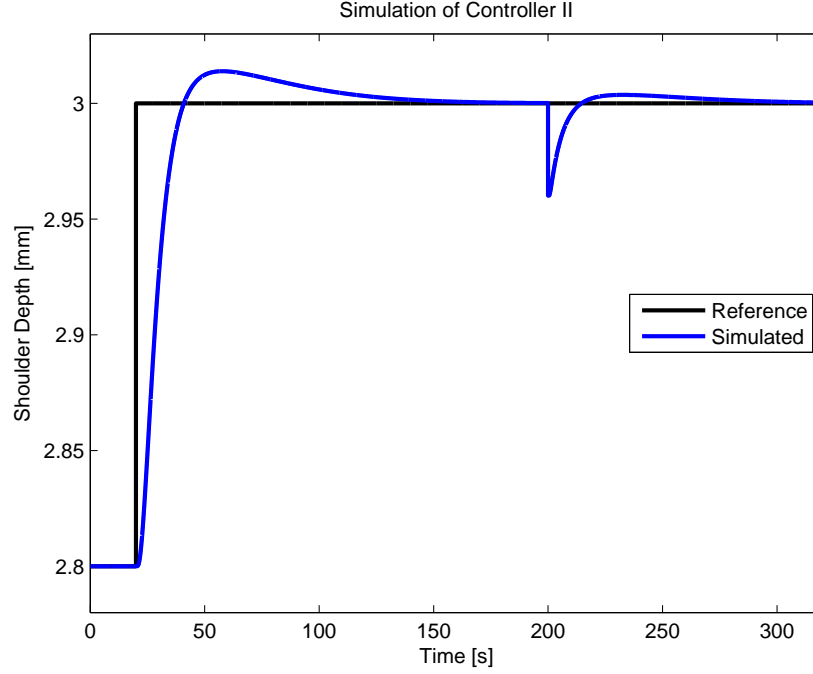


Figure 5.15. Simulation of Controller II. At time 20 seconds a step in reference from 2.8 mm to 3 mm is applied. A step change in the process gain is applied at time 200 seconds.

By changing the objective function and/or the constraints, different control performances are achieved. Figure 3.4 shows the block diagram of the feedback solution using NMPC to control depth and stir zone temperature (the block depicted by "Controller" is now the NMPC). The NLP problem is solved *every iteration* of the control loop, using the measurements as initial values on the measured states to get feedback from the process. Table 5.2 describes the nomenclature used for NMPC.

An extensive description of model predictive control is given in Maciejowski [19], where the basic idea is described together with other subjects. Only linear model predictive control is described in this literature, but the basic idea of MPC is the same as for NMPC.

5.3.1 Optimization Problem

The objective function and constraints can be formulated in different ways and the basic idea when constructing the objective function is that deviations from the setpoints of the controlled variables should add a cost of some sort. Depending

Nomenclature in optimization problems	
Φ	objective function
y_m	model values $(y_{m,0}, \dots, y_{m,n})^T$
y_s	measured values $(y_{s,0}, \dots, y_{s,n})^T$
$y_{t,hi}, y_{t,lo}$	desired trajectory dead-band
w_{hi}, w_{lo}	penalty outside trajectory dead-band
$c_y, c_u, c_{\Delta u}$	cost of y, u and Δu , respectively
f	equation residuals
x	states
u	inputs
d	parameters or unmeasured disturbances
g	output function
h	inequality constraints
a	upper limits
b	lower limits
τ_t	time constant of desired controlled variable response
e_{lo}	slack variable below the trajectory dead-band
e_{hi}	slack variable above the trajectory dead-band
sp	setpoint for the controlled variables
sp_{hi}	upper dead-band setpoint
sp_{lo}	lower dead-band setpoint

Table 5.2. Nomenclature of the constants and variables used in the NLP problems given by (5.5) and (5.6).

on the choice of objective function, the optimization is either a minimization or a maximization. The controller in this thesis uses objective functions that are minimized. One commonly used approach is to use the \mathcal{L}_2 -norm to create an NLP problem according to

$$\begin{aligned}
\min_u \Phi &= \min_u (y_m - y_t)^T W_t (y_m - y_t) + y_m^T c_y + u^T c_u + (\Delta u)^T c_{\Delta u} \\
s.t. \quad &0 = f(\dot{x}, x, u, d) \\
&0 = g(y_s, x, u, d) \\
&a \geq h(x, u, d) \geq b \\
&\tau_t \frac{\partial y_t}{\partial t} + y_t = sp.
\end{aligned} \tag{5.5}$$

The \mathcal{L}_2 -norm of the deviation of the controlled variables (y_m) from their setpoints (y_t) adds a cost to the minimization, hence this deviation will be kept small by the controller. The cost is given by the cost matrix W_t and there are also costs added for the control signal and the delta movement in the manipulated variable.

The minimization is subjected to a set of constraints that represent the model of the system together with some constraints on the variables.

Another choice, used in the controller proposed in this section, uses instead the \mathcal{L}_1 -norm to calculate the objective function. This choice is better at explicitly prioritizing the control objectives, Hedengren et al. [14]. The idea with this approach is to define a dead-band within which the controlled variable should be kept. If the value is outside this dead-band, it will be penalized by an increased cost. The NLP problem is given by

$$\begin{aligned}
\min_u \Phi &= \min_u w_{hi}^T \cdot e_{hi} + w_{lo}^T \cdot e_{lo} + y_m^T \cdot c_y + u^T \cdot c_u + (\Delta u)^T \cdot c_{\Delta u} \\
s.t. \quad &0 = f(\dot{x}, x, u, d) \\
&0 = g(y_s, x, u, d) \\
&a \geq h(x, u, d) \geq b \\
&\tau_t \frac{\partial y_{t,hi}}{\partial t} + y_{t,hi} = sp_{hi} \\
&\tau_t \frac{\partial y_{t,lo}}{\partial t} + y_{t,lo} = sp_{lo} \\
&e_{hi} \geq (y_m - y_{t,hi}) \\
&e_{lo} \geq (y_{t,lo} - y_m),
\end{aligned} \tag{5.6}$$

where the slack variables e_{hi} and e_{lo} together with the inequalities are introduced to relax the use of absolute values. This makes the objective function smooth and continuously differentiable which is a requirement for large-scale NLP solvers. Besides the constraints given by the model and limits on the variables, there are also constraints for the upper and lower limits on the dead-band. The limits will be described by first order linear differential equations with time constants given by τ_t . These time constants are thus the desired time constants for the controlled variable responses and can be tuned to change the closed loop performance. The objective function will add a cost to the minimization if the controlled variables are outside the dead-band, but it will also add a cost for delta movements in the control signal. A cost for the manipulated variable and the controlled variable are also included.

The optimization problem is not changed if all weights are scaled by a constant k . This is realized by looking at the objective function Φ . If all weights are scaled, then the equation for the minimization is

$$\begin{aligned}
\min_u \bar{\Phi} &= \\
&\min_u (k \cdot w_{hi}^T \cdot e_{hi} + k \cdot w_{lo}^T \cdot e_{lo} + k \cdot y_m^T \cdot c_y \dots \\
&+ k \cdot u^T \cdot c_u + k \cdot (\Delta u)^T \cdot c_{\Delta u}) = k \cdot \min_u \Phi
\end{aligned}$$

which will calculate the same u (but of course a different minimal value). As a

consequence, only the relation between the weights are important, not the actual values.

The optimization problem is solved over a finite time horizon every iteration. The controller in this thesis uses the time horizon

$$t = [0 : 0.1 : 5, 7, 10, 15]^T,$$

where MATLAB syntax has been used. The second part of the vector ($[7, 10, 15]^T$) is added to get predictions further ahead without adding a large number of extra variables to the optimization problem.

5.3.2 Controller Parameter Tuning

The model derived in Section 4.10 (without the torque dependence on rotation speed) is used to design and tune the non-linear model predictive controller. The tuning to get the desired performance is made by changing the settings of the optimization problem. The most important tuning parameters are the weights used in the objective function, but there are also settings for the NLP solver that can be tuned to get good results, e.g. the number of nodes used in each horizon step. The time constant of the response (τ_t) is another tuning parameter and this is set to 5 seconds in the controller proposed here. This parameter may be tuned to fit the desired response of the real process, but since this has not been evaluated, a fix value of τ_t is used.

In this thesis, the tuning was done mainly in two steps, first the settings for the NLP solver was set to get a solution that converged with good numerical properties and then the weights were tuned to get the desired closed loop response. Since the default solver in APMONITOR (APOPT) has proven to work well, this large-scale NLP solver has been used in all simulations in this section. The optimization settings can be changed using the APMONITOR interface, and for all settings except one, the default values has been used. The number of nodes used in every prediction horizon has been set to 2 (default 4) to decrease the solution time. The step sizes in the manipulated variables have been constrained to 10 kN respectively 30 RPM, preventing excessive movement in the control signal.

The tuning of the weights is an iterative process; first apply a weight and then simulate the closed loop system and then re-tune the weights and simulate again. This is done until a desired performance is achieved. Looking at the objective function in (5.6) gives a guidance on how to change the weights to affect certain properties of the closed loop system. All terms in the objective function are on the form $w \cdot e$, where w is the weight and e is the corresponding variable. Increasing the weight w will force the optimization to decrease the variable e , and this is the main idea when tuning the controller. Besides this, the tuning will be a compromise between fast response, disturbance suppression and a control signal without excessive magnitudes.

The cost c_u and c_y are set to zero, since there should not be a penalty of a non zero controlled variable and control signal (to keep the controlled variable at the non zero setpoint, a non zero control signal is required). The objective function is thus

$$\Phi = w_{hi}^T \cdot e_{hi} + w_{lo}^T \cdot e_{lo} + (\Delta u)^T \cdot c_{\Delta u},$$

and the weights are set to $w_{hi} = w_{lo} \equiv w$ since a deviation above the dead-band should be penalized equally as a deviation below the dead-band. Hence, there are two vector valued weights $w = [w_{Pz} \ w_T]^T$ and $c_{\Delta u} = [c_{Fz} \ c_\omega]^T$ that have to be tuned. The dead-bands are set to be $\pm 0.1^\circ C$ from the desired stir zone temperature and $\pm 0.002 \text{ mm}$ from the desired plunge depth. Those values are chosen in an ad hoc manner, and they might be too restrictive for the real process and could be changed when doing real time control.

The closed loop system is simulated for step changes in the reference of plunge depth and temperature. Figure 5.16 shows the simulated controlled variables from two simulations with different weights in the objective function (everything else the same). Figure 5.17 shows the corresponding control signals and the first set of weights are referred to as "Tuning I". The weights on the controlled variables were chosen to one and the cost on the delta movement were chosen to the default values 10^{-5} , i.e.:

$$w = \begin{bmatrix} 1 \\ 1 \end{bmatrix}, \quad c_{\Delta u} = \begin{bmatrix} 10^{-5} \\ 10^{-5} \end{bmatrix},$$

and the simulated closed loop responses for step changes in the references are depicted as the red curve in Figure 5.16 (and the same for the control signal in Figure 5.17). The figures reveal that the effect of a step change in plunge depth is handled well but the step change in temperature affects the plunge depth. The control signal (in particular the axial force command) oscillates quite a lot in some time intervals, which is not desired.

In order to increase the performance, the weights were changed iteratively until a satisfying result was obtained. The weight for the temperature is kept from the first iteration since its response is considered satisfactory. To be able to decouple the depth from the temperature, a larger weight is set on the depth. Hence, the deviation in depth will be penalized harder and the optimization algorithm will thus keep this deviation smaller. To get a smoother axial force command, the cost for the delta movement in axial force command was increased. The final set of weights, referred to as "Tuning II", is

$$w = \begin{bmatrix} 100 \\ 1 \end{bmatrix}, \quad c_{\Delta u} = \begin{bmatrix} 1 \\ 0.01 \end{bmatrix},$$

and the simulation using these weights are seen as the blue curves in Figures 5.16 and 5.17. With this choice of weights, the depth and temperature are almost completely decoupled and the step changes in one controlled variable do not affect the other. The commanded axial force is also much smoother while the commanded spindle rotation speed is almost the same as before. A deviation in plunge depth

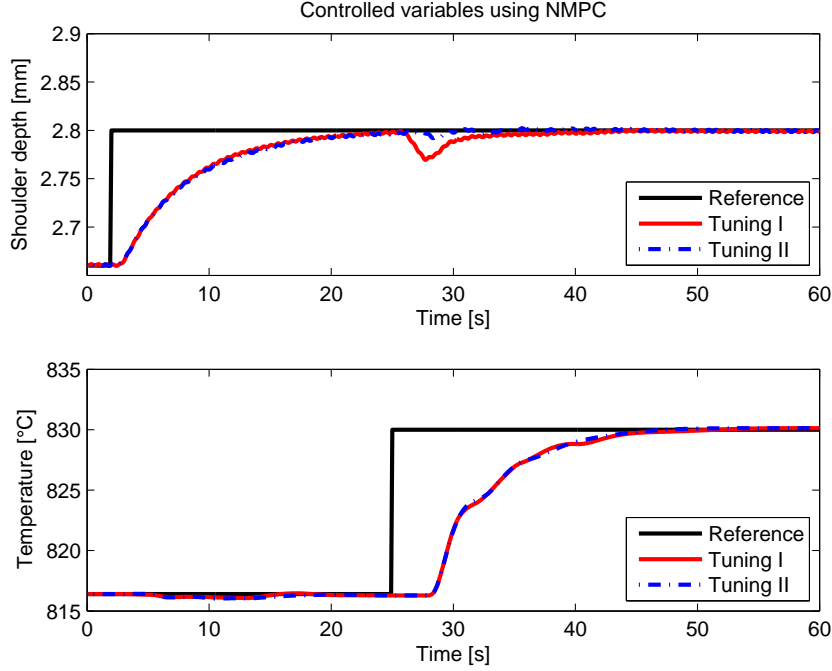


Figure 5.16. Simulated controlled variables for two different tunings. Tuning I is the first attempt and Tuning II is the final attempt. The simulations using Tuning II gives an almost completely decoupled response with nice behaviour. The black lines are the reference values for respective output variable.

with magnitude equal to one dead-band width is penalized twice as much as a comparable deviation in the temperature.

Using Tuning II gives a satisfactory reference tracking, but the disturbance suppression and robustness can not be investigated as straightforward as was done in Sections 5.1 and 5.2. For example, there are no analytically robustness results proving closed loop stability when the model deviates from the nominal plant. Those properties of the control system will be addressed in Section 5.4 where a comparison of the controllers is presented. Although no analytical results can be derived, a hint of the robustness and disturbance suppression is obtained by simulate the closed loop system for different modeling errors and disturbances.

5.4 Comparison of Control Strategies

The two different controller structures proposed in this thesis have been evaluated according to the criteria from Section 1.3, and the results are summarized in this

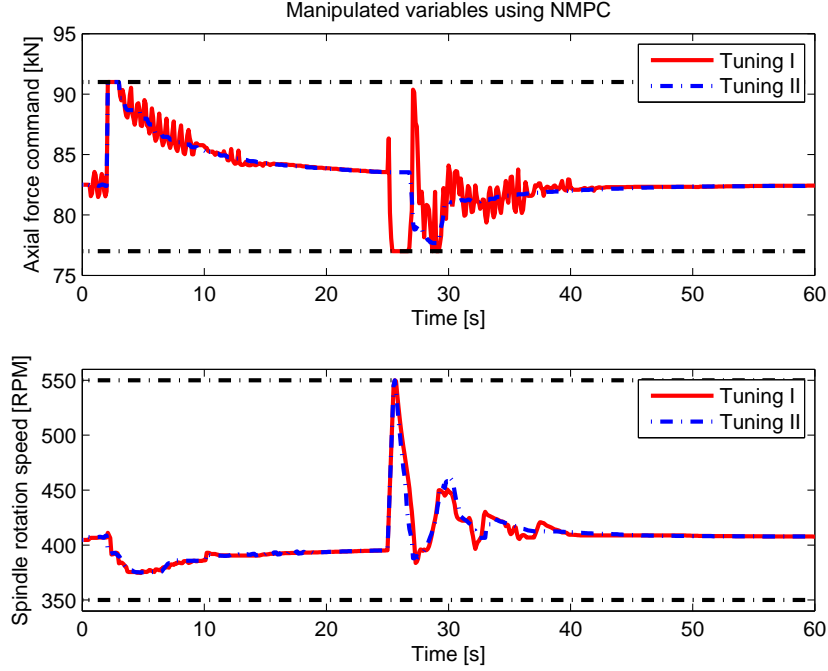


Figure 5.17. Simulated manipulated variables for two different tunings. Tuning I is the first attempt and Tuning II is the final settings. The dash-dotted black lines are the upper and lower limits on the control signals.

section. Even though there were two different controller tunings for the decentralized control, only Controller II will be used in the comparison. The difference between the *controller structure* is then compared without influences from a *controller tuning* based on another model. This fact is confirmed by Figure 5.14 where Controller I is used to control Model II. The performance is much less than with Controller II, and using Controller I to compare the controller strategies might give misleading results. The evaluation has been made using simulations in AP-MONITOR and MATLAB with the full model without the spindle speed rotation correction factor derived in Section 4.10. This version of the model was chosen since it is a hypothesis of the author that the accuracy of the ad hoc correction factor used to model the torque's dependence on rotation speed is low. The simulated temperature is more accurate when the correction factor is not used, and it is more important to have an accurate model of the temperature than of the torque.

The main focus when comparing the controllers is how well they cope with the cross-connections. The cascaded controller already used in the system is tuned to be very robust and its response is slower than the NMPC-controller. The depth controller and the NMPC controller might be too aggressive and it is possible that

those have to be re-tuned after implementation. This should be kept in mind while evaluating the two controller designs.

5.4.1 General Differences

The two proposed control strategies are both feedback solutions, but they are quite different. The major drawbacks with the NMPC-solution is its need for a fairly complex model of the system, the computational complexity and the absence of guaranteed convergence of the optimization problem. The simulations of the NMPC in this thesis takes about 3-4 seconds per iteration, which is far too much for an on-line real time controller. This could however be reduced significantly by using fast non-linear model predictive control, but this topic is outside this thesis and will not be addressed. There are neither any guarantees that the optimization problem will converge nor how fast the solver will find a solution, and this could be a problem in a real time implementation of the controller. This problem is not addressed in this thesis either, since the main goal is to evaluate the possible increase in controller performance using NMPC, not implementing it on the real process. None of those problems are encountered using the decentralized control. The computational complexity is low and there are no problems to calculate the control signal at 10 Hz.

The NMPC-solution though has benefits over the less complex solution with the PI-controllers; it can handle the cross-connections in an effective way, and bounds and limits on the state variables, controlled variables and manipulated variables are simple to add.

5.4.2 Reference Tracking

A comparison of the reference tracking performance is made by applying two steps; one in desired plunge depth and one in desired temperature. The result is seen in Figure 5.18 with the control signals in Figure 5.19. The depth is controlled almost equally well by the two controllers, but the NMPC-controller has a slightly better response. The step in desired plunge depth however results in a quite large bump in the temperature for the decentralized controller. This is a consequence of increased axial force command. The cascaded controller compensates for this disturbance, but the compensation is quite slow. The NMPC-controller manages to decouple the depth response from the temperature, keeping the temperature at the reference. At the step in temperature, both controllers manage to keep the depth close to the reference.

The step responses in desired temperature are quite different; the NMPC-controller manages to increase the temperature without any oscillations or overshoot, while the cascaded temperature controller gives an overshoot and is much slower to settle. The time constant of the NMPC-response is set to $\tau_t = 5$ but this might be

an optimistic value, and increasing this would get a response that is more equal in rise-time.

The corresponding control signals are seen in Figure 5.19. The manipulated variables are quite similar, except for the fact that the NMPC-controller uses larger and more rapid changes to compensate for the cross-connections. Whether these changes are too abrupt or not for the real process is not validated. Both controllers have control signals without any large oscillations.

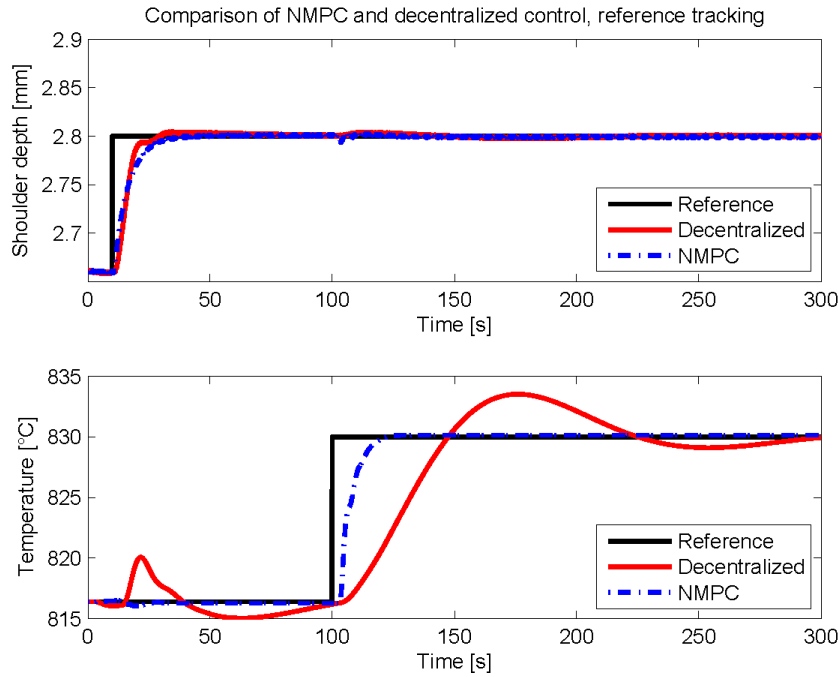


Figure 5.18. Simulations for step changes in desired plunge depth and desired temperature for the two controller structures. The cascaded temperature controller has a slower response than the NMPC, but it could be that the NMPC-controller is too aggressive.

5.4.3 Disturbance Suppression and Robustness

The robustness of the controllers has been compared by simulating the system for modeling errors in the gains of the depth and temperature models. The second column in Figure 5.20 shows the multiplicative disturbances in the gains and the simulation result is seen in Figure 5.21 with the corresponding control signals in Figure 5.22. Both controllers handle the abrupt errors in the models well, but the NMPC is a lot faster to control the variables to their setpoints. It does not seem to be any strange oscillations in the response for the modeling errors

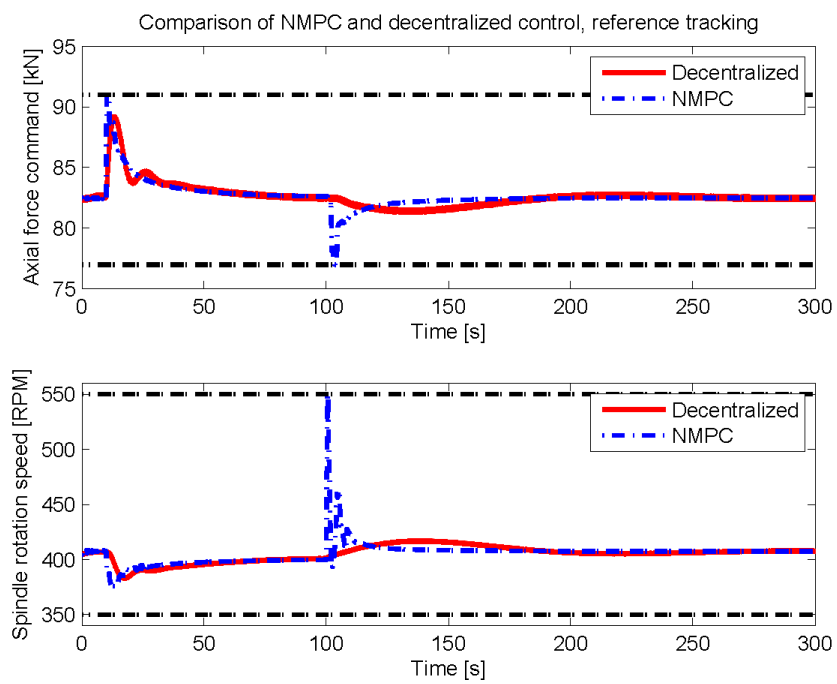


Figure 5.19. Simulation of the control signals when a step in desired plunge depth and temperature is applied. The controllers gives similar control signals, but the NMPC-controller uses the signals more actively to decouple the system.

and the controllers seems to not have any robustness issues for this type and magnitude of errors. Figure 5.21 also reveals that there are cross-connections that are not considered in the decentralized control; at approximately 70 seconds the temperature starts to rise as a consequence of an increased axial force. This type of cross-connections are handled well by the NMPC-solution.

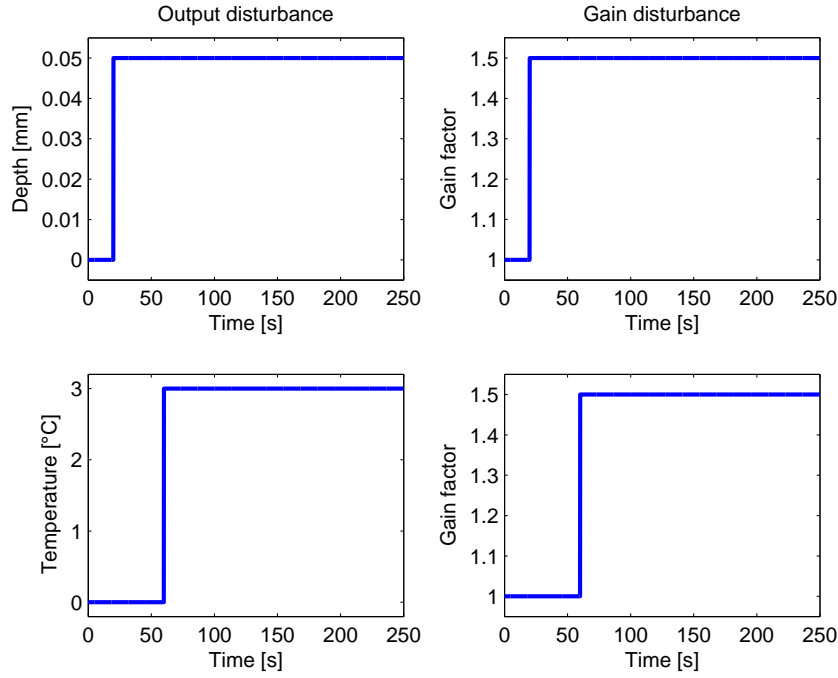


Figure 5.20. The first column is the output disturbances for depth and temperature which are used to simulate the closed loop disturbance suppression. In the second column, the multiplicative gain factors are presented. The changes are made at 20 respectively 60 seconds.

The controller performances when step disturbances acts on the plunge depth and temperature have been simulated to evaluate the disturbance suppression. The result is seen in Figure 5.23 with the corresponding manipulated variables in Figure 5.24, and it is very similar to the robustness simulation. The disturbance in depth at 20 seconds induces a notch of 3°C in the decentralized control, and the temperature starts to increase at about 70 seconds due to an increase in the axial force. Both depth controllers manage to keep the depth close to the reference, and the PI-controller is somewhat faster to suppress the disturbance than the NMPC. A too fast PI-controller might be a problem in the real implementations, since it is hard for the cascaded temperature controller to compensate for the fast changes in torque induced by the rapid change in axial force.

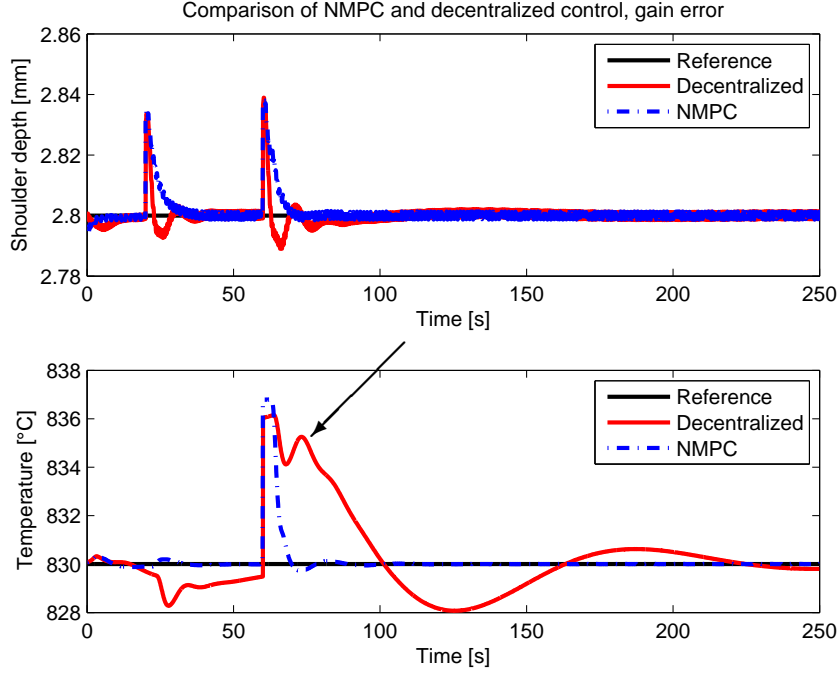


Figure 5.21. Simulation of the response for abrupt modeling errors. At 20 seconds a step change in the gain for the depth model is applied and at 60 seconds a similar error is applied to the temperature gain. The NMPC gives a fast and damped response while the decentralized control gives more oscillations.

5.4.4 Violation of Bounds

The simulations in the two previous sub-sections have had quite small changes in the controlled variables, and hence the decentralized controller has not calculated control signals outside the limits. Figure 5.25 shows a simulation for a step change in the desired depth of magnitude 0.5 mm. This is significantly larger than the ones used in the previous simulations. The corresponding control signals are seen in Figure 5.26, and it is clear that the decentralized controller calculates a control signal that is outside the limits. This would imply that the control signal will be saturated, resulting in a decreased performance. The implementation of this controller therefore includes anti-windup (i.e. prevents the integral part to increase when the control signal is saturated) to reduce the effect if the saturation. The NMPC, however, copes with the limits well since they are included in the optimization problem. This is one of the cases when NMPC/MPC outperforms most other controller designs.

The decentralized depth controller manages not to keep the plunge depth at the

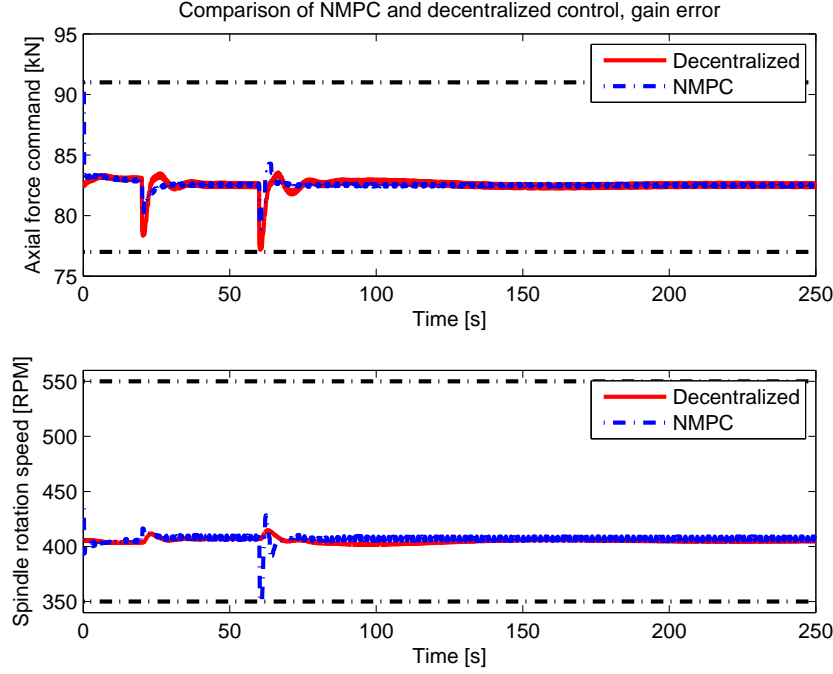


Figure 5.22. Simulated control signals for abrupt modeling errors in the temperature and depth models.

reference in the beginning (although it uses an excessive control signal). This might be an indication that the time constant in the reference filter is set too low in the simulations. This fact is also confirmed by the experimental evaluation in Section 5.1.5 where a time constant of 20 seconds is used.

5.4.5 Simplicity to Tune and Maintain

During the years of operation the controller might need to be re-tuned, and this is done slightly different for the two controller structures. The decentralized control is simpler to tune if it is done using step responses for the process, while manually tuning the NMPC-solution is more intuitive than manually tuning the PI-controller. Depending on the operator that will tune the controller, either of these methods could be used. There is a clearer connection between the NMPC parameters (the weights) and the controlled variables response than between the PI-gains and the output variables; the operator increases the weight on the controlled variable that needs to be regulated better instead of changing the gains in the PI-controller.

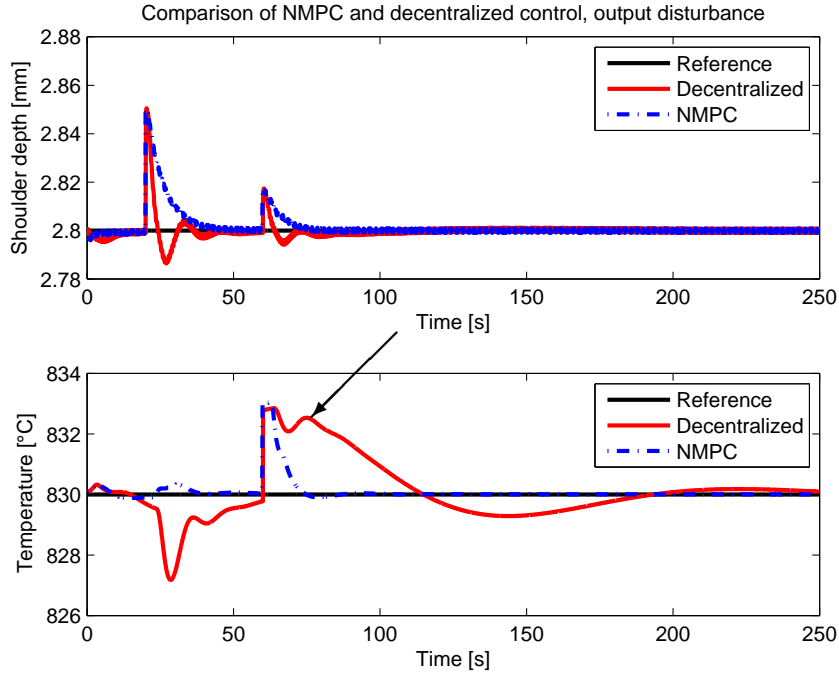


Figure 5.23. Simulation of an output disturbance at the plunge depth and the temperature. The NMPC-controller handles the disturbances better than the decentralized control.

However, the best way to tune the parameters would probably be to change the models for the system and then tune the gains using the new model. In this case, the decentralized control is much more convenient to use, since the modeling work is much less complex than the modeling for the NMPC-solution. It is easier to do step responses in axial force and fit a process model to the measured data, use this model to tune the PI-gains according to some rule (e.g. the methods used in this thesis) than to find a new version of the full model used in the NMPC-design.

The conclusion is that if the process needs to be modeled again, then the decentralized solution is much simpler to use than the NMPC-solution. If the controllers are however manually tuned, then the NMPC is more intuitive to tune.

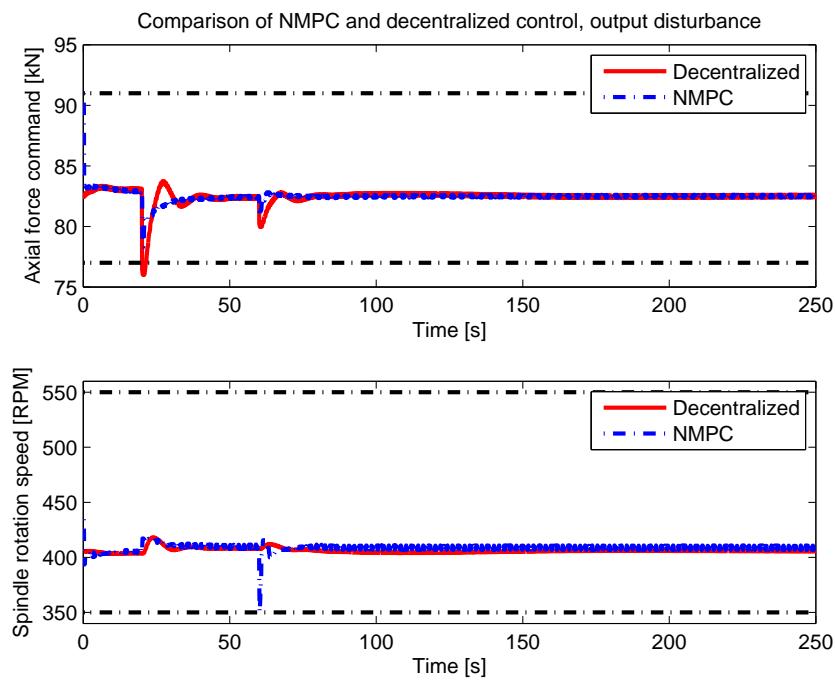


Figure 5.24. Simulated control signals when step disturbances entering at the outputs are applied. The manipulated variables are similar, but the NMPC changes the spindle rotation speed more rapid to decouple the system.

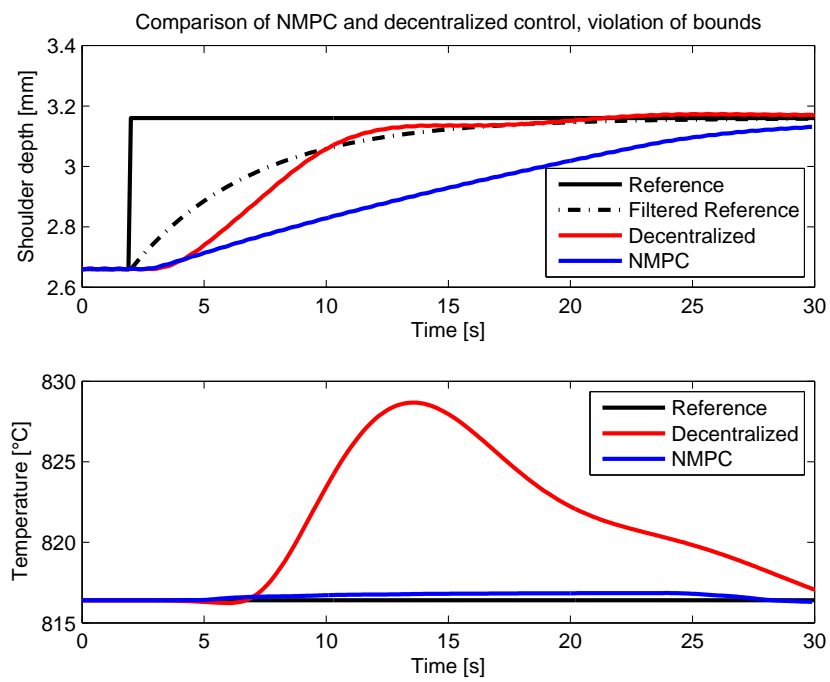


Figure 5.25. Simulation of a large step in the desired plunge depth. Even though the decentralized controller calculates excessive control signals, it manages not to keep the desired plunge depth in the beginning.

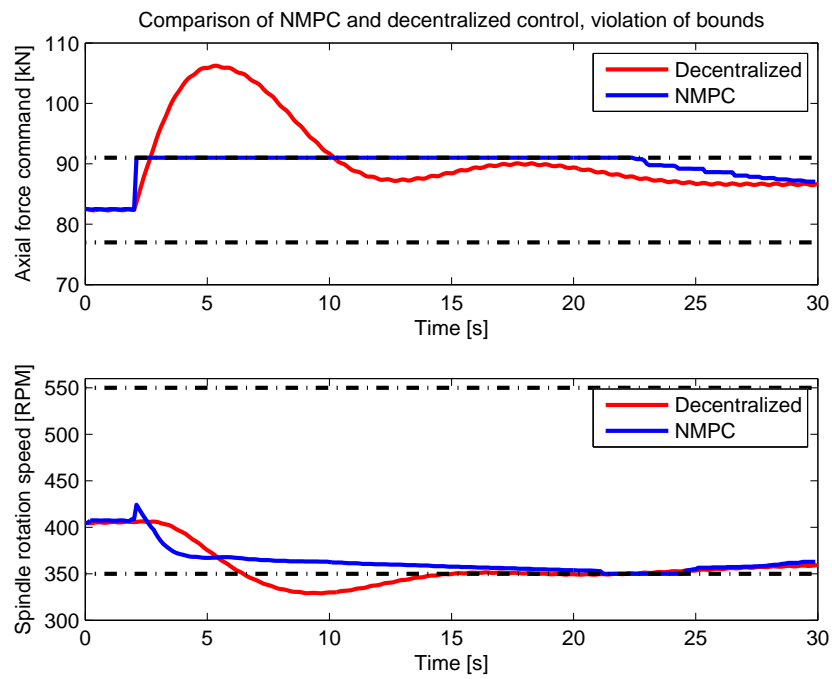


Figure 5.26. The simulated control signals for a large step in the desired plunge depth. The decentralized PI-controller calculates a control signal that is far outside the allowed limits.

Chapter 6

Results and Further Work

The work of this thesis has produced both results and new insight into the task of controlling the welding depth in friction stir welding. This insight has raised new questions and further work to be done has been discovered. This chapter intends to summarize the results obtained during the work of the thesis, but also present the further work that could be done in this research area.

6.1 Results

The results obtained in this thesis are promising and the main purposes and goals of the thesis are met. Two different model structures have been designed; a SISO-system for the plunge depth only and one complete model of the full system. Those have been used to design the controllers proposed in the thesis.

A decentralized solution to control the plunge depth during start and downward sequence has been implemented and the first welds have given satisfying results. There is still work to be done regarding the tuning of this controller, but the main design and strategy seems to work well. Simulations have shown that the cross-connections in the system could be handled fairly well by the PI-controllers, but this has not yet been fully experimentally evaluated. The implemented controller uses the tool position measurements as feedback, but an evaluation of the sensors states that it would be better to use a sensor that measures the actual plunge depth instead. The LVDT-sensor could be used to evaluate the controller with this type of feedback, but for the final control solution another sensor is probably needed. It is a hypothesis of the author that the position measurement should not be used to control the depth during the joint line, and it requires more effort spent on modeling the thermal expansion to use it effectively at the start and downward sequence.

The complete model has been used to evaluate an NMPC-solution for the combined depth and temperature control. An increase in performance is gained by using the more complex structure and an almost decoupled closed loop system is achieved, where a change in the desired plunge depth is not affecting the temperature and vice versa. The NMPC-controller has only been evaluated using simulations since there are limitations in the control system that prevents an implementation today. The solution time for the NMPC is also far too long to be used in a real time situation and more effort need to be spent if the NMPC should be implemented on the real system. Depending on how the decentralized control will perform in reality, NMPC could however be a very attractive control design.

6.2 Further Work

Some ideas and plans for future work on plunge depth control have been developed and are presented here. Some of them are closely related to the proposed controllers in this thesis, while some of the ideas are regarding the control during the joint line.

The controllers proposed in this thesis must be thoroughly evaluated by running several welds before it is decided which one to use. There are two different controller tunings for the decentralized control, and which one is the best could be evaluated by comparing the performance of the controllers during the welds. Besides this, the limits on axial force should be further investigated to get as large process window as possible, without jeopardizing the process window of the temperature. The experimental results in Section 5.1.5 indicate that the upper limit might be too conservative and that it could be increased up to maybe 95 kN or even larger values.

A more extensive research regarding the depth's dependence on temperature could also be made. The ad hoc solution proposed in this thesis might be improved by deriving a relation based on physical relations to get a model that is valid in a larger set in the state space. An analysis of how much the models are changing between different lids and welds could also be done more thoroughly to get a better model validation than is made in this thesis. The disturbances that affect the process should also be more thoroughly investigated. This thesis includes only a brief discussion of which disturbances might enter the system.

This thesis investigated the control during the initial start and downward sequence and the next step is to look at the control during the joint line. This weld sequence ranges over more than half an hour and is subjected to thermal expansion and possible movement of the canister. The control during the joint line must thus be further investigated. Since the LVDT-sensor can not be used during the full circumferential welds, there are three options left to evaluate further; using the position measurements, adding a new sensor to the system or changing control strategy. Trying to use the position measurements requires a lot of effort spent in

modeling the thermal expansion of the copper canister and investigations on how the copper canister is deformed and moved during the weld. Since this approach would partly result in open loop control, these models must be quite good and valid for all copper canisters that should be welded. The second approach with adding a new sensor to the system gives a more desirable situation with a feedback signal that measures the real tool depth regardless of thermal expansion and canister movement. The third option is to change the controller structure and choose another feedback solution. This may be the most attractive approach, since it could use the benefits of both the previous options; it relaxes the need for a new sensor and still is not subjected to the thermal expansion and canister movement. The idea could be to combine the controller in this thesis with a control structure similar to the one proposed by Longhurst et al. [18]. This would imply using the position measurements during the (relatively short) start and downward sequence where the thermal expansion might be easy to model, and then, when reaching the joint line, a torque controller is activated. This would need quite a lot of effort spent into finding a good structure for the torque controller, but would relax the need for a new sensor.

An evaluation of the possibility to design a control structure other than NMPC that could decouple the depth and temperature control loops could also be done. This would combine the simpler controllers with possibly higher performance and less interaction between the controller variables. A feedforward loop that compensate for the changes in force might be included to get less torque disturbances in the cascaded controller.

The torque's dependence on spindle rotation speed is another topic that could be further studied. A more fundamental understanding of this phenomenon could be used both in the further development of the NMPC-controller, but also in the existing cascaded temperature controller. If this dependence could be modeled properly and predicted in the welds, a higher control performance could be expected. Cui et al. [6] have observed a correlation between rotation speed and torque, which they explain with a change in the material flow resistance around the tool. This hypothesis could be validated and incorporated in the control system.

APMONITOR supports on-line parameter estimation, and it could be interesting to look at an NMPC with real time parameter estimation. At least the state parameter δ and the yield stress τ_{yield} could be estimated to improve the predictive accuracy of the model between different welds and parts of the state space.

The main reason to introduce depth control is to avoid hooking defects, and an NDT will reveal how well the plunge depth controller has performed. Hence, the welds made with the implemented plunge depth controller will be evaluated using NDT and the result from this test should be used to determine whether the controller keeps the depth at the desired levels or not.

Bibliography

- [1] APMONITOR. <http://www.apmonitor.com>, May 2012.
- [2] L. Cederqvist, O. Garpinger, T. Hägglund, and A. Robertsson. Cascade control of the friction stir welding process to seal canisters for spent nuclear fuel. *In review for Control Engineering Practice*.
- [3] L. Cederqvist, A. P. Reynolds, C. D. Sorensen, and O. Garpinger. Reliable sealing of copper canisters using new tool geometry and regulator controlling tool temperature and power input. In *8th International Symposium on Friction Stir Welding*, Timmendorfer Strand, Germany, May 2010.
- [4] L. Cederqvist, C. D. Sorensen, A. P. Reynolds, and T. Öberg. Improved process stability during friction stir welding of 5 cm thick copper canisters through shoulder geometry and parameter studies. *Science and Technology in Welding and Joining* 46(2).
- [5] Lars Cederqvist. *Friction Stir Welding of Copper Canisters Using Power and Temperature Control*. PhD thesis, Lund University, 2011.
- [6] S. Cui, Z. W. Chen, and J. D. Robson. A model relating tool torque and its associated power and specific energy to rotation and forward speeds during friction stir welding/processing. *International Journal of Machine Tools & Manufacture* 50, Sep. 2010.
- [7] Richard C. Dorf and Robert H. Bishop. *Modern control systems*. Pearson Prentice Hall, Upper Saddle River, N.J., 11th edition, 2008.
- [8] A. Fehrenbacher, N. J. Ferrier, N. A. Duffie, M. R. Zinn, and F. E. Pfefferkorn. Temperature measurement and closed-loop control in friction stir welding. In *8th International Symposium on Friction Stir Welding*, Timmendorfer Strand, Germany, May 2010.
- [9] Wilhelm Flügge. *Viscoelasticity*. Springer-Verlag, 1975.
- [10] M. W. Foley, R. H. Julien, and B. R. Copeland. Proportional-integral-derivative λ -tuning for integrating processes with deadtime. *IET Control Theory and Applications*, May 2009.

- [11] Olof Garpinger. *Design of Robust PID Controllers with Constrained Control Signal Activity*. Lic. thesis, Lund University, 2009.
- [12] Olof Garpinger, Tore Hägglund, and Karl Johan Åström. Criteria and Trade-offs in PID Design. In *IFAC Conference on Advances in PID Control*, Brescia, Italy, 2012.
- [13] Torkel Glad and Lennart Ljung. *Reglerteknik - Grundläggande teori*. Studentlitteratur, 2006.
- [14] J. D. Hedengren and R. Asgharzadeh. Tutorial overview of solving dynamic optimization and advanced control for large scale industrial systems. *Control Engineering Practice*. To appear.
- [15] D. H. Lammlein, W. R. Longhurst, D. R. DeLapp, P. A. Fleming, A. M. Strauss, and G. E. Cook. The friction stir welding of hemispheres - a technique for manufacturing hollow spheres. *International Journal of Pressure Vessels and Piping*, Aug. 2010.
- [16] Daniela Lohwasser and Zhan Chen. *Friction stir welding, From basics to applications*. Woodhead Publishing Limited, 2010.
- [17] W. R. Longhurst, A. M. Strauss, and G. E. Cook. Enabling Automation of Friction Stir Welding: The Modulation of Weld Seam Input Energy by Traverse Speed Force Control. *Journal of Dynamic Systems, Measurement, and Control*, Jul. 2010.
- [18] William R. Longhurst, Alvin M. Strauss, George E. Cook, and Paul A. Fleming. Torque control of friction stir welding for manufacturing and automation. *The International Journal of Advanced Manufacturing Technology*, Apr. 2010.
- [19] J. M. Maciejowski. *Predictive Control with Constraints*. Pearson Education Limited, 2002.
- [20] S. Mandal, J. Rice, and A. A. Elmustafa. Experimental and numerical investigation of the plunge stage in friction stir welding. *Journal of Materials Processing Technology (203)*, 2008.
- [21] D. W. Mayfield and C. D. Sorensen. An improved temperature control algorithm for friction stir welding. In *8th International Symposium on Friction Stir Welding*, Timmendorfer Strand, Germany, May 2010.
- [22] R. S. Mishra and Z. Y. Ma. Friction stir welding and processing. *Materials Science and Engineering R* 50, Aug. 2005.
- [23] R. Nandan, T. DebRoy, and H. K. D. H. Bhadeshia. Recent Advances in Friction Stir Welding - Process, Weldment, Structure and Properties. *Progress in Materials Science* 53, Aug. 2008.
- [24] Katsuhiko Ogata. *Modern control engineering*. Prentice Hall, Upper Saddle River, N.J., international 4th edition, 2002.

- [25] J. W. Qian, J. L. Li, J. T. Xiong, F. S. Zhang, W. Y. Li, and X. Lin. Periodic variation of torque and its relations to interfacial sticking and slipping during friction stir welding. *Science and Technology of Welding and Joining*, Jan. 2012.
- [26] H. Schmidt, J. Hattel, and J. Wert. An analytical model for the heat generation in friction stir welding. *Modelling and Simulation in Material Science and Engineering*, Nov. 2003.
- [27] SKB. Encapsulation, when, where, how and why? <http://www.skb.se/upload/publications/pdf/Inka2008Eng.28.1NY.pdf>, 2005.
- [28] S. Skogestad. Probably the best simple PID tuning rules in the world. *Journal of Process Control*, Sep. 2001.
- [29] Thomas WM, Nicholas ED, Needham JC, Murch MG, Temple-Smith P, and Dawes CJ. Friction stir butt welding. Patent PCT/GB92/02203, 1991.

Upphovsrätt

Detta dokument hålls tillgängligt på Internet — eller dess framtida ersättare — under 25 år från publiceringsdatum under förutsättning att inga extraordinära omständigheter uppstår.

Tillgång till dokumentet innebär tillstånd för var och en att läsa, ladda ner, skriva ut enstaka kopior för enskilt bruk och att använda det oförändrat för icke-kommersiell forskning och för undervisning. Överföring av upphovsrätten vid en senare tidpunkt kan inte upphäva detta tillstånd. All annan användning av dokumentet kräver upphovsmannens medgivande. För att garantera äktheten, säkerheten och tillgängligheten finns det lösningar av teknisk och administrativ art.

Upphovsmannens ideella rätt innefattar rätt att bli nämnd som upphovsman i den omfattning som god sed kräver vid användning av dokumentet på ovan beskrivna sätt samt skydd mot att dokumentet ändras eller presenteras i sådan form eller i sådant sammanhang som är kränkande för upphovsmannens litterära eller konstnärliga anseende eller egenart.

För ytterligare information om Linköping University Electronic Press se förlagets hemsida <http://www.ep.liu.se/>

Copyright

The publishers will keep this document online on the Internet — or its possible replacement — for a period of 25 years from the date of publication barring exceptional circumstances.

The online availability of the document implies a permanent permission for anyone to read, to download, to print out single copies for his/her own use and to use it unchanged for any non-commercial research and educational purpose. Subsequent transfers of copyright cannot revoke this permission. All other uses of the document are conditional on the consent of the copyright owner. The publisher has taken technical and administrative measures to assure authenticity, security and accessibility.

According to intellectual property law the author has the right to be mentioned when his/her work is accessed as described above and to be protected against infringement.

For additional information about the Linköping University Electronic Press and its procedures for publication and for assurance of document integrity, please refer to its www home page: <http://www.ep.liu.se/>